DESIGN AND EVALUATION OF A HELICOPTER MAIN ROTOR ELECTROHYDRAULIC CONTROL SYSTEM

A THESIS SUBMITTED TO
THE GRADUATE SCHOOL OF NATURAL AND APPLIED SCIENCES
OF
MIDDLE EAST TECHNICAL UNIVERSITY

BY

HASAN ALİ DÜZAĞAÇ

IN PARTIAL FULFILLMENT OF THE REQUIREMENTS
FOR
THE DEGREE OF MASTER OF SCIENCE
IN
MECHANICAL ENGINEERING

AUGUST 2022

Approval of the thesis:

DESIGN AND EVALUATION OF A HELICOPTER MAIN ROTOR ELECTROHYDRAULIC CONTROL SYSTEM

submitted by **HASAN ALİ DÜZAĞAÇ** in partial fulfillment of the requirements for the degree of **Master of Science** i**n Mechanical Engineering, Middle East Technical University** by,

Prof. Dr. Halil Kalıpçılar
Dean, Graduate School of **Natural and Applied Sciences** _____

Prof. Dr. Mehmet Ali Sahir Arıkan
Head of the Department, **Mechanical Engineering** _____

Assist. Prof. Dr. Hakan Çalışkan
Supervisor, **Mechanical Engineering, METU** _____

Prof. Dr. Raif Tuna Balkan
Co-Supervisor, **Mechanical Engineering, METU** _____

Examining Committee Members:

Assoc. Prof. Dr. Buğra Koku
Mechanical Engineering, METU _____

Assist. Prof. Dr. Hakan Çalışkan
Mechanical Engineering, METU _____

Prof. Dr. Raif Tuna Balkan
Mechanical Engineering, METU _____

Assoc. Prof. Dr. Ulaş Yaman
Mechanical Engineering, METU _____

Assist. Prof. Dr. Kutluk Bilge Arıkan
Mechanical Engineering, TED University _____

Date: 26.08.2022

I hereby declare that all information in this document has been obtained and presented in accordance with academic rules and ethical conduct. I also declare that, as required by these rules and conduct, I have fully cited and referenced all material and results that are not original to this work.

Name, Last name: Hasan Ali Düzağaç

Signature:

ABSTRACT

DESIGN AND EVALUATION OF A HELICOPTER MAIN ROTOR ELECTROHYDRAULIC CONTROL SYSTEM

Düzağaç, Hasan Ali
Master of Science, Mechanical Engineering
Supervisor: Assist. Prof. Dr. Hakan Çalışkan
Co-Supervisor: Prof. Dr. Raif Tuna Balkan

August 2022, 165 pages

Helicopters are widely used aircrafts for several purposes. Main Rotor of a Helicopter creates necessary flight forces for performing flight operation. Orientation of a Helicopter Rotor System is determined and controlled manually by pilot and automatically by automatic control system via hydraulically operated flight control actuators. In this research, a novel electrohydraulically operated helicopter main rotor control system is mathematically designed and developed to improve overall performance of control system and to extend controllable frequency range. Besides, resonant frequency is modified to a rarely used frequencies and amplitude of resonant frequency response is reduced. Mathematical model of Flight Control Actuator is verified and mathematical model is validated using test results obtained in a test bench that reflects main rotor control system of helicopter. Theoretical and experimental test results are compared. A novel control actuator and feedback actuator are introduced and implemented within the system for application of proposed control strategies.

Keywords: Hydraulic, Control Theory, System Dynamics, Helicopter, Fluid Power Control

ÖZ

BİR HELİKOPTER ANA ROTOR ELEKTROHİDROLİK KONTROL SİSTEMİNİN TASARIMI VE DEĞERLENDİRMESİ

Düzağaç, Hasan Ali
Yüksek Lisans, Makina Mühendisliği
Tez Yöneticisi: Assist. Prof. Dr. Hakan Çalışkan
Ortak Tez Yöneticisi: Prof. Dr. Raif Tuna Balkan

Ağustos 2022, 165 sayfa

Helikopterler, çeşitli amaçlar için yaygın olarak kullanılan hava araçlarıdır. Helikopterin ana rotoru, uçuş operasyonu için gerekli olan uçuş kuvvetlerini üretir. Helikopter rotor sisteminin oryantasyonu, hidrolik ile çalışan uçuş kontrol eyleyicileri kullanılarak pilot tarafından manuel ve otomatik kontrol sistemi tarafından otomatik olarak belirlenir ve kontrol edilir. Bu çalışmada, yeni bir elektrohidrolik helikopter ana rotor control sistemi, genel performans artırımı ve kontrol edilebilir frekans aralığını genişletmek amacıyla matematiksel olarak tasarlanıp geliştirilmiştir. Bunun yanında rezonans frekansı, nadir kullanılan bir frekans olarak modifiye edilmiş ve rezonans frekansın genliği azaltılmıştır. Uçuş kontrol eyleyicisinin matematiksel modeli doğrulanmış ve matematik model, helikopter rotor kontrol sistemini yansıtan bir test düzeneği kullanılarak geçerli kılınmıştır. Teorik ve deneysel sonuçlar mukayese edilmiştir. Yeni bir kontrol eyleyicisi ve geri besleme eyleyicisi, önerilen kontrol stratejilerinin uygulanması amacıyla tanımlanmış ve sistem içerisinde adaptasyonu yapılmıştır.

Anahtar Kelimeler: Hidrolik, Kontrol Teorisi, Sistem Dinamiği, Helicopter, Akışkan Gücü Kontrolü

To my father, my aunt, my grandmother, my deceased uncle…

and to Neslihan…

ACKNOWLEDGMENTS

First, I would like to thank my supervisor Assoc. Prof Dr. Hakan Çalışkan and my co-supervisor Prof. Dr. Raif Tuna Balkan for their great contribution and for giving this opportunity to me. I learned a lot of things throughout this research. Without comments and suggestions of them, I would not be able to learn and understand what is mentioned in this research. I learned to approach on divergent perspectives to any information that I learned thanks to their vision and ideas.

I would like to thank my friends and family for their priceless support during my studies. I would not be able to stay mentally focused and motivated without them. I would like to specially thank to my friends Oğuzhan, Onur, Mücahit and Sina for their support.

I would like to thank Neslihan for her undefinable help and support. With her great support when I need, I believe and stay motivated about what I can achieve.

And I would like to thank any other person who wants to help, encourage and support me during my studies.

TABLE OF CONTENTS

LIST OF TABLES

TABLES

LIST OF FIGURES

FIGURES

LIST OF ABBREVIATIONS

CG	Center of Gravity
COL	Collective Input
ELA	External Load Actuator
FC	Flight Computer
FL	Feedback Lever
FLC	Fuzzy Logic Controller
FWD	Forward
HP	Hydraulic Pump
HPS	Hydraulic Power System
IBC	Initial Bell Crank
IL	Input Lever
LAT	Lateral Input
LON	Longitudinal Input
LVDT	Linear Variable Displacement Transducer
MCV	Main Control Valve
P	Proportional
PD	Proportional-Derivative
PI	Proportional-Integral
PID	Proportional-Integral-Derivative
PIA	Pilot Input Actuator
PL	Pitch Link
RSP	Rotational Swashplate
SCA	Stability Control Actuator
SL	Stick Length
SSP	Stationary (Fixed) Swashplate
SV	Safety Valve

LIST OF SYMBOLS

λ	Translational Motion of Collective to Swashplate
α	Pitch Angle of Stationary Swashplate
β	Roll Angle of Stationary Swashplate
q	Helicopter Body Pitch Degree of Freedom
p	Helicopter Body Roll Degree of Freedom
r	Helicopter Body Yaw Degree of Freedom
x	Helicopter Body Longitudinal Degree of Freedom
y	Helicopter Body Lateral Degree of Freedom
z	Helicopter Body Vertical Degree of Freedom
x_1	Collective Input
y_1	Longitudinal Cyclic Input
y_2	Lateral Cyclic Input
z_1	Pedal Input
C_1	Gearing Ratio of Longitudinal Cyclic
C_2	Gearing Ratio of Lateral Cyclic
C_3	Gearing Ratio of Collective
C_4	Gearing Ratio of Pedal
d_1, D_1	Displacement of Forward Flight Control Actuator
d_2, D_2	Displacement of Left Flight Control Actuator
d_3, D_3	Displacement of Forward Flight Control Actuator
$D_{1(2)(3)}$	Displacement of Forward (Left) (Right) Actuator
$D_{1(2)(3),H}$	Horizontal Displacement of Forward (Left) (Right) Actuator
$D_{1(2)(3),V}$	Vertical Displacement of Forward (Left) (Right) Actuator
R_S	Radius of Fixed Swashplate Trajectory
d_{pl}	Radial Distance of Pitch Link to Rotor Mast Axis
d_h	Hinge Length
$\omega_{COL(LON)(LAT)}$	Collective (Longitudinal) (Lateral) Control Angle
$x_{SL,COL(LON)(LAT)}$	Collective (Longitudinal) (Lateral) Stick Mechanism Length

Q_1	Flow from Pressure Source to Chamber 1
x_v	Valve Input
x_i	Pilot Input
x_p	Cylinder Output
x_b	Blade Displacement
x_s	Lug Displacement
x_{body}	Body Displacement
$x_{v,Pilot}$	Pilot Valve Input
$x_{v,Stability}$	Stability Actuator Input
$x_{v,SCA}$	SCA Input
$x_{v,1}$	Total Valve Input
H	Valve Height
C_D	Valve Coefficient
A_v	Valve Area
ρ	Fluid Density
P_1	Pressure of Chamber 1
P_2	Pressure of Chamber 2
P_A	Pressure of Chamber A
P_B	Pressure of Chamber B
P_S	Pressure of High-Pressure Source
P_R	Pressure of Return Tank
x_v^0	Vicinity Point of Valve Input
P_1^0	Vicinity Point of Chamber Pressure
$\alpha_{P,St}$	Coefficient of Structural Elasticity
R_{Leak}(R)	Leakage between Chambers of the Piston
E_v	Bulk Modulus of Hydraulic Oil
$R_{1(2)(3)(4)}$	Orifice Resistance Through Line 1(2)(3)(4) in MCV
$Q_{R1(R2)(R3)(r4)}$	Flow Through Line 1(2)(3)(4) in MCV
$P_{R1(R2)(R3)(R4)}$	Pressure Difference Through Line 1(2)(3)(4) in MCV

C	Capacitance of Hydraulic Fluid
M_1	Equivalent Mass for 1-Mass System
K_1	Equivalent Stiffness for 1-Mass System
B_1	Equivalent Damping for 1-Mass System
P_A	Pressure Difference on Piston
V_A	Velocity of Cylinder
F_A	Force Exerted by Cylinder
Q_A	Flow Rate of Cylinder
K_{vf}	Coefficient of Valve Flow
K_{pf}	Coefficient of Pressure Flow
A_P	Piston Area
K_{ls}	Layshaft Coefficient
M_P, M_{Pt}	Mass of Piston
M_B	Equivalent Mass of Blade Assembly
M_S	Equivalent Mass of Swashplate Assembly
M_{Body}	Mass of Actuator Body
M_R	Equivalent Mass of Rotor System
B_B	Equivalent Damping of Blade Assembly
B_S	Equivalent Damping of Blade Assembly
K_B	Equivalent Stiffness of Swashplate Assembly
K_S	Equivalent Stiffness of Swashplate Assembly
V_A	Volume of Chamber A
V_B	Volume of Chamber B
F_F	External Force
t_{rise}	Rise Time
$t_{settling}$	Settling Time
$C_{y1(y2)(x1)}$	Mechanism Proportion of Cyclic (Collective)
K_{lS}	Layshaft Reduction

CHAPTER 1

INTRODUCTION

1.1 Helicopter Hydraulics: History and Motivation

Helicopters are large aircrafts that are used for many different applications over decades. Having a such advantage in terms of flexibility and mobility, provides wide usage area for helicopters such as transportation for both military and civilian purposes, health as an ambulance vehicle, firefighting as a carrier vehicle. As a huge aircraft, helicopters have many operations that require high power and loads. To fulfill the power demand in high loads from such applications, hydraulic power control systems are used commonly. Most common ones are given below;

- Pitch Angle Control of Main Rotor Blades
- Pitch Angle Control of Tail Rotor Blades
- Position Control of Stability Augmentation Actuator
- Extension and Retraction of Retractable Landing Gear Systems
- Control of Wheel Brake Braking Pressure
- Control of Rotor Brake Braking
- Lock/Unlock of Tail or Nose Wheel

Helicopter performs its motions from the forces that are created by main rotor blades due to their pitch angles. Angles are determined by the positions of a rod and position control of the pitch angles of all rotor blades are controlled by electrohydraulic rotor control system. For the helicopters that are under 3 tons, hydraulic power systems are not compulsorily involved as the flight forces acting on the rotor system are compatible with the forces acting on the pilot's hand during handling. However, hydraulic power system is used in helicopters which are over 3 tons due to decrease the pilot workload during handling. Additionally, helicopter control has strict requirements to enhance the handling

quality of the vehicle. For that reason, control system is required to be highly responsive under huge number of forces. For that reasons, hydraulic power systems are quite beneficial considering the handling performance of the vehicle. There are some crucial benefits of including hydraulic control systems in a helicopter main rotor control, which can be listed as [1];

- Installation Capability in a Compact Volume
- Fast Rate of Response
- Load Retaining Capacity
- High Power/Weight Ratio
- Durability Under Severe Conditions
- Ability of Sensitive Control

Considering these benefits compared to other control systems, usage of hydraulic systems are reasonable. In order to comprehend how rotor assembly responds to outputs of the linear hydraulic actuators, it is required to be explained.

1.1.1 Helicopter Main Rotor and Rotor Control Theory

Helicopter main rotor is a huge assembly that contains significant subcomponents that provides an arrangement of main rotor blades pitch angle to create necessary forces to perform flight operation. These subcomponents are demonstrated and explained below.

1.1.1.1 Input Levers

Input Levers are directly controlled sticks by pilot to create the necessary maneuver of the aircraft. Helicopter can be controlled at 4 different directions directly, which are Pitch (q), Roll (p), Yaw (r) and Vertical (z). Movement on these directions can be achieved by three different Input Levers that supply four different types of input to main and tail rotor assembly. Inputs Levers are called Cyclic ($y_{1,2}$), Collective

(x_1) and Pedal (z_1). Cyclic input can be given two different axis which are called Longitudinal Cyclic (y_1) and Lateral Cyclic (y_2). Longitudinal (x) and Lateral (y) motion of the helicopter occurs resulting from Pitch and Roll motion, respectively. All helicopter input and corresponding motion of the air vehicle are listed in Table 1.1.

Table 1.1 Helicopter Motion and Resultant Helicopter Input

Helicopter Motion	Helicopter Input
Pitch (q)	Longitudinal Cyclic (y_1)
Roll (p)	Lateral Cyclic (y_2)
Yaw (r)	Pedal (z_1)
Longitudinal (x)	Result of Pitch (q)
Lateral (y)	Result of Roll (p)
Vertical (z)	Collective (x_1)

These Input Levers are mechanically connected with the input point of the Flight Control Actuator (FCA) via assemblies consist of rods and bell cranks. In other words, transmission of the input on the helicopter is achieved with mechanical connection. There is a ratio between the displacement of an Input Lever and input point of the FCA, which is called mechanical gearing ratio, and it is bounded to certain mechanical design parameters of rotor system that are to be described in 2.1 Gearing ratios of y_1, y_2, x_1, z_1 are represented as C_1, C_2, C_3 and C_4 respectively.

1.1.1.2 Rotor Assembly

Rotor assembly is a rotating assembly of the helicopter that is used to create necessary forces to perform flight. The most significant components of the rotor assembly can be listed as Stationary Swashplate (SSP), Rotating Swashplate (RSP), Pitch Links (PL), Hub, Control Rod, Rotor Blades. These components and their missions are explained below, and they are demonstrated in Figure 1.1.

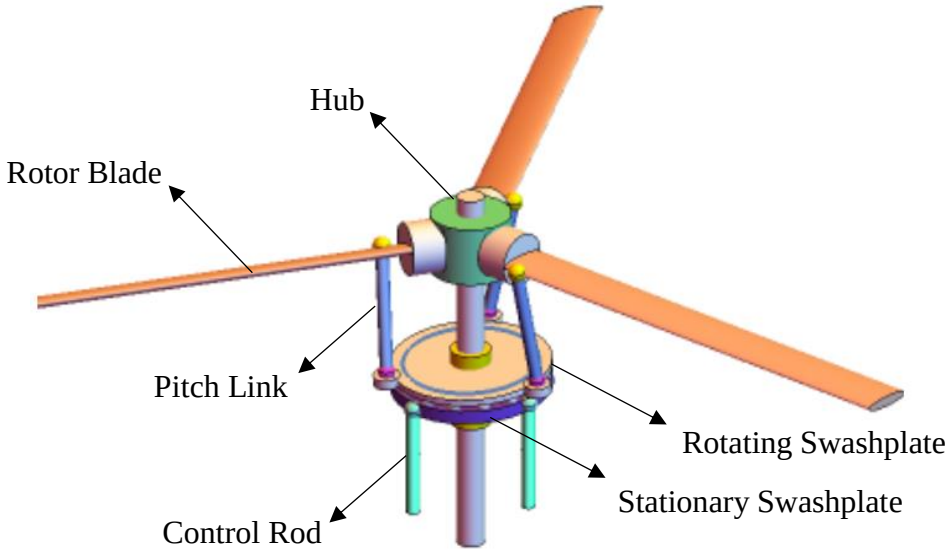

Figure 1.1 Fundamental Components of Helicopter Rotor Assembly [2]

Rotor Blade: These are used to create aerodynamic forces for necessary lifting of the helicopter. Increasing value of the angle of attack causes more lifting during flight. Besides, Disturbance loads and aerodynamic loads are acting directly to rotor blades.

Hub: The structural component that provides a mechanical installation interface for Rotor Blades. Centre axis of the main rotor hub is aligned with the rotor mast.

Pitch Link: These are used to change the pitch angle of the Rotor Blades. Number of the Pitch Links are equal with the number of Rotor Blades.

Rotating Swashplate (RSP): It is used to arrange the displacement of each pitch link at the specific rotation angle. As a result of the motion of this component, each Pitch Link has a constantly changing displacement values for any angle.

Stationary Swashplate (SSP): It is the stationary component that is used to arrange the orientation of Rotating Swashplate. There is a ball bearing between these components. SSP is connected with the control rods of the each FCAs from three different location. From the combined displacements of these FCAs, orientation of SSP is determined and it is transmitted to RSP. It ultimately affects blades pitch angle as the angle of all blades are bounded to orientation of the SSP at any time.

Orientation of the stationary swashplate can be identified by three degrees of freedom of itself which are α, β and λ; pitch, roll and vertical degrees of freedom of the SSP itself. These are obtained by mathematical combination of Input Levers that are reducted as predetermined rates with rotor control links.

Control Rod: It is the rod of FCA that is connected to lug of the SSP. It transmits the cylinder output directly to the corresponding lug of the SSP.

As a brief summary, combined action of FCAs is SSP via Control Rods. Tilting angles of α, β and z are transferred directly to RSP. A Ball Bearing assembly is installed between Rotating and Nonrotating Swashplate to performs smooth transformation of SSP orientation to rotating components. Varying orientation of RSP gives input to each Pitch Link that is used to control the pitch angle of each Rotor Blades separately and independently. Flight forces are created with changing rate of pitch angles of Rotor Blades through desired degree of freedom. SSP is demonstrated as a triangle because there are three different lug to which rod ends of FCA are connected.

1.1.2 Hydraulic Flight Control Actuator

Flight Control Actuators (FCA) are the components that are operated by the power of hydraulic pump and transmits pilot input as cylinder output with an amplified ratio. Amplification can be acquired by nominal operational pressure which is ideally selected as 3000 psi that equals to 20.7 MPa pressure acting on a cylinder with a ratio. Ratio that arranges the pressure which is acting to hydraulic cylinder is determined by the Main Control Valve (MCV) inside the FCA. With the significant help of MCV, pilot input is converted to desired output with an amplified force. Lacking hydraulic power system causes necessity of extremely high forces that are to be applied by pilot or automatic pilot; thus, control of the helicopter would be unfeasibly hard and improper handling characteristic would occur. Fundamental subcomponents of a FCA can be listed as Linear Piston-Rod Assembly, Main

Control Valve, Feedback Lever, Cylinder Body, Mechanical Linkage and Electrical Input Module. These subcomponents are explained as follows;

Piston-Rod Assembly: It is an assembly that transmits force, resulting from the pressure difference of two different chambers, converting it to an acting force via a rod. Linear cylinder moves only in axial direction backward and forward considering the direction of the force. Rod end of the cylinder is connected to SSP lug with a single attachment that provides displacement within a specified range that is at least equal to the complete stroke of the FCA. Thus, displacement of the FCA that consist as a result of pilot input is converted an output and transmitted to rotor system via SSP.

Main Control Valve (MCV): It is a component that is used to arrange the flow rate through two different chambers of the linear cylinder as one of the chambers is expanding while the other one retracting, simultaneously. MCV has a mechanical connection for taking input; however, Servo valve inputs are electrically powered input that are transmitted to control valve via independent mechanical connection. Control valve is basically a sleeve spool mechanism of which orifices are adjusted as critically lapped.

Feedback Lever (FL): It is a linkage mechanism basically linked to end rod of the pilot input, electrical input rod, MCV and Cylinder output. It is used to give cylinder output as feedback to obtain a closed loop control system. Summing of input and feedback output are given as an input to MCV. Pilot input and electrical input are also pre summed via a summing link. Besides, Feedback lever length and ratio of its arms are critical for the stability of the feedback control system.

Cylinder Body: It contains the necessary hydraulic fluid for the operation of the system as well as cylinder rod assembly and seals.

Mechanical Linkage: It is a linkage that is used for the reduction of feedback that is given to the MCV to acquire more stable system, which is called Layshaft Reduction. Without this component, stability is severely impacted because of instantaneous

amplified input that is directly transmitted to MCV. Reduction rate by this component is critical and sensitively influences the system behavior in terms of response times. Layshaft reduction is demonstrated in Figure 1.2.

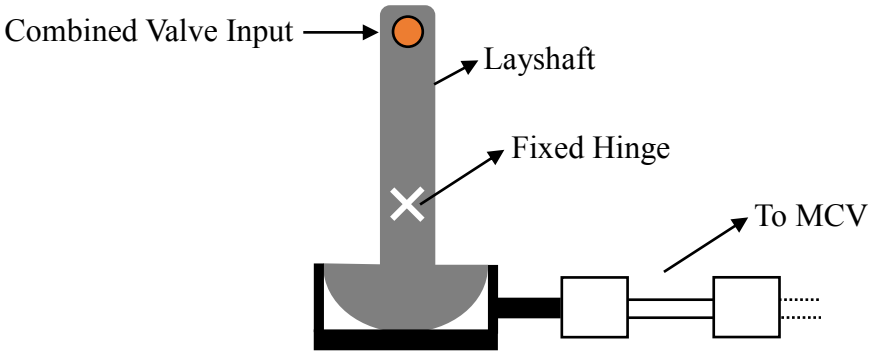

Figure 1.2 Demonstration of Layshaft Reduction

Electrical Input Module: Stability of the SSP is provided by using controllers additional to the mechanical input. Controllers are creating supplementary input by the aid of electrical input module. Note that these inputs are for the stability and performance improvement of the SSP instead of complete vehicle. Complete vehicle stability is provided with Stability Augmentation System which is a different system that uses helicopter positions as feedback for the closed loop. Instead, control of SSP uses cylinder output as feedback; still, considering the impact of rotor equivalent mass inertia, blades inertia, aerodynamic loads, and disturbances.

1.1.3 Installation of FCAs on Main Rotor SSP

Considering the availability of different installation techniques and mechanism designs, various installation principles are developed for main rotor such as 90° installation and 120° installation, or even in 120° installations, there can be various installations and difference occurs from the orientation angles γ and ψ_0 [3]. In the evaluated helicopter main rotor swashplate, 120° installation is used with three Servo FCAs which are called Forward FCA, Left FCA and Right FCA. From the top view, installation of FCAs is given in Figure 1.3.

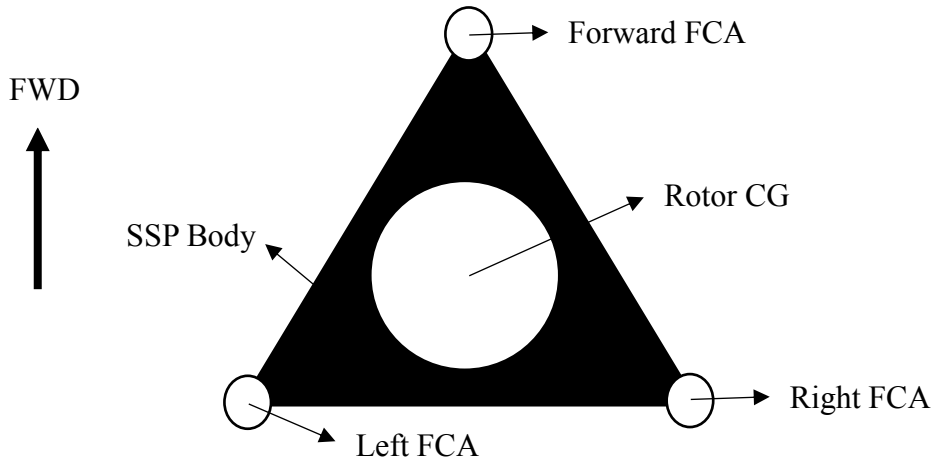

Figure 1.3 Top View of Helicopter Main Rotor SSP Installation

Forward FCA is the 1st, Left FCA is the 2nd and Right FCA is the 3rd FCA while numbering the parameters. With the given information, perspective view of the SSP and FCAs assembly are given in Figure 1.4.

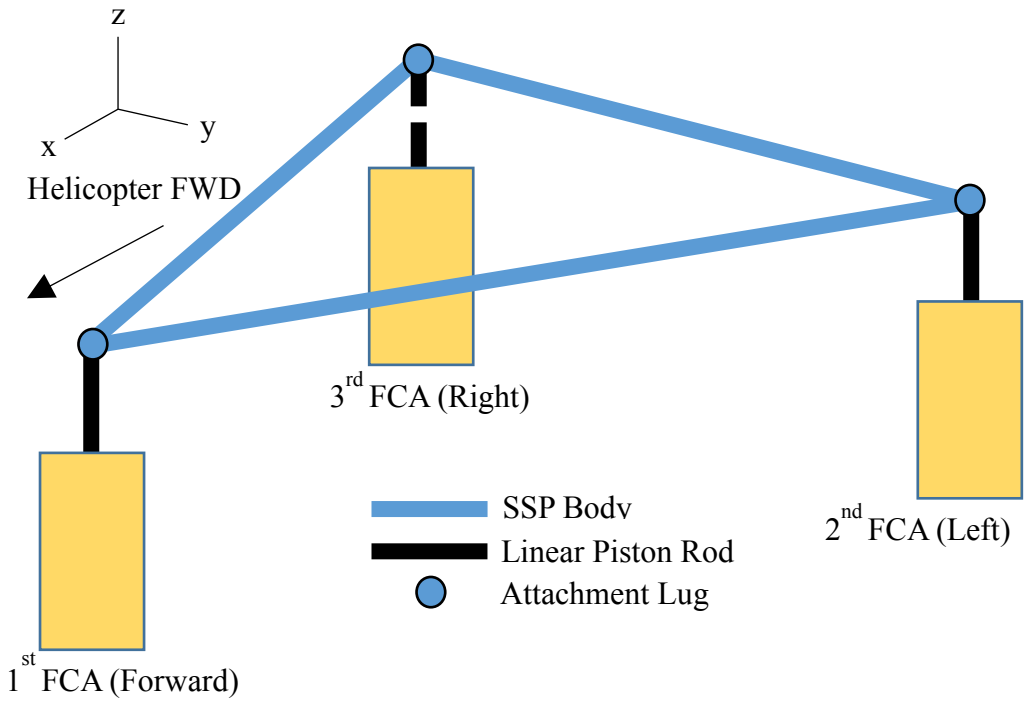

Figure 1.4 Perspective View of Main Rotor SSP Assembly

Orientation of Main Rotor SSP is determined by three different inputs which are Collective (COL), Longitudinal Cyclic (LON) and Lateral Cyclic (LAT). Each FCA moves either positive or negative on their own axis with a given specific input. Relation between given input and corresponding effected SSP degree of freedom are given in Table 1.2.

Table 1.2 Main Rotor SSP Affected Motion for Given Input

Main Rotor SSP Motion	Helicopter Input
Pitch (α)	Longitudinal Cyclic (y_1)
Roll (β)	Lateral Cyclic (y_2)
Vertical (λ)	Collective (x_1)

1.1.3.1 Motion of Pitch (α)

Pitch motion (α) is the rotational motion of SSP about y-axis on the frame of its own CG. In this motion, Forward FCA moves, in either direction, two times faster than other actuators; meanwhile, left and right FCAs move through opposite direction with Forward FCA simultaneously. Forward (+) LON input causes Forward actuator to retract and Left/Right actuator to extend. Backward (-) LON input causes Forward actuator to extend and Left/Right actuator to retract. Demonstration of positive LON and positive α, negative LON and negative α are demonstrated in Figure 1.5 and Figure 1.6 respectively.

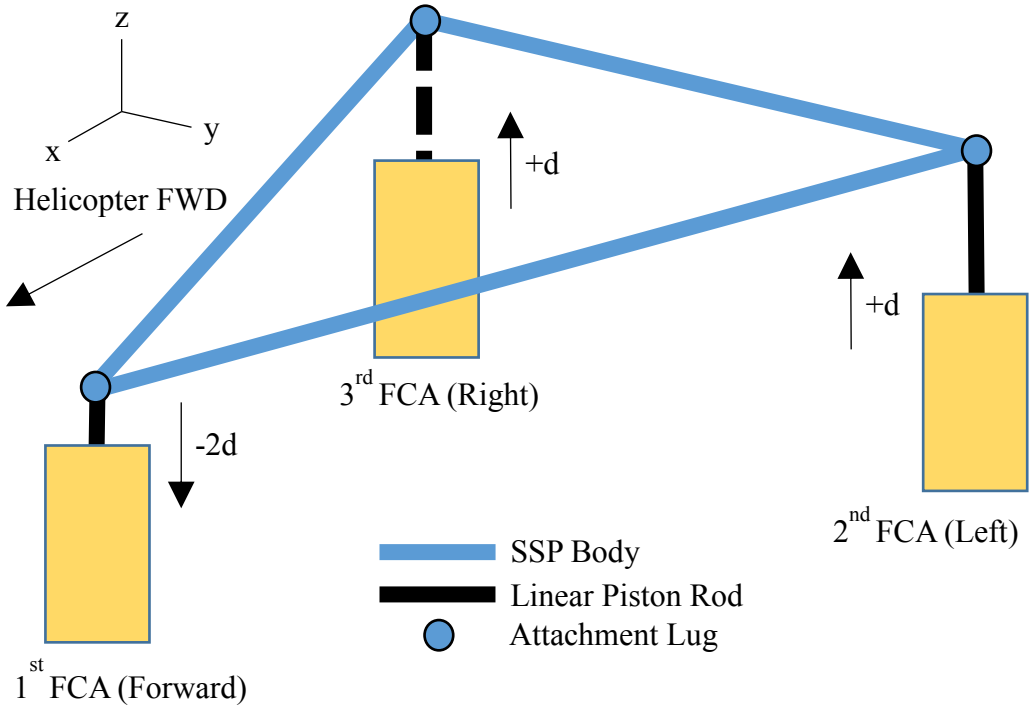

Figure 1.5 Positive Pitch Angle Resulting from Positive LON Input

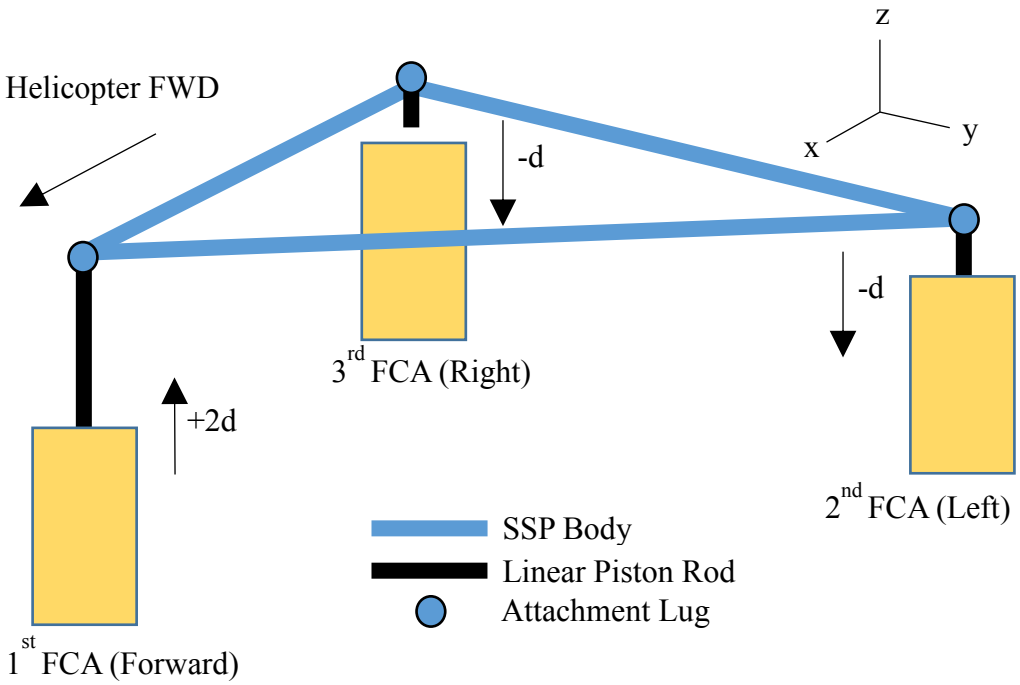

Figure 1.6 Negative Pitch Angle Resulting from Negative LON Input

1.1.3.2 Motion of Roll (β)

Roll Motion (β) is the rotational motion of SSP about the x-axis on the frame of its own CG. In this motion, Forward FCA does not move in any direction. Left FCA moves in either direction; meanwhile, Right FCA moves in the opposite one with the same velocity but simultaneously. Rightwards (+) LAT input causes Right FCA to retract and Left FCA to extend. Leftwards (-) LAT input causes Right FCA to extend and Left FCA to retract. Demonstration of positive LAT and positive β, negative LAT and negative β are demonstrated in Figure 1.7 and Figure 1.8 respectively.

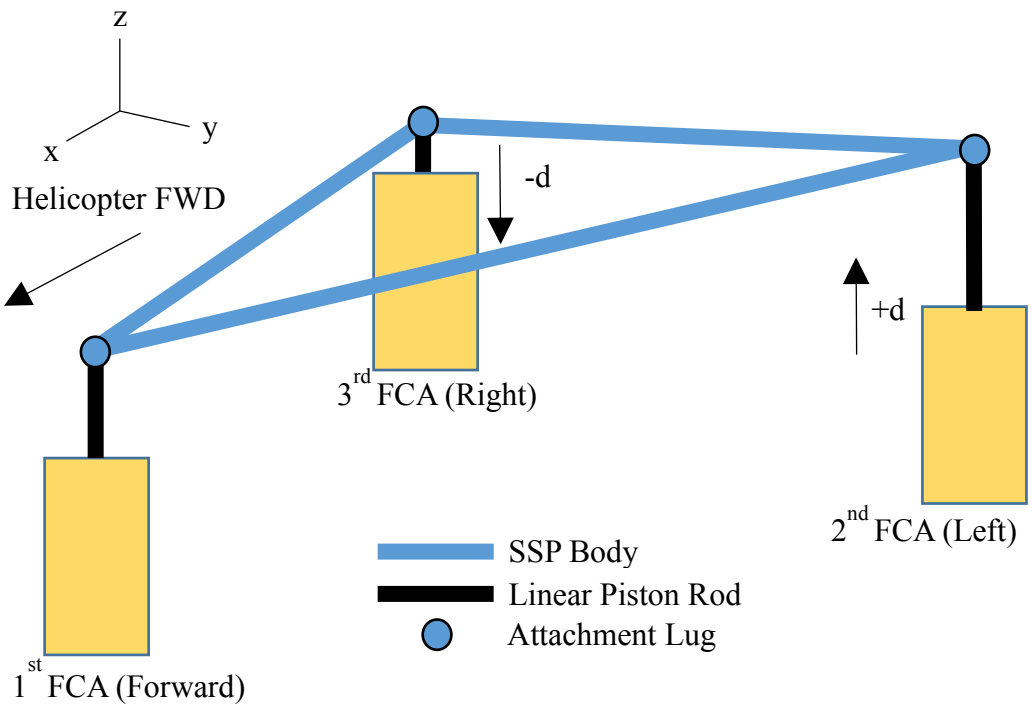

Figure 1.7 Positive Roll Angle Resulting from Positive LAT Input

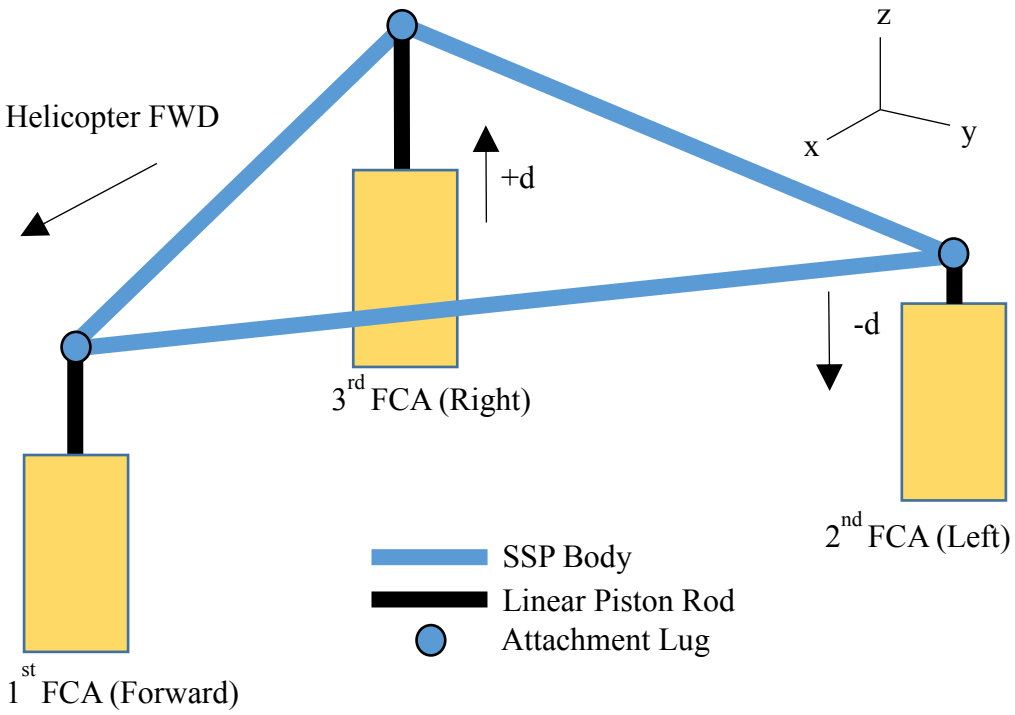

Figure 1.8 Negative Roll Angle Resulting from Negative LAT Input

1.1.3.3 Vertical Motion (λ)

Vertical Motion (λ) is the longitudinal motion of SSP along z axis on the frame of its own CG. Vertical motion of the SSP causes increment of the pitch angles, angle of attack, of all rotor blades simultaneously by the same amount; thus, creates an overall lift for the aircraft. To perform motion along z axis smoothly, all FCAs installed on SSP moves simultaneously by the same amount in either direction. Upwards (+) COL input causes extension of all FCAs. Downwards (-) COL input causes retraction of all FCAs. Demonstration of positive COL and positive λ is demonstrated in Figure 1.9.

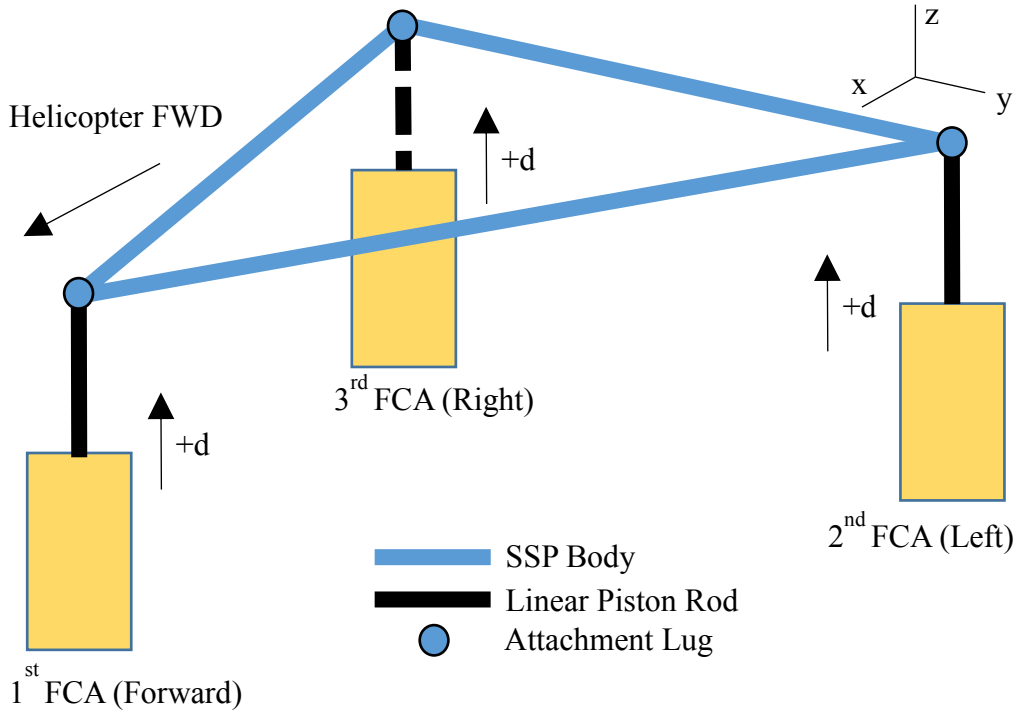

Figure 1.9 Positive Vertical Motion Resulting from Positive COL Input

For any possible input that can be given by the pilot, displacements of each FCA are tabulated in .

Table 1.3 Displacements and Directions of Each FCA by Given Pilot Input

Helicopter Input	Forward FCA	Left FCA	Right FCA
Positive LON ($y_1 > 0$)	-2d	+d	+d
Negative LON ($y_1 < 0$)	+2d	-d	-d
Positive LAT ($y_2 > 0$)	0	+d	-d
Negative LAT ($y_2 < 0$)	0	-d	+d
Positive COL ($x_1 > 0$)	+d	+d	+d
Negative COL ($x_1 < 0$)	-d	-d	-d

1.1.3.4 Geometric Singularities

During SSP pitch and roll motion, lugs are assumed to be moved only vertical in a single reference frame. However, as one side length of the SSP equilateral triangle is rigid and does not elongate during motion of SSP, vertical motion in a single reference frame causes a singularity of motion. For example, actual geometrical position of actuators in a positive lateral cyclic input with an extreme amplitude in demonstrated in Figure 1.10.

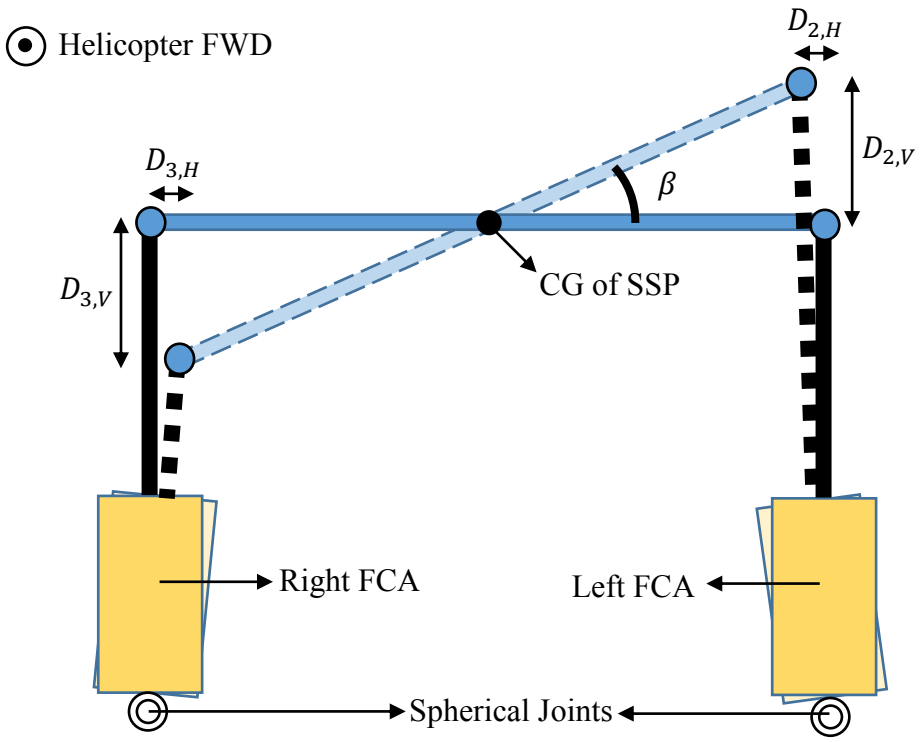

Figure 1.10 Actual Geometric Orientation of SSP Roll Motion

Vertical and horizontal displacement of each actuator is represented for roll motion. Same diagram is applied in the pitch motion of SSP and D_1 can also be divided as $D_{1,H}$ and $D_{1,V}$. As it can be seen in Figure 1.10, horizontal displacements are negligibly small compared to vertical displacements. Thus, displacements of each actuator can be assumed throughout analysis as follows;

$$D_1 = \sqrt{{D_{1,H}}^2 + {D_{1,V}}^2} \cong D_{1,V} \tag{1.1}$$

$$D_2 = \sqrt{{D_{2,H}}^2 + {D_{2,V}}^2} \cong D_{2,V} \tag{1.2}$$

$$D_3 = \sqrt{{D_{3,H}}^2 + {D_{3,V}}^2} \cong D_{3,V} \tag{1.3}$$

Displacements of each FCA are taken as directly horizontal displacement of the corresponding actuator. Meanwhile, kinematic representation of SSP linked with displacements can easily be found without making kinematic equations complex unnecessarily. Thus, geometric singularities of pitch and roll motions are eliminated by using (1.1), (1.2) and (1.3) with a trivial manipulation of SSP kinematics.

1.2 Literature Review

Hydraulically powered linear actuators are commonly used within a servo valve that is to perform a sensitive control on the actuator. Due to demonstration of highly nonlinear characteristics, Simulink® is generally used to represent this nonlinear behavior. However, valve dynamics can also be obtained by linearization and valve is allowed to exhibit its behaviors with such a linearity in the defined linear range. State-space representation is easier to obtain in linear systems as well as all parameters can be tracked more easily. On the other hand, linear systems cannot be used in wide ranges because as far as the system response become distant from the linear range of the actuator, responses can not to be considered as consistent. Linear Graph method is widely used in obtaining such linear systems to simulate the system response easier. Linear graph method allows obtaining first order nonlinear differential equations that belongs to the system components and converting them into linear form. System can be controlled in both two ways which are position control and force control. Position control is commonly based on proportional feedback control. PID controller can be implemented within the system to get better responses. In order to perform a force control, model-based controller is to be developed. In these types of controllers, system is not closed with feedback. Instead,

system observes the parameters other than position such as force or pressure in either chamber or creates control input to perform the stable control. It is more compatible to design such model-based controllers in linear systems that allows position tracking as well as force control [4].

As soon as the position control of an actuator is sufficiently sensitive to be utilizable, force control is to be implemented to acquire a more sensitively controlled system is applications such as hydraulic presses. Inherent nature of hydraulic presses requires to get an overdamped system because an overshoot from the reference behavior may cause unbearable forces for the applied material. Force control prevents such instantaneous peaks of forces. Šıtum [5] argues such a hydraulic press that is controlled by two different feedback: position and applied force. Dynamic system of the context is considered as a first order system. Force is controlled before entering the system as it is known the steady state force value of the system under which the material does not fail. Besides, position is controlled as feedback taken as output of the cylinder. Servo valve function is developed which represents a common controller for force and position; however, gain coefficient can be differently selected before entering the servo valve function. Hydraulic system is represented with a first order linear transfer function. Hybrid controller that is used in the test setup uses PD controller for position control and PID controller for force control that is developed by using MATLAB/Simulink®.

Modeling of a hydraulic servo system brings correct and reliable results either in linear or nonlinear model depending on the system parameters. For example, including the friction model of the linear actuator brings such nonlinearities to the system. Thus, it is beneficial to use a nonlinear system if there is any friction model. Due to differences among different types of models, various methods can be developed using linear and nonlinear tools. Besides, for the inspection of a specific system parameter, linear model can also be simplified further. For a wide range of input in terms of amplitude and frequencies, verification of each model can be performed, and corresponding model can be used within this specific range in which the system is verified. Efe [6] developed a hydraulic servo control system by using

three different typs of methods which are nonlinear, linear, and simplified linear models. System is also experimentally developed, and a predetermined valve input signal is given to the servo valve. Simulation results for both models and experimental results are compared in terms of system outputs such as displacement, pressure differences between the chambers of the actuator. It is observed that increasing signal rate that is given to the servo valve brings more accurate results in all simulations. However, nonlinear model has more overshoots compared to other systems and linear models tend to be more stable compared to nonlinear model. As it is described above, even with the varying rate of the given input, models behave differently from each other, and all models give correct results in different regions of the valve input. It can be concluded that nonlinear model brings the more compatible results with respect to experimental results; however, it has huge number of overshoots and undershoots that makes the observation of the system responses inaccurate.

While developing the nonlinear models for the system simulation, it is significant to consider the models that brings nonlinearities to the system. Nonlinearities from the valve characteristics are generally be added to the system. Especially in the low-pressure system, friction parameters of Coulomb and Stribeck can be demonstrated to enhance the overall accuracy of the system. For example, a nonlinear type of model is verified with all nonlinearities that are mentioned above [7]. Two types of controllers are developed which are nonlinear feedback controller and adaptive controller. Adaptive controller diverges from other types of controllers because it includes the adaptation to the system behavior even all parameters are not known. IT can be beneficial while simulating a currently used system without a mathematical model because some physical parameters cannot be taken out from the design of the actuator. Even for the adaptive controllers, system performance relies on the number of accurate parameters because any assumption for the parameter that is not known accurately brings instabilities.

Servosystems can be controlled by fully electrically instead of mechanical control. To perform such a control, a torque motor is to be developed. Current that is applied

to the torque motor is converted to a voltage signal for the input of the valve. This input can be processed either with a transfer function of PID controller that is eventually also a transfer function. Besides, a Linear Variable Displacement Transducer (LVDT) is to be modeled in order to convert the displacement of the cylinder to a electrical signal that creates a feedback for closed loop control. A PID type control with an LVDT is developed and simulated [8]. Outputs of the simulation are compared with the data of a Moog servo valve. Time responses are taken for step inputs. Pressure differences that allow movement of the cylinder is observed. It is concluded that nonlinear model of the servo valve is highly consistent with the experimental results of Moog servo valve under similar voltage ranges.

Considering a linear system design for a position tracking application in a three-dimensional surface [9], three different control methods are applied which are called Block Control, Sliding Mode Control and Integral Control. Block control method is developed for position tracking, sliding mode control method is applied to perform a stable control under chaotic sliding surfaces that can exhibit a different mode of frequency. Sliding mode controller responds the mod exchange of the input. Integral control method is applied to get rid of the disturbances coming from external sources. Results demonstrate that position control of the actuator is achieve. Furthermore, by using this linear model and three controller that are developed, force control can also be achieved.

To eliminate the effects of nonlinearities causes instabilities, several control methods are to be used instead of PID controller because in some cases classical PID control method does not demonstrate the desired result. In a classical servo hydraulic system developed for the position control, backstepping approach is used with feedback control system [10]. Backstepping is the method in which Lyapunov control function is determined within the feedback controller, and it guarantees the stability of the system by using a recursive design technique of the controller [11]. By using the backstepping method, error between the reference values is considerable reduced for transient conditions of position control. However, it is a more complicated method

compared to classical PID control and it is required to be simplified in order to be used in industrial applications especially for the system that required rapid responses.

On the other hand, classical PD control can be evaluated as adequate in multiple cases involving high speed systems in which the response time of the actuator is extremely low. For a designated hydraulic position control system with a single mass a PD regulation is applied to high-speed position control of the hydraulic actuator [12]. In this article, relation between control input voltage u and valve input x_v is represented via second order linear transfer function. For the hydraulic servo system, a third-order approach is applied, and it is fit to an experimental result to make system identification of the hydraulic servo system. After making the system identification, a PD controller is designed and implemented to the system as well as it is experimentally simulated. Performance of the system is adequate for the desired application and results of simulation and experiment are strictly correlated. PD controller can perform sufficiently with the reference velocity of 125 mm/s.

Another example of the combined force and position method is offered by Bobrow and Sohl [13]. In this article, a Lyapunov function is used to path tracking application of force and it is extended for the usage of position control. Servo dynamics are assumed to be linear and effects from torque motor are not included within the system. However; Spool dynamics, cylinder dynamics are included which are acting to a single mass. Proposed control method includes pressure, cylinder position, cylinder velocity, desired force, and actual force control in a combined way. By the developed model, dynamic and static friction characteristics of the hydraulic system are observed, and they are compared with experimental results. For the position tracking application, sinusoidal wave is given to the system and response of the cylinder is tracked. It can be extracted that proposed controller shows an adequate performance up to 6 Hz with a phase shift not exceeding the limits. However, cylinder output does not reach to peak amplitude of the reference signal after 8 Hz. It is a sign of the degradation in the performance of the system. Furthermore, peak value of the observed sign has deteriorations that are not observed in small frequencies. Besides, step response of the system with proposed controller is also

observed. Compared to classical proportional controller, responses for step inputs are quite accomplished in terms of reducing the shift between reference and actual output. Developed control method shows much more faster settling time $t_{settling}$ compared to proportional controller. In a path tracking case for 80 seconds, error values are compared for proposed controller and P controller. It is observed that tracking error in proposed controller is reduced to 10% of the tracking error of P controller.

Servo valve is a crucial component that is used to transform LVDT feedback signal into a control input for the MCV. Frequency range of the valve is to be higher than the MCV frequency range of over -3 dB. Several Moog servo valves are examined and compared in terms of their frequency ranges and phase lag degrees for inputs within a wide range of frequencies [14]. In this article, Moog servo valves from Series 30 to Series 35 are compared. As a result of this comparison, servo valves respond the reference of the output up to 30 Hz without any loss in the peak value of the reference. After 30 Hz, Series 30, 31 and 32 servo valves are exceeding the reference output signal. On the other hand, Series 34 and 35 are started to degrade in terms of reaching the peak value of output. Limit amplitude ratio for the response of the servo valves is selected generally as -3 dB. All servo valves demonstrate sufficient performance up to 80 Hz. Likewise, phase shift (□) of all servo valves are to be compared in the same frequency range from 5 Hz up to 500 Hz. Acceptable limit for the phase is generally selected as 45°. All servo valves demonstrate adequate performance up to 35 Hz inputs. However, comparing with amplitudes of each valve, Phase lag degree determines the boundary for performance. Based on another comparison that can be found in the article, similar conclusion can be evaluated for the Moog servo valves of Series 260, 261, 262, 263, 264 and 265.

For the rapid simulations of the hydraulic rams, Simscape Fluids® (previously Simhydraulic®) can be used in the with Simulink®. In a cylinder-ram simulation [15], Simhydraulic® tool is used to obtain displacement, velocity and force that is created by the actuator. Results of the simulation demonstrates that the hydraulic

actuator that is simulated in this article highly exhibits underdamped characteristics, which can result in severe increments of the force that is applied to the material in a hydraulic press application. To eliminate these overshoots from the underdamped characteristics of the actuator, a different fluid with lower Bulk modulus can be involved. By applying a force control method in software environment, applied force are decreased to acquire more overdamped ram.

While modeling and simulating hydraulic components especially for main control valve and cylinder-ram assembly, leakage is to be a significant parameter. Leakage occurs within the sliding seals of valve and cylinder. For the wide manufacturing tolerances that are applied for monetary reasons, operation of the system is to be sustained under high leakage rates without losing any force of rate but losing efficiency of the system. In a hydraulic servo control system that acts on a simple mass-spring-damper, leakage is considered for main control valve and hydraulic actuator separately [16]. In this article, torque motor is considered as a first order differential equation while servo valve dynamics are considered as a second order differential equation. Flow schematic of the hydraulic valve is developed including the leakage rates for the closed ports. Leakage rates are bounded to spool position that slides inside sleeve. Cylinder external leakage rates are defined with a leakage coefficient that is linearly bounded to the pressure of each chamber. Internal leakage between chamber A and chamber B has also its own leakage coefficient and internal leakage is bounded to pressure difference between the chambers rather than the individual pressure of each chamber. LuGre friction model is implemented within the system that computes friction force acting the linear cylinder by its varying velocity. A Fuzzy Logic type controller (FLC) is designed, and it is compared with classical P, PD and PID controllers. It is observed that FLC demonstrates a greater performance in terms of error value that is calculated for trajectory tracking applications, while P controller demonstrates the worst performance among all actuators.

Working with linear systems are easier to implement controller based on modern control applications because it is convenient to observe internal states and design the

controller regarding that manner. In a simulation and control application [17], a servo hydraulic system is modeled and identified. System modeling includes pressure-flow equations, continuity equation, pressure-load equations, linear friction model. Servo valve is assumed as a second order differential equation. Moog G671 series servo valve is used to perform such control application as the given current-flow transfer function is obtained as a first order linear system. As a result of them, overall transfer function between servo valve input and cylinder output is obtained. System identification is performed adding a PID controller and selecting the constants to obtain experimental results accurately. After system identification, a novel method of linearization is proposed which is called Exact Linearization Theory. This theory is used to implement a Sliding Mode Control application for the position control of hydraulic servo system. Using state feedback, controller is developed, and necessary simulations are performed.

Hydraulic test benches have great significance as the design of each component, valves, cylinder assemblies, loading systems and developed controller are implemented to testing environment for the verification and validation of the control system. In aircraft applications, testing systems are also very important for the simulation of aerodynamics loads and disturbances that air vehicle experience during its flight profile. A test rig is developed for the simulation of an aircraft actuator involving both hydraulic servo control system and external loading system [18]. External loading system has its own independent servo valve and force gage to control the applied force at the tip of the FCA. For the modeling of the loading system, a fifth order transfer function is considered likewise for flight actuator. For the servo valve, a second order linear system is considered. Models of each component are put into Simulink® environment. Loading system is designed to make a force control on the actuator. Thus, three different types of controllers are designed which are PI, PI feedforward and Fuzzy PI feedforward. It is concluded that Fuzzy PI feedforward demonstrates a god performance in terms of eliminating disturbances of the cylinder output position which cause instabilities in the applied forces.

For the real-time simulations of servo hydraulic systems, several realistic methods are developed. One the methods is called Hardware-In-Loop (HIL) method [19]. This method tends to be brought more realistic results compared to pure simulations because it is required to add a real component for processing electrical data. In this article, a first order mass-spring-damper system is actuated, and position control of the hydraulic actuator is performed. Servo dynamics are represented with a second order linear equation and other parameters are physically represented. Results are inspected for step inputs with different internal leakage parameters of the cylinder. Force tends to be higher while using a higher resistant internal leakage coefficient. It is stated that the model can simulate the system behavior using HIL plant.

1.3 Ingredients of Thesis

Content of thesis can be given in three main parts. In main purpose part, fundamental target of this research is described in terms of what is targeted to be achieved, function of the method and techniques that are mentioned and inspected. In outline part, main concerns of each chapter are described shortly. After that, Methods and tools that are used in the thesis are given.

1.3.1 Main Purpose

Main purpose of this thesis research can be divided into three main purposes. Initial purpose is to comprehend fundamental control system of a helicopter main rotor powered with a hydraulic power system and controlled using hydraulically powered flight control actuators and executing a system identification to obtain internal parameters and states of designed control system to express them in a mathematical model. Second purpose is to verify hydraulic control system of the helicopter using a test setup that reflects exact scale of the helicopter main rotor control system. The last purpose is to propose a new control system that improves overall performance

of the main rotor control using identified system parameters as input parameters for controller.

Comprehension of helicopter hydraulic control system is achieved through mathematical model of the control system. Mathematical model includes hydraulically powered servo actuator that is described as Flight Control Actuator, Kinematic model between input levers control system that can be controlled manually by pilot and automatically by flight computer, Force distribution model that calculates tilting angles of SSP. As far as pitch angle of each rotor blade is determined independently by SSP, compound forces are calculated for each FCA and distributed them considering tilting angles. It is complicated to implement rotor system including all details. Therefore, whole rotor system is reduced to a 2 Degrees of Freedom mass-spring-damper model. Coefficients are taken as equivalent dynamic coefficients. Mathematical model of rotor system is included as target system that takes forces from hydraulic control system.

After gathering complete theoretical mathematical of control system, it is required to verify and validate theoretical model by using a test setup. Features of test setup is designated, and it is developed to validate mathematical model. Test setup has a strong infrastructure that allows axial application of any load on FCAs independently by using ELAs. Besides, it is also allowed to give control inputs for each FCA by using PIAs. Tests are determined and executed, and data is collected. Executed tests are simulated by using mathematical model and results are compared. Based on these results, mathematical model is verified, and it is assessed that mathematical model can be used for further applications such as improvement of the control system by manipulating system parameters and designing a control system.

Proving the mathematical model by using a test setup allows usage of mathematical model for designing and developing a control system. Thus, classical P and PI controllers are designed to get better performance in terms of rise time and peak value of the response. Design of P and PI controllers are achieved by implementing a Swashplate Control Actuator that improves stability of SSP and operate by the

principle of position feedback. Additionally, a 2-mass position control method is introduced to improve stability of the control system, improve frequency band, decrease amplitude of the response, and increase peak frequency of the control system.

1.3.2 Outline

Thesis includes four chapters except the current one. It is explained what is included by each chapter as follows;

In Chapter 2, Mathematical model of all included systems are mentioned. Derivation of mathematical model starts with explanation of kinematic model between control inputs of pilot and automatic control system between FCAs and SSP position. After that, force distributions based on the position of SSP is derived. Next, linear system dynamics of 1-Mass FCA is developed as open-loop and closed-loop system. Transfer functions and Bode diagram of developed system is provided. Next, 3-Mass equivalent dynamics of combined rotor and FCA system is developed as open-loop and closed loop. Design parameters and assumptions that are made to decrease complexity of system are explained. Finally, nonlinear dynamic relationship between actuator and rotor systems are derived. Nonlinear derivation is used instead of linear derivations because it is easier to observe system states and design a control system using nonlinear system. Note that dynamic characteristics of both linear and nonlinear system are found and compared in terms of compatibility between derivations.

In Chapter 3, Experimental test setup is described, and properties of test setup are explained. Schematic representation of test setup, properties of components that are used in the setup, configurations of executed tests and detailed results of each executed test are provided. As far as main purpose for construction of test setup is to verify and validate mathematical model, comparison between both linear and nonlinear system is performed to observe if mathematical model is correctly derived.

At the end of this chapter, a compatibility assessment between test results and developed models is provided.

In chapter 4, a novel control system is proposed for overall performance enhancement of the hydraulic control system. As far as 3 Degrees of Freedom system is more complicated, a reduction is performed from 3 Degrees of Freedom into 2 Degrees of Freedom. Then, proposed novel system of Swashplate Control Actuator (SCA) is introduced. Stability actuator that has already been installed on the helicopter is introduced and the cooperation between SCA is explained by designing an internal mechanism. Two different controllers are proposed which are classical PID controller and 2-Mass controller. Although classical control included PID terms, differential gain is kept at zero because it is evaluated as unnecessary. Thus, P and PI controllers are designed. After that, a 2-Mass control system is developed. By using these control systems, rise time of control system is decreased as well as frequency band is increased. Besides, amplitude of resonant response is significantly decreased, and resonant frequency is increased to rarer frequencies.

In Chapter 5, main conclusions are provided and recommendations upon future work are shared.

While obtaining mathematical model, MATLAB® is used for linear systems and Simulink® is used for nonlinear systems. For data processing, both programs are extendedly used.

CHAPTER 2

MATHEMATICAL MODELING

Physical system can be inspected and modeled by four different parts. Initially, kinematic model of the SSP in terms of displacements of three different FCAs is obtained. Acquirement of the kinematic model starts from pilot input lever displacements to the end of displacements of all cylinders including the geometric parameters of the SSP. Hydraulic actuator that includes several components are modeled as the second part. Hydraulic valve parameters, cylinder parameters and fluid parameters are the most crucial parameters that are to be selected for having a properly operating system. Third, Rotor assembly is considered in different degrees of freedom integrated within the bodies of hydraulic actuator. Four degrees of freedom system is considered in which the masses are selected as Blades, Swashplate Assembly, Piston-Rod Assembly and Actuator Body. Finally, angle and force calculation is executed and aerodynamic loads are calculated by using pitch angles of Rotor Blades. Additional to the aerodynamic loads, disturbances are also given to the blades as forces. The most greatest advantage of modeling all masses seperately, inertial effects are included within the analysis. Including inertial effects brings more realistic system, physically. Four main steps of obtaining the mathematical model are explained [4].

2.1 Kinematic Relationships Between FCAs and SSP

Installation of the FCAs ae selected as separated by 120° as explained in 1.1.3. Phasing between FCAs are considered for kinematic relationship. Based on this installation principle, fundamental geometric definitions are to be made to comprehend control mechanism of blades pitch angles although these geometric definitions are design selections. In the very end of this part, design parameters are

converted to constant parameters and it is demonstrated that they influence mechanism just as constant ratios. Fundamental dimensions of design parameters are demonstrated in Figure 2.1.

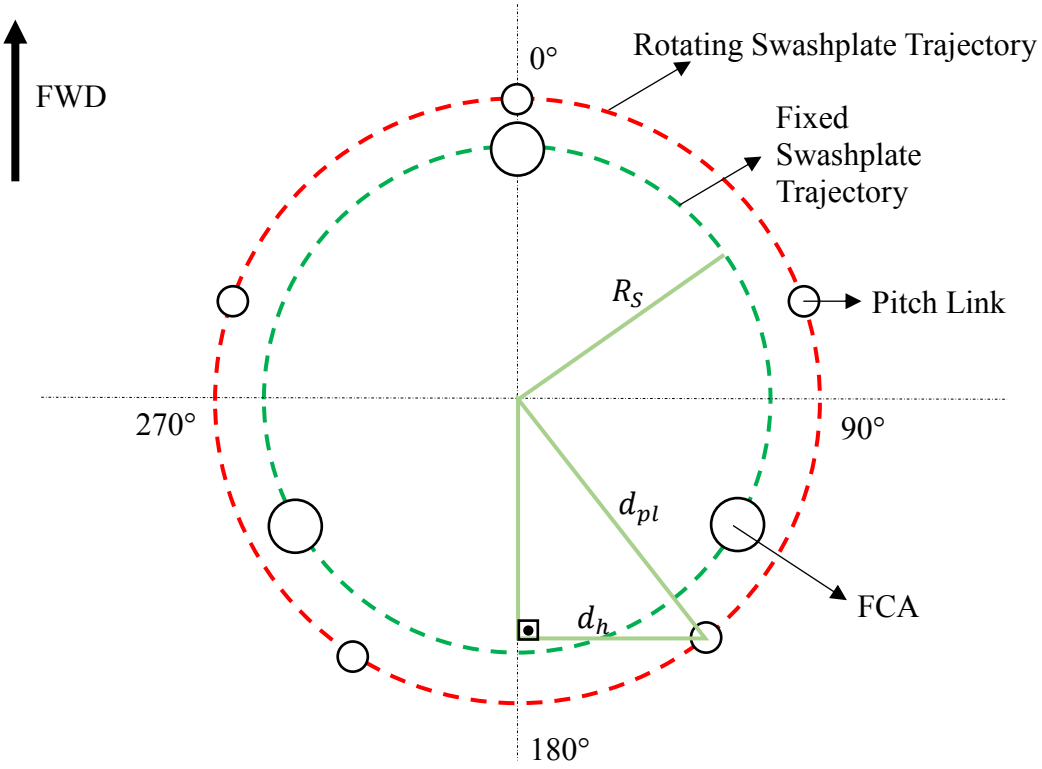

Figure 2.1 Fundamental Dimensions or Rotor Blade Pitch Angle Mechanical Control

Radial distance of any pitch link to rotor mast axis is represented by d_{pl} and it is a design parameter. Hinge length is defined as the minimum distance between pitch link and vertical control axis while Hinge length is perpendicular with vertical control axis because the angle between d_{pl} and hinge length is a constant designed angle. Hinge length is demonstrated by d_h throughout derivations. Rotation of Rotating Swashplate is Clockwise. Thus, initial pitch link on the right side of vertical control axis is to be considered while observing d_h. Note that it is not required to provide perpendicularity of hinge and 0° pitch link angle at the same time, but it is given in the condition represented by Figure 2.1.

For the given pilot input, actuator displacements and their rates are found. Defining the displacements of Forward, Left and Right FCAs as D_1, D_2 and D_3 respectively, yields following equations, in which inverse kinematic relationship provides displacements. Note that axial perpendicularities of any FCA to the helicopter upper deck is considered to be always 90° currently, without any change as it extends of retracts.

$$d_1 = \lambda_1 - R_S sin(\alpha) \tag{2.1}$$

$$d_2 = \lambda_1 + R_S sin\left(\frac{\pi}{3}\right)\sin(\beta) + R_S cos\left(\frac{\pi}{3}\right)\sin(\alpha) \tag{2.2}$$

$$d_3 = \lambda_1 - R_S sin\left(\frac{\pi}{3}\right)\sin(\beta) + R_S cos\left(\frac{\pi}{3}\right)\sin(\alpha) \tag{2.3}$$

Derivatives of these relationship are taken to obtain the velocities of each FCAs, which is as follows;

$$\dot{d}_1 = \dot{\lambda}_1 - R_S cos(\alpha)\dot{\alpha} \tag{2.4}$$

$$\dot{d}_2 = \dot{\lambda}_1 + R_S sin\left(\frac{\pi}{3}\right) cos(\beta)\dot{\beta} + R_S cos\left(\frac{\pi}{3}\right) cos(\alpha)\dot{\alpha} \tag{2.5}$$

$$\dot{d}_3 = \dot{\lambda}_1 - R_S sin\left(\frac{\pi}{3}\right) cos(\beta)\dot{\beta} + R_S cos\left(\frac{\pi}{3}\right) cos(\alpha)\dot{\alpha} \tag{2.6}$$

All input levers have its own Initial Bell Crank (IBC) which is the initial bell crank to which last rod of the rotor control mechanism end is connected directly. There is a relationship between the angle of each IBC and controlled angle/position of SSP. These angles are determined for COL, LON and LAT as ω_{COL}, ω_{LON} and ω_{LAT}; respectively. Based on these definitions, IBC angles can be gathered as;

$$\omega_{COL} = \arcsin\left({\lambda_1}/{d_h}\right) \tag{2.7}$$

$$\omega_{LON} = \arcsin\left({d_{pl}\sin(\alpha)}/{d_h}\right) \tag{2.8}$$

$$\omega_{LAT} = \arcsin\left({d_{pl}\sin(\beta)}/{d_h}\right) \tag{2.9}$$

Taking sin function of each side extracting out λ_1, α, β and gives that;

$$\lambda_1 = d_h \sin(\omega_{COL}) \tag{2.10}$$

$$\sin(\alpha) = \frac{d_h \sin(\omega_{LON})}{d_{pl}} \tag{2.11}$$

$$\sin(\beta) = \frac{d_h \sin(\omega_{LAT})}{d_{pl}} \tag{2.12}$$

Taking derivatives of the controlled angle/displacement, gives the rate of change in terms of IBC angle as follows;

$$\dot{\lambda}_1 = d_h \dot{\omega}_{COL} \cos(\omega_{COL}) \tag{2.13}$$

$$\cos(\alpha)\,\dot{\alpha} = \frac{d_h \dot{\omega}_{LON} \cos(\omega_{LON})}{d_{pl}} \tag{2.14}$$

$$\cos(\beta)\,\dot{\beta} = \frac{d_h \dot{\omega}_{LAT} \cos(\omega_{LAT})}{d_{pl}} \tag{2.15}$$

Using derivations from (2.9) to (2.15), cylinder velocities can be obtained directly in terms of IBC angles and their rates, as given between (2.16) and (2.18).

$$\dot{d}_1 = d_h \dot{\omega}_{COL} \cos(\omega_{COL}) - R_S \frac{d_h \dot{\omega}_{LON} \cos(\omega_{LON})}{d_{pl}} \tag{2.16}$$

$$\dot{d}_2 = d_h \dot{\omega}_{COL} \cos(\omega_{COL}) + R_S sin\left({}^{\pi}/_{3}\right) \frac{d_h \dot{\omega}_{LAT} \cos(\omega_{LAT})}{d_{pl}} + R_S cos\left({}^{\pi}/_{3}\right) \frac{d_h \dot{\omega}_{LON} \cos(\omega_{LON})}{d_{pl}} \tag{2.17}$$

$$\dot{d}_3 = d_h \dot{\omega}_{COL} \cos(\omega_{COL}) - R_S sin\left(\frac{\pi}{3}\right) \frac{d_h \dot{\omega}_{LAT} \cos(\omega_{LAT})}{d_{pl}} + R_S cos\left(\frac{\pi}{3}\right) \frac{d_h \dot{\omega}_{LON} \cos(\omega_{LON})}{d_{pl}} \tag{2.18}$$

Additionally, relation between IBC angles and pilot input ranges is to be obtained to finalize the connection between all input lever ranges and cylinder displacements. Thus, it is provided as following by defining stick mechanism lengths of $x_{SL,LON}$, $x_{SL,LAT}$ and $x_{SL,COL}$ for ω_{LON}, ω_{LAT} and ω_{COL}; respectively. Note that small angle assumption is applicable as IBC angles are generally smaller than 5°.

$$sin(\omega_{COL}) = \tan(\omega_{COL}) = \omega_{COL} = {}^{x_1}/_{x_{SL,COL}} \tag{2.19}$$

$$sin(\omega_{LON}) = \tan(\omega_{LON}) = \omega_{LON} = {}^{y_1}/_{x_{SL,LON}} \tag{2.20}$$

$$sin(\omega_{LAT}) = \tan(\omega_{LAT}) = \omega_{LAT} = {}^{y_2}/_{x_{SL,LAT}} \tag{2.21}$$

Using derivations of (2.19), (2.20) and (2.21); relation with rates of the pilot inputs can be found as follows;

$$\dot{\omega}_{COL} = {}^{\dot{x}_1}/_{x_{SL,COL}} \tag{2.22}$$

$$\dot{\omega}_{LON} = {}^{\dot{y}_1}/_{x_{SL,LON}} \tag{2.23}$$

$$\dot{\omega}_{LAT} = {}^{\dot{y}_2}/_{x_{SL,LAT}} \tag{2.24}$$

Putting the derivations from (2.19) to (2.24) into (2.1) to (2.3), relation between pilot input positions and cylinder displacements that can be found as follows;

$$d_1 = \frac{d_h}{x_{SL,COL}} x_1 - \frac{R_S d_h}{d_{pl} x_{SL,LON}} y_1 \tag{2.25}$$

$$d_2 = \frac{d_h}{x_{SL,COL}} x_1 + \frac{R_S sin\left(\frac{\pi}{3}\right) d_h}{d_{pl} x_{SL,LAT}} y_2 + \frac{R_S cos\left(\frac{\pi}{3}\right) d_h}{d_{pl} x_{SL,LON}} y_1 \tag{2.26}$$

$$d_3 = \frac{d_h}{x_{SL,COL}} x_1 - \frac{R_S sin\left(\frac{\pi}{3}\right) d_h}{d_{pl} x_{SL,LAT}} y_2 + \frac{R_S cos\left(\frac{\pi}{3}\right) d_h}{d_{pl} x_{SL,LON}} y_1 \tag{2.27}$$

Putting the derivations from (2.19) to (2.24) into (2.16) to (2.18), relation between pilot input rates and cylinder velocities can be found as follows;

$$\dot{d}_1 = \frac{d_h \cos\left(\frac{x_1}{x_{SL,COL}}\right)}{x_{SL,COL}} \dot{x}_1 - \frac{R_S d_h \cos\left(\frac{y_1}{x_{SL,LON}}\right)}{d_{pl} x_{SL,LON}} \dot{y}_1 \tag{2.28}$$

$$\dot{d}_2 = \frac{d_h \cos\left(\frac{x_1}{x_{SL,COL}}\right)}{x_{SL,COL}} \dot{x}_1 + \frac{R_S sin\left(\frac{\pi}{3}\right) d_h \cos\left(\frac{y_2}{x_{SL,LAT}}\right)}{d_{pl} x_{SL,LAT}} \dot{y}_2 + \frac{R_S cos\left(\frac{\pi}{3}\right) d_h \cos\left(\frac{y_1}{x_{SL,LON}}\right)}{d_{pl} x_{SL,LON}} \dot{y}_1 \tag{2.29}$$

$$\dot{d}_3 = \frac{d_h \cos\left(\frac{x_1}{x_{SL,COL}}\right)}{x_{SL,COL}}\dot{x}_1 - \frac{R_S sin\left(\frac{\pi}{3}\right) d_h \cos\left(\frac{y_2}{x_{SL,LAT}}\right)}{d_{pl} x_{SL,LAT}}\dot{y}_2 + \frac{R_S cos\left(\frac{\pi}{3}\right) d_h \cos\left(\frac{y_1}{x_{SL,LON}}\right)}{d_{pl} x_{SL,LON}}\dot{y}_1 \quad (2.30)$$

In the end of these derivations, relation between pilot inputs and cylinder displacement/rate is obtained. For the comprehension of them and using in a linear control application, they are written in a transformation matrix form. Initially, displacement matrix of all FCAs is obtained as follows;

$$\begin{bmatrix} d_1 \\ d_2 \\ d_3 \end{bmatrix} = \begin{bmatrix} \frac{d_h}{x_{SL,COL}} & -\frac{R_S d_h}{d_{pl} x_{SL,LON}} & 0 \\ \frac{d_h}{x_{SL,COL}} & \frac{R_S cos\left(\frac{\pi}{3}\right) d_h}{d_{pl} x_{SL,LON}} & \frac{R_S sin\left(\frac{\pi}{3}\right) d_h}{d_{pl} x_{SL,LAT}} \\ \frac{d_h}{x_{SL,COL}} & \frac{R_S cos\left(\frac{\pi}{3}\right) d_h}{d_{pl} x_{SL,LON}} & -\frac{R_S sin\left(\frac{\pi}{3}\right) d_h}{d_{pl} x_{SL,LAT}} \end{bmatrix} \begin{bmatrix} x_1 \\ y_1 \\ y_2 \end{bmatrix} \quad (2.31)$$

Similarly, rates of FCAs are obtained in a velocity transformation matrix in terms of pilot input rates can be obtained. Before obtaining transformation matrix, definitions that are given below are proposed for simplification. Simplification parameters are given as;

$$C_{x1} = \frac{d_h \cos\left(\frac{x_1}{x_{SL,COL}}\right)}{x_{SL,COL}} \quad (2.32)$$

$$C_{y1} = \frac{d_h \cos\left(\frac{y_1}{x_{SL,LON}}\right)}{d_{pl} x_{SL,LON}} \quad (2.33)$$

$$C_{y2} = \frac{d_h \cos\left(\frac{y_2}{x_{SL,LAT}}\right)}{d_{pl} x_{SL,LAT}} \quad (2.34)$$

Thanks to these simplification parameters, rate transformation matrix can be obtained as;

$$\begin{bmatrix} \dot{d}_1 \\ \dot{d}_2 \\ \dot{d}_3 \end{bmatrix} = \begin{bmatrix} C_{x1} & -R_S C_{y1} & 0 \\ C_{x1} & \frac{R_S C_{y1}}{2} & \frac{\sqrt{3} R_S C_{y2}}{2} \\ C_{x1} & \frac{R_S C_{y1}}{2} & -\frac{\sqrt{3} R_S C_{y2}}{2} \end{bmatrix} \begin{bmatrix} \dot{x}_1 \\ \dot{y}_1 \\ \dot{y}_2 \end{bmatrix} \tag{2.35}$$

2.2 Linear System Dynamics of Single FCA

Linear system repesentation of a FCA is to be obtained in order apply control methods and observe the effect of state parameters. Due to the nonlinear characteristic of the MCV, linearization is to be performed on the valve dynamic equation. Linearization is made based on Taylor Series exansion principle.

2.2.1 Linearization of Valve Using Taylor Series Expansion

Main Control Valve (MCV) has a highly nonlinear characteristic because of the square root term inside the equations. Operating with dynamic pressure variations and considerably high pressure regimes results in increases of valve sensitivity. For that reason, linearized valve equations in a vicinity of common operating point allows to mexecute linear analysis. Besides, linearization is required to obtain linear model of the complete actuation system. To make such linearization of the valve dynamics, Taylor Series expansion method is used. For a flow equation with two unknowns of node pressure P_1 and valve width x_v, flow equation can be found as follows;

$$Q_1(x_v, P_1) = C_D x_v H \sqrt{\frac{2}{\rho}(P_S - P_1)} \tag{2.36}$$

For (2.36), Taylor's Series expansion [21] can be applied. Assuming that $\varphi = Q_1(x_v, P_1)$ as the Taylor's Series function, expansion about vicinity point of x_v^0 and P_1^0 gives the following.

$$\varphi = Q_1(x_v^0, P_1^0) + (x_v - x_v^0)\frac{\partial \varphi}{\partial x_v} + (P_1 - P_1^0)\frac{\partial \varphi}{\partial P_1} + O(2) \tag{2.37}$$

Higher order terms of Taylor's Series are neglected. As given in the Merritt [22], (2.37) can be rewritten as follows;

$$Q_1 = Q_1(x_v^0, P_1^0) + \frac{\partial \varphi}{\partial x_v}\Big|_{x_v^0}(x_v - x_v^0) + \frac{\partial \varphi}{\partial P_1}\Big|_{P_1^0}(P_1 - P_1^0) \tag{2.38}$$

Where;

$$\frac{\partial \varphi}{\partial x_v} = C_D H\sqrt{\frac{2}{\rho}(P_1 - P_R)} \tag{2.39}$$

$$\frac{\partial \varphi}{\partial P_1} = C_D A_v \frac{1}{\sqrt{2\rho(P_S - P_1^0)}} \tag{2.40}$$

Vicinity point can be selected as $(10^{-3}, \frac{P_S + P_R}{2})$ for simplicity. Thus, considering the sign convention, flow equation becomes as follows by taking coefficient of valve flow as K_{vf} and coefficient of pressure as K_{pf}, which are simplified as follows. Note that P_B is selected from high pressure source to chamber and P_A is selected from chamber to low pressure.

$$Q_1(x_v, P_B) = C_D H\sqrt{\frac{P_S - P_B^0}{\rho}}x_v - C_D A_v \frac{1}{\sqrt{\rho(P_S - P_B^0)}}P_B \tag{2.41}$$

$$Q_1(x_v, P_B) = K_{vfb}x_v - K_{pfb}P_B \tag{2.42}$$

$$Q_2(x_v, P_A) = C_D H\sqrt{\frac{P_S - P_A^0}{\rho}}x_v + C_D A_v \frac{1}{\sqrt{\rho(P_A^0 - P_R)}}P_A \tag{2.43}$$

$$Q_2(x_v, P_A) = K_{vfa}x_v + K_{pfa}P_A \tag{2.44}$$

2.2.2 Open-loop Linear Model of Single FCA

Open-loop model of a single FCA includes linearized valve dynamics, cylinder dynamics and first order mass-spring-damper system to track the displacement and velocity outputs of the linear system. For the representation of open-loop system, Inlet pressure of P_S, outlet tank pressure of P_R, chamber pressures of P_A and P_B are defined. Between two chambers of the cylinder; structural elasticity of the cylinder ($\alpha_{P,St}$), bulk modulus of the hydraulic oil (E_v) and leakage between the chambers of the cylinder (R) is assumed. Physical representation of linearly derived model is given in Figure 2.2.

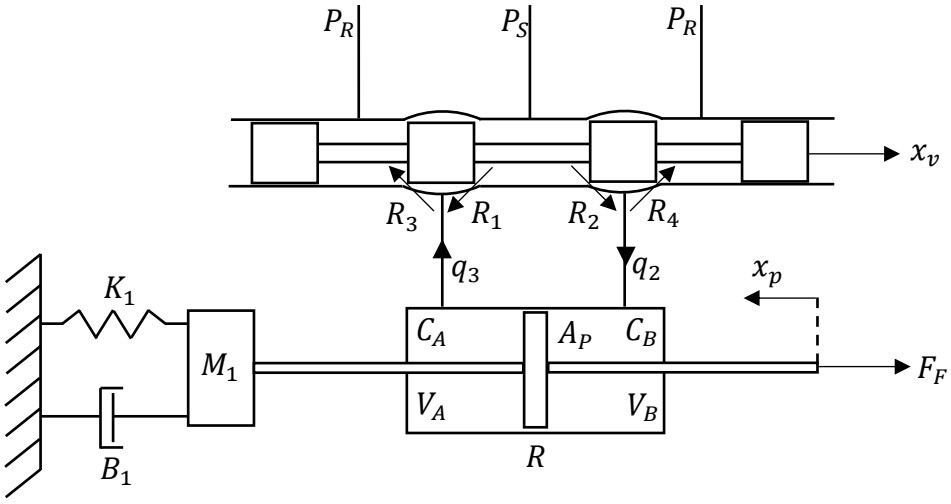

Figure 2.2 Open Loop 1-Mass Linear System

Note that R_1, R_2, R_3 and R_4 represents the linearized valve resistance corresponding to valve orifice area. Depending on the sign of x_v, either R_1 and R_4 or R_2 and R_3 are active while other pair does not have any effect on the linear system at that moment. For example; if sign of x_v is greater than 0, R_2 and R_3 are active while R_1 and R_4 are not active. Linear graph method is used for acquisition of the linear model. Considering that the valve is critically lapped and x_v is a positive value, Linear Graph representation of the model is given in Figure 2.3.

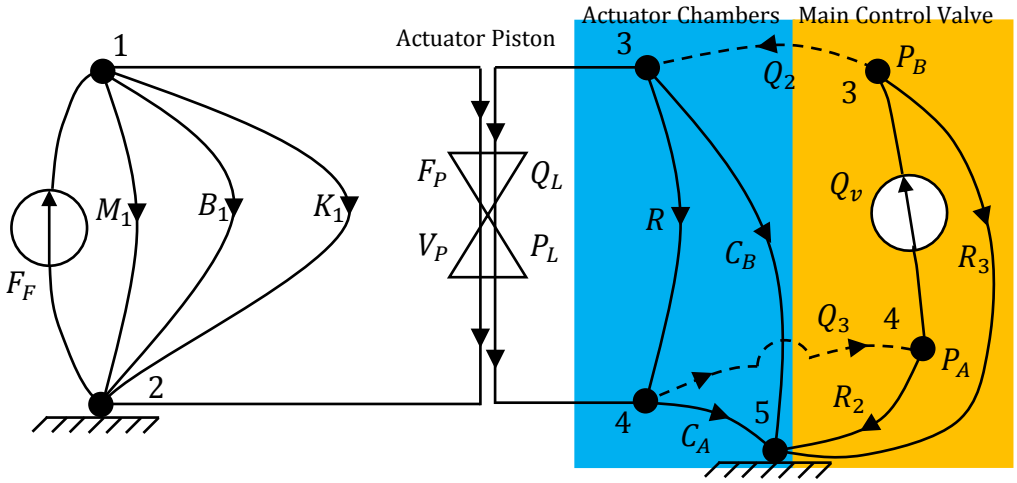

Figure 2.3 Linear Graph of Open Loop Single Mass System

In Figure 2.3, hydraulic valve section is demonstrated as linear system instead of a physical system to understand better. Hydraulic valve is represented based on (2.41) and (2.43). As seen in Figure 2.3, the valve in not an ideal source but have two loss terms R_2 and R_3. Considering that manner, properties of the Linear Graph is provided in Table 2.1.

Table 2.1 Properties of Linear Graph of Open Loop Linear Representation

Linear Graph Property	# of the Property in Linear Graph
Branches (B)	12
Nodes (N)	5
Across Sources (S_A)	0
Through Sources (S_T)	2
Nodes in Normal Tree ($N - N_D$)	4
Variables ($2B$)	24

Considering the properties of Linear Graph, Normal Tree can be obtained as given in Figure 2.4.

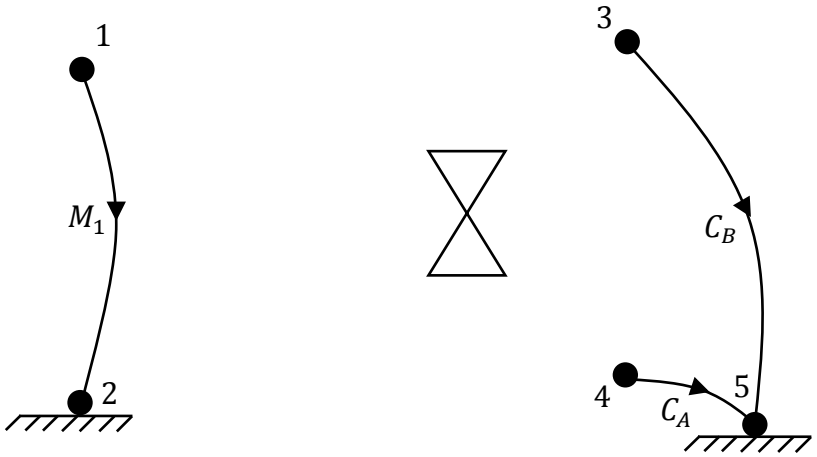

Figure 2.4 Normal Tree of 1-Mass Open Loop System

Primary and secondary variables are selected based on the method defined in [23],[24]. Thus, across variables on the normal tree and through variables on the link are taken as primary variables. Other variables are selected as secondary variables. All primary and secondary variables are provided in Table 2.2.

Table 2.2 Primary and Secondary Variables of Open Loop System

Primary Var.	Q_v ,P_A, P_B, V_{M1}, F_{B1}, F_{K1}, F_P, Q_L, F_F, Q_R, Q_{R2}, Q_{R3},
Secondary Var.	P_v ,Q_A, Q_B F_{M1}, V_{B1}, V_{K1}, V_P, P_L, V_F, P_R, P_{R2}, P_{R3},

After finding primary and across variables, it is required to determine the state variables of the linear system, which can be determined by taking across type variables on the tree and through type variables on the link. Thus, four states are coming from tree and link which are F_{K1}, V_{M1}, P_A and P_B. Thus, open loop has three state variables. Number of unknowns, elemental equations, continuity equations and compatibility equations are found with equations from (2.45) to (2.48), respectively;

$$2(B-S) = 2(12-2) = 20 \tag{2.45}$$

$$B - S = 12 - 2 = 10 \tag{2.46}$$

$$N - N_D - S_A = 5 - 2 - 0 = 3 \tag{2.47}$$

$$B - (N - N_D) - S_T = 12 - 4 - 1 = 7 \tag{2.48}$$

Elemental equations are given as follows;

$$\dot{V}_{M1} = \frac{1}{M_1} F_{M1} \tag{2.49}$$

$$\dot{F}_{K1} = K_1 V_{K1} \tag{2.50}$$

$$\dot{P}_A = \frac{1}{C_A} Q_A \tag{2.51}$$

$$\dot{P}_B = \frac{1}{C_B} Q_B \tag{2.52}$$

$$F_{B1} = B_1 V_{B1} \tag{2.53}$$

$$F_P = A_P P_L \tag{2.54}$$

$$Q_L = -A_P V_P \tag{2.55}$$

$$Q_R = \frac{1}{R} P_R \tag{2.56}$$

$$Q_{R2} = \frac{1}{R_2} P_{R2} \tag{2.57}$$

$$Q_{R3} = \frac{1}{R_3} P_{R3} \tag{2.58}$$

Note that Q_{R2} and Q_{R3} are written referring to the derivation that is made in (2.42) and (2.44), using steady state variation of the pressure with respect to linearized point and taking $R_2 = {}^1/_{K_{pfa}}$, $R_3 = {}^1/_{K_{pfb}}$; continuity equations are given as follows;

$$F_{M1} = F_F - F_{B1} - F_{K1} - F_P \tag{2.59}$$

$$Q_A = Q_L + Q_R - Q_{R3} - Q_v \tag{2.60}$$

$$Q_B = -Q_L - Q_R + Q_{R2} + Q_v \tag{2.61}$$

Where Q_v is the flow source which is defined in (2.42) and (2.44) as$Q_v = K_{vf} x_v$. Compatibility equations are given as follows;

$$V_{K1} = V_{M1} \tag{2.62}$$

$$V_{B1} = V_{M1} \tag{2.63}$$

$$P_L = P_A - P_B \tag{2.64}$$

$$V_P = V_{M1} \tag{2.65}$$

$$P_R = P_B - P_A \tag{2.66}$$

$$P_{R2} = -P_B \tag{2.67}$$

$$P_{R3} = P_A \tag{2.68}$$

Initial definition for the state equations is obtained as follows, regarding the derivations that are made above.

$$\dot{F}_{K1} = K_1 V_{K1} = K_1 V_{M1} \tag{2.69}$$

$$\dot{V}_{M1} = \frac{1}{M_1} F_{M1} = \frac{1}{M_1}(F_F - F_{B1} - F_{K1} - F_P) \tag{2.70}$$

From (2.70), 2nd state equation can be found in (2.71), as the 1st state equation have already been found in (2.69).

$$\dot{V}_{M1} = \frac{1}{M_1}(F_F - B_1 V_{M1} - F_{K1} - A_P P_L) \tag{2.71}$$

Following equation (2.72) are derived to obtain the 3rd state equation.

$$\dot{P}_A = \frac{1}{C_A} Q_A = \frac{1}{C_A}(Q_L + Q_R - Q_{R3} - Q_v) \tag{…}$$

$$\dot{P}_A = \frac{1}{C_A}\left(A_P V_P + \frac{1}{R} P_R - K_{vfa} x_v - K_{pfa} P_{R3}\right) \tag{…}$$

$$\dot{P}_A = \frac{1}{C_A}\left(A_P V_{M1} + \frac{1}{R}(P_B - P_A) - K_{vfa} x_v - K_{pfa} P_A\right) \tag{2.72}$$

Finally, following equation (2.73) are derived to obtain the 4th state equation.

$$\dot{P}_B = \frac{1}{C_B} Q_B = \frac{1}{C_B}(-Q_L - Q_R + Q_{R2} + Q_v) \tag{…}$$

$$\dot{P}_B = \frac{1}{C_B}\left(-A_P V_{M1} - \frac{1}{R}(P_B - P_A) + K_{vfb} x_v - K_{pfb} P_{R2}\right) \tag{…}$$

$$\dot{P}_B = \frac{1}{C_B}\left(-A_P V_{M1} + \frac{1}{R}(P_B - P_A) + K_{vfb} x_v + K_{pfb}(P_B)\right) \tag{2.73}$$

State-space representation derived from 4 states are given as follows;

$$\begin{bmatrix} \dot{F}_{K1} \\ \dot{V}_{M1} \\ \dot{P}_A \\ \dot{P}_B \end{bmatrix} = \begin{bmatrix} 0 & K_1 & 0 & 0 \\ \frac{-1}{M_1} & -\frac{B_1}{M_1} & -\frac{A_P}{M_1} & \frac{A_P}{M_1} \\ 0 & \frac{A_P}{C_A} & -\frac{(K_{pfa}R+1)}{RC_A} & \frac{1}{RC_A} \\ 0 & \frac{-A_P}{C_B} & \frac{-1}{RC_B} & \frac{(K_{pfb}R+1)}{RC_B} \end{bmatrix} \begin{bmatrix} F_{K1} \\ V_{M1} \\ P_A \\ P_B \end{bmatrix} + \begin{bmatrix} 0 & 0 \\ \frac{1}{M_1} & 0 \\ 0 & \frac{K_{vfa}}{C_A} \\ 0 & -\frac{K_{vfb}}{C_B} \end{bmatrix} \begin{bmatrix} F_F \\ x_v \end{bmatrix} \tag{2.74}$$

To obtain a simplified linear system as it is unnecessary to obtain pressure values of each chamber separately, pressure acting to acting cylinder is defined as P_C as P_A and P_B are dependent to same pressure states. Considering position of actuator at the middle under linearization, following definition of a new state is made. Also note that these are applicable in the following sections.

$$C_A = C_B = C \tag{2.75}$$

$$K_{vfa} = K_{vfb} = K_{vf}, K_{pfa} = K_{pfb} = K_{pf} \tag{2.76}$$

$$\dot{P}_C = \dot{P}_A - \dot{P}_B \tag{2.77}$$

Defined state can be found as follows as 3rd state equation itself;

$$\dot{P}_C = \dot{P}_A - \dot{P}_B = \frac{1}{C}\left(2A_P V_{M1} + \frac{2}{R}P_C + 2K_{vf}x_v - K_{pf}P_C\right) \tag{2.78}$$

Founded four state equations that are linearly bounded to state variables, are converted to state space form as follows;

$$\begin{bmatrix} \dot{F}_{K1} \\ \dot{V}_{M1} \\ \dot{P}_C \end{bmatrix} = \begin{bmatrix} 0 & K_1 & 0 \\ \frac{-1}{M_1} & -\frac{B_1}{M_1} & -\frac{A}{M_1} \\ 0 & \frac{2A_P}{C} & \frac{(2-K_{pf}R)}{RC} \end{bmatrix} \begin{bmatrix} F_{K1} \\ V_{M1} \\ P_C \end{bmatrix} + \begin{bmatrix} 0 & 0 \\ \frac{1}{M_1} & 0 \\ 0 & \frac{2K_{vf}}{C} \end{bmatrix} \begin{bmatrix} F_F \\ x_v \end{bmatrix} \tag{2.79}$$

As a result of all derivations, a state-space representation is obtained with state matrix and input matrix. Open loop system can be controlled by valve input x_v and external forces can be simulated by using F_F.

2.2.3 Transfer Functions of Open-Loop Model

Transfer functions of the open loop system can be found by using the commonly known method as it is described by Bequette [20]. This method can be applied for an obtained state-space method. Having 3 inputs and 3 state variables yields that there are 3 different transfer functions of the linear system. Among these transfer functions, one that demonstrates the bode plot representation that demonstrates the relationship between valve input and actuator output is obtained and given in Figure 2.5.

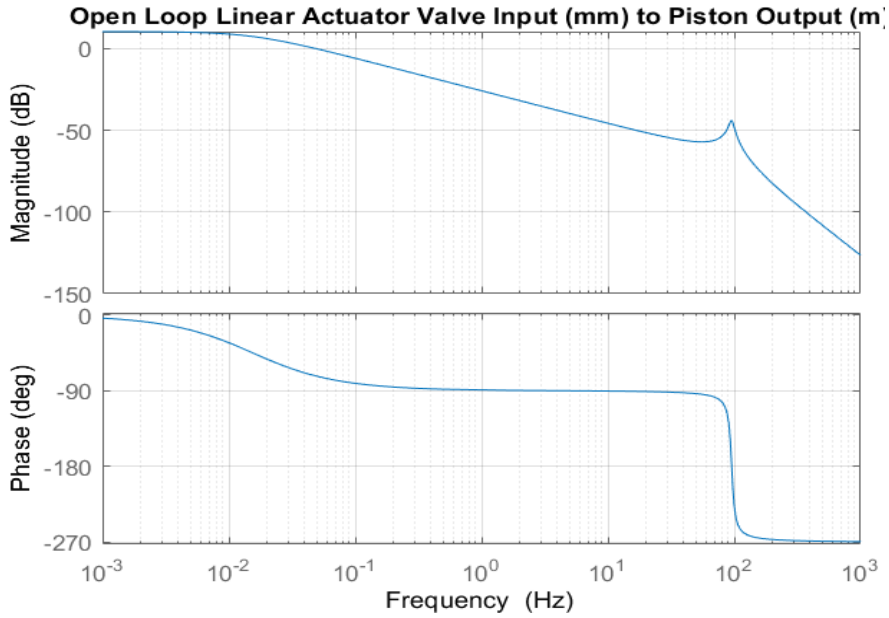

Figure 2.5 Bode Plot of Open Loop System - Valve Input and Cylinder Output

It is observed that system has a resonant frequency at 91 Hz. However, this level frequency is much higher compared to what pilot and servo valve and give to the system. Thus, 91 Hz resonant frequency does not have any drawback regarding system operation.

2.2.4 Closed Loop Linear Model of Single FCA

Closed loop model is derived to involve pilot input within the system by adding a simple feedback lever and actuating lever for summation of pilot input and cylinder output; thus, all derivations that are performed for open loop system are also applicable for closed loop system. Actuating lever is connected to 3 hinge points. Note that all connected points are movable instead of being stationary. First point is demonstrated with x_i that takes input from the last rod of input mechanism that starts moving with the input of pilot. Second point is demonstrated with x_v and it has already been defined as the pilot input. In state space representation, x_v will be replaced and automatically controlled without being able to manipulate. Third point is demonstrated with x_p and it is the output position of the cylinder that consist of a

basis of feedback control. Feedback lever is connected to cylinder output and end tip of the actuating lever. All locations of connection are provided in Figure 2.6.

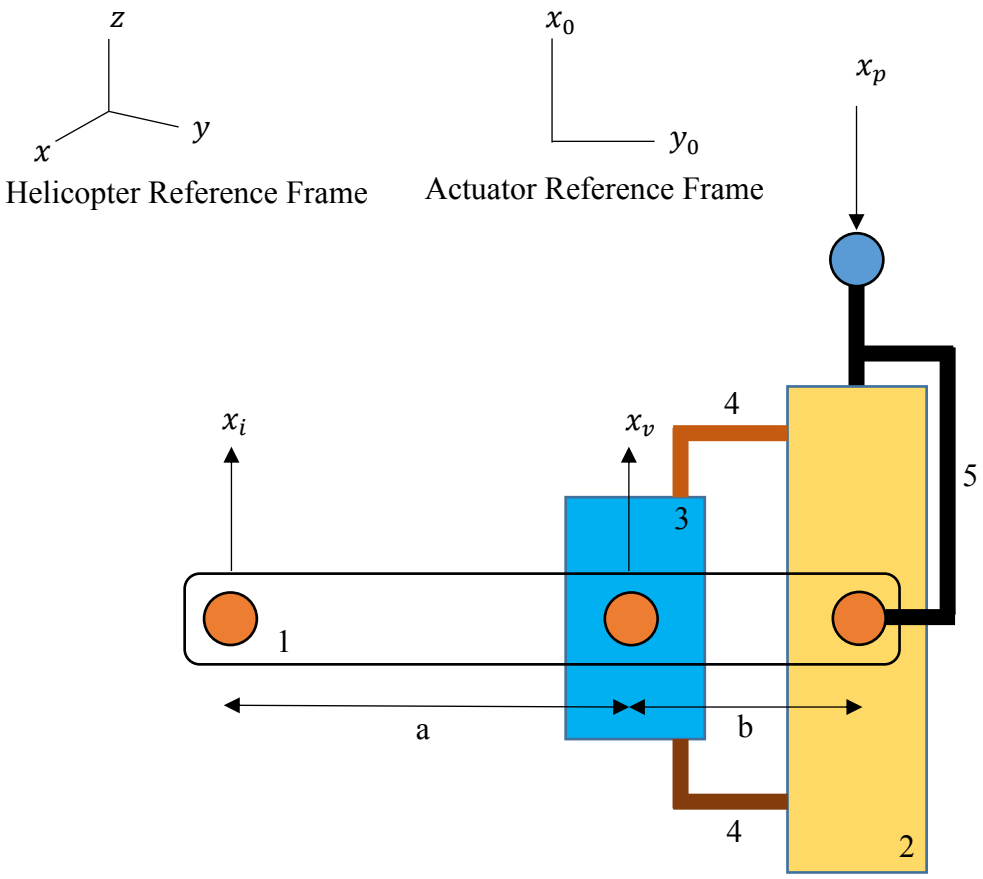

Figure 2.6 FCA Represented Upgraded with Feedback Lever and Actuating Lever

Subcomponents of a single FCA that are numbered in Figure 2.6 from 1 to 5 are described at Table 2.3.

Table 2.3 Subcomponents of Closed Loop FCA

Subcomponent	Description
#1	Actuating Lever
#2	Flight Control Actuator
#3	Main Control Valve
#4	Hydraulic Lines
#5	Feedback Lever

For the transient situations, geometric relations among three different hinge points are to be provided. First assuming the cylinder position as a fixed point and get the relation between pilot input x_i and valve input x_v, by extracting of valve input, is as follows;

$$x_v = \frac{K_{ls} b}{(a+b)} x_i \tag{2.80}$$

In this equation, $K_{layshaft}$ is defined as the reduction ratio of valve input. After calculation of valve input, it is not directly given to FCA. Instead, a layshaft is used to transmit valve input to main control valve. Layshaft reduction ratio is added to the system as a linear coefficient.

Next, assuming the pilot input position as fixed and get the relation between valve input x_v and cylinder output x_p, by extracting the cylinder output is as follows;

$$x_v = \frac{K_{ls} a}{(a+b)} x_p \tag{2.81}$$

After writing in terms of state variables yields that;

$$x_v = \frac{K_{ls} a}{(a+b) K_1} F_{K1} \tag{2.82}$$

Combining valve input relation in a single equation gives (2.83. Note that sign of cylinder output and pilot input are selected inversely to provide sign convention.

$$x_v(x_i, F_{K1}) = K_{ls} \left(\frac{b}{(a+b)} x_i + \frac{a}{(a+b) K_1} F_{K1} \right) \tag{2.83}$$

Putting valve input equation into 3rd state equation arises the new state equation that provides closed loop feedback control of the system. 3rd state equation becomes in the form of (2.84).

$$\dot{P}_C = \frac{1}{C} \left(-2 A_P V_{M1} + \frac{2}{R} P_C - \frac{2 K_{vf} K_{ls} b}{(a+b)} x_i - \frac{2 K_{vf} K_{ls} a}{(a+b) K_1} F_{K1} + K_{pf} P_C \right) \tag{2.84}$$

As a result, recent state space representation of the linear closed loop system can be found in (2.85). Note that input is directly given as x_i in a closed loop system.

$$\begin{bmatrix} \dot{F}_{K1} \\ \dot{V}_{M1} \\ \dot{P}_C \end{bmatrix} = \begin{bmatrix} 0 & K_1 & 0 \\ \frac{-1}{M_1} & -\frac{B_1}{M_1} & -\frac{A}{M_1} \\ -\frac{2K_{vf}K_{ls}a}{(a+b)K_1} & \frac{2A_P}{C} & \frac{(2-K_{pf}R)}{RC} \end{bmatrix} \begin{bmatrix} F_{K1} \\ V_{M1} \\ P_C \end{bmatrix} + \begin{bmatrix} 0 & 0 \\ \frac{1}{M_1} & 0 \\ 0 & -\frac{2K_{vf}K_{ls}b}{C(a+b)} \end{bmatrix} \begin{bmatrix} F_F \\ x_i \end{bmatrix} \tag{2.85}$$

2.2.5 Transfer Function of Closed-Loop Model

Transfer functions of the close loop system can be found again by using the commonly known method as it is described by Bequette's method likewise open loop transfer functions. It is observed that for the first column that represents transfer functions of external load and system states, numerators are exactly similar compared to open loop model. However, transfer function is to change as determinant of the state matrix is changed. There are, once again, 9 different transfer functions are found between inputs and system states. Among these transfer functions, bode plot representation that demonstrates the relationship between pilot input and actuator output is obtained and given in Figure 2.7.

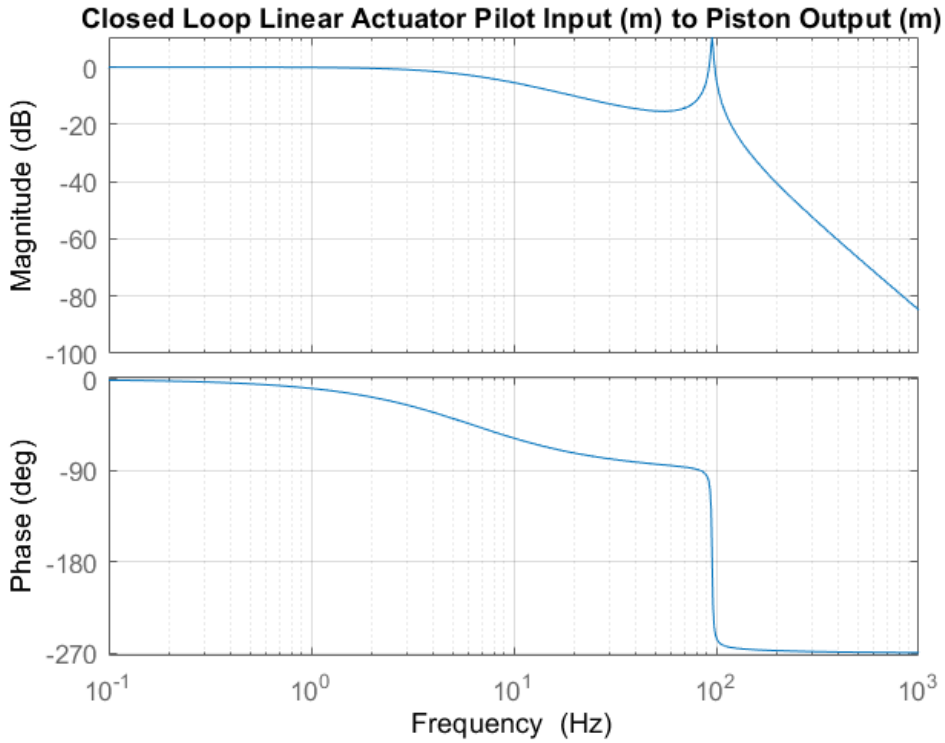

Figure 2.7 Bode Plot of Closed Loop System - Pilot Input and Cylinder Output

As it was seen in the open loop system, closed loop system has also a resonant frequency at 91 Hz considering acting dynamic system. It is quite far away from reference input levels in terms of frequency; thus, it does not have any effect to operation of the system. It is obvious that no resonant frequency is observed caused from hydraulic system.

2.3 Linear System Dynamics of Equivalent Actuator-Rotor Model

Rotor System is modeled as three independent degrees of freedom which represents mass of cylinder as M_P, mass of swashplate assembly as M_S and mass of rotor blades assembly as M_B. These masses are modeled to comprehend the inertial effects that are acting on the actuators while giving input to the system. Thus, these masses are inertial masses instead of being exact masses that are used in the helicopter. Actuator is considered as stationary which is placed on the helicopter structure. Equivalent

masses that are used in the derivation of mathematical model and corresponding rotor elements of these equivalent masses are demonstrated in Figure 2.8

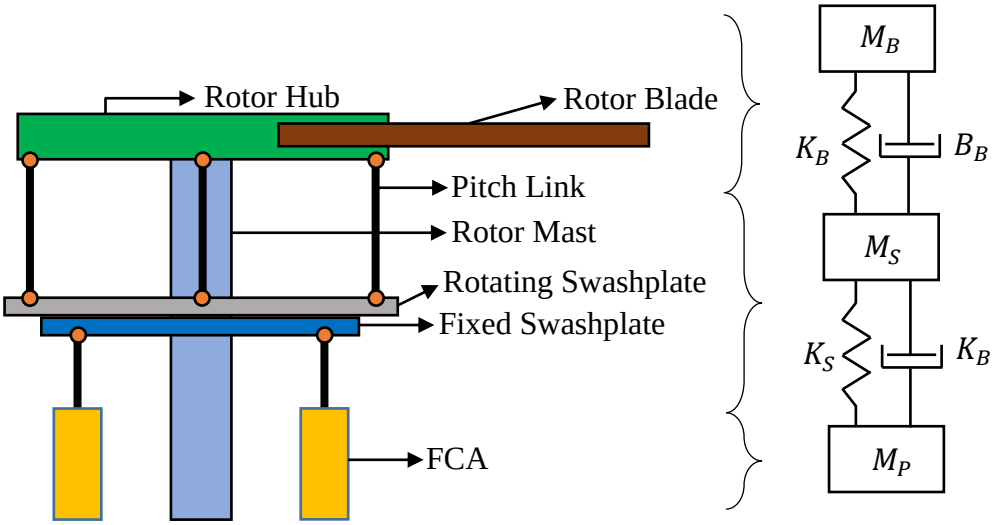

Figure 2.8 Corresponding Rotor Components of Equivalent Masses

2.3.1 Open Loop Linear Equivalent Actuator-Rotor

Open loop system is derived likewise in 1-Mass open loop system, by adding two additional rotor mass components. Physical representation of linearly derived model for three mass system is given in Figure 2.9.

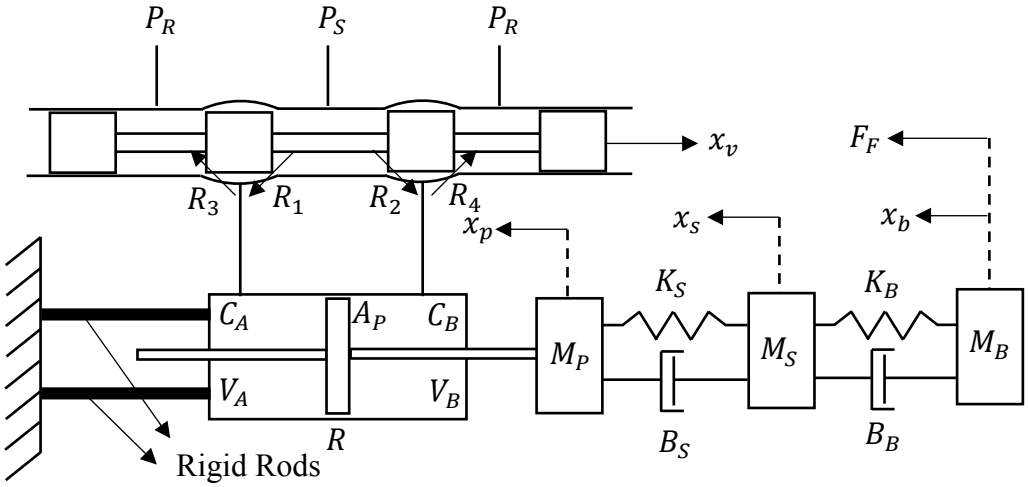

Figure 2.9 Open Loop 3-Mass Linear System

Linear graph of 3-Mass equivalent actuator and rotor system are provided in Figure 2.10.

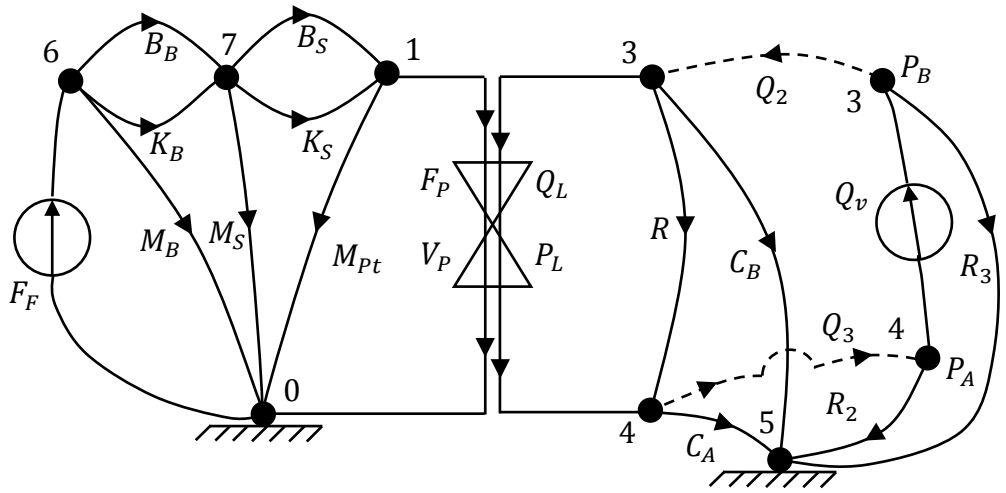

Figure 2.10 Linear Graph Representation of 3-Mass Rotor and Actuator Equivalent Model

Properties of linear graph for the equivalent actuator-rotor model are provided in Table 2.4.

Table 2.4 Linear Graph Properties of Equivalent Actuator-Rotor Model

Linear Graph Property	# of the Property in Linear Graph
Branches (B)	16
Nodes (N)	7
Across Sources (S_A)	0
Through Sources (S_T)	2
Nodes in Normal Tree ($N - N_D$)	6
Variables ($2B$)	32

Based on the parameters in the given linear graph, normal tree of equivalent dynamic system is provided in Figure 2.11.

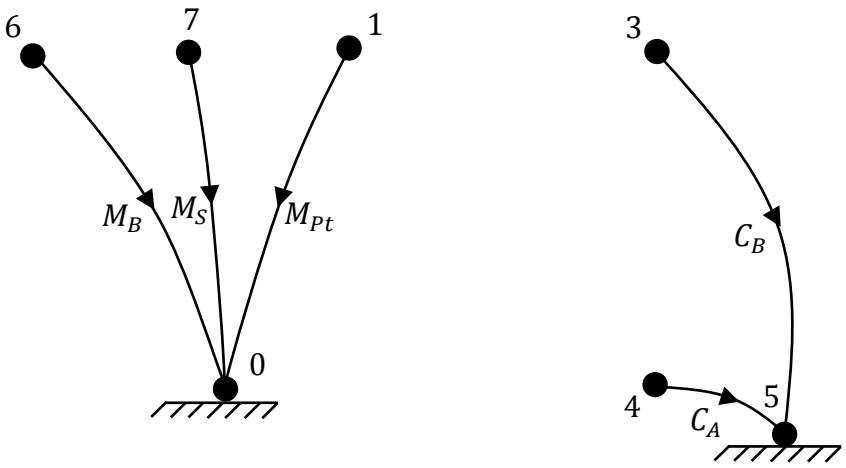

Figure 2.11 Normal Tree of Equivalent 3-Mass Dynamic System

Next, primary and secondary variables of the equivalent system is found [23,24]. Thus, across variables on the normal tree and through variables on the link are taken as primary variables. Other variables are selected as secondary variables. For the valve side, primary and secondary variables are selected same as open/closed loop model development. All primary and secondary variables of the system components are given as follows;

Table 2.5 Primary and Secondary Variables of Equivalent Model

Primary Var.	$V_B, V_S, V_{Pt}, P_A, P_B, Q_v, F_{BB}, F_{KB}, F_{BS}, F_{KS}, F_F, F_P, Q_L, Q_R,$ $Q_{R2}, Q_{R3},$
Secondary Var.	$F_B, F_S, F_{Pt}, Q_A, Q_B, P_v, V_{BB}, V_{KB}, V_{BS}, V_{KS}, V_F, V_P, P_L, P_R,$ P_{R2}, P_{R3}

States of the dynamic system are found by taking the A-Type variables on the normal tree and T-type variables on the links. Therefore, states of dynamics system are F_{KB}, $F_{KS}, V_B, V_S, V_{Pt}, P_A, P_B$. For 7 different state variables; elemental, compatibility and continuity equations can be found by using equations between (2.45) and (2.48). As a result of this, there are 14 elemental equations, 5 continuity equations and 9

compatibility equations are used to construct system dynamics. Elemental equations are provided below.

$$\dot{V}_B = \frac{1}{M_B} F_B \tag{2.86}$$

$$\dot{V}_S = \frac{1}{M_S} F_S \tag{2.87}$$

$$\dot{V}_{Pt} = \frac{1}{M_{Pt}} F_P \tag{2.88}$$

$$\dot{P}_A = \frac{1}{C_A} Q_A \tag{2.89}$$

$$\dot{P}_B = \frac{1}{C_B} Q_B \tag{2.90}$$

$$F_{BB} = B_B V_{BB} \tag{2.91}$$

$$\dot{F}_{KB} = K_B V_{KB} \tag{2.92}$$

$$F_{BS} = B_S V_{BS} \tag{2.93}$$

$$\dot{F}_{KS} = K_S V_{KS} \tag{2.94}$$

$$F_P = A_P P_L \tag{2.95}$$

$$Q_A = -A_P V_A \tag{2.96}$$

$$Q_R = \frac{1}{R} P_R \tag{2.97}$$

$$Q_{R2} = \frac{1}{R_2} P_{R2} \tag{2.98}$$

$$Q_{R3} = \frac{1}{R_3} P_{R3} \tag{2.99}$$

Next, continuity equations are written mainly consist of force equilibrium and flow equilibrium within the nodes of the system. Continuity equations are provided below;

$$F_F = F_{BB} + F_{KB} + F_B \tag{2.100}$$

$$F_{BB} + F_{KB} = F_S + F_{BS} + F_{KS} \tag{2.101}$$

$$F_{BS} + F_{KS} = F_{Pt} + F_P \tag{2.102}$$

$$Q_A = Q_L + Q_R - Q_{R3} - Q_v \tag{2.103}$$

$$Q_B = -Q_L - Q_R + Q_{R2} + Q_v \tag{2.104}$$

Continuing with the 13 compatibility equations; however, some of them are merged. Thus, representations between (2.105) and (2.113) contains 9 compatibility equations and these are given below.

$$P_L = P_A - P_B \tag{2.105}$$

$$P_{R3} = P_A \tag{2.106}$$

$$P_R = P_A - P_B \tag{2.107}$$

$$P_{R2} = -P_B \tag{2.108}$$

$$V_{BB} = V_{KB} \tag{2.109}$$

$$V_{BS} = V_{KS} \tag{2.110}$$

$$V_B = V_{BB} + V_S \tag{2.111}$$

$$V_S = V_{BS} + V_P \tag{2.112}$$

$$V_{Pt} = V_P \tag{2.113}$$

Starting to create state equations from$\dot{F}_{KB}$ gives the 1st state equations as follows;

$$\dot{F}_{KB} = K_B V_{KB} = K_B V_{BB} = K_B(V_B - V_S) \tag{2.114}$$

Continuing with $\dot{F}_{KS}$, 2nd state equation is found as;

$$\dot{F}_{KS} = K_S V_{KS} = K_S V_{BS} = K_S(V_S - V_{Pt}) \tag{2.115}$$

Continuing with $\dot{V}_B$, 3rd state equation is found as;

$$\dot{V}_B = \frac{1}{M_B} F_B = \frac{F_F - B_B(V_B - V_S) - F_{KB}}{M_B} \tag{2.116}$$

Continuing with $\dot{V}_S$, 4th state equation is found as;

$$\dot{V}_S = \frac{1}{M_S} F_S = \frac{1}{M_S}(F_{BB} + F_{KB} - F_{BS} - F_{KS}) \tag{…}$$

$$\dot{V}_S = \frac{1}{M_S}(-B_S(V_S - V_{Pt}) - F_{KS} + B_B(V_B - V_S) + F_{KB}) \tag{2.117}$$

Continuing with V_{Pt}, 5th state equation is found as;

$$\dot{V}_{Pt} = \frac{1}{M_P}F_P = \frac{1}{M_P}(F_{BS} + F_{KS} - F_G) \tag{…}$$

$$\dot{V}_{Pt} = \frac{1}{M_P}(B_S(V_S - V_{Pt}) + F_{KS} + A_P P_C) \tag{2.118}$$

Continuing with P_C, for the 6th state equation, P_C can be written in terms of P_A and P_B;

$$\dot{P}_C = \dot{P}_A - \dot{P}_B = \frac{1}{C}\left(2A_P V_{M1} + \frac{2}{R}P_C + 2K_{vf}x_v - K_{pf}P_C\right) \tag{2.119}$$

State space representation of the open loop system is provided as follows.

$$\dot{x} = \boldsymbol{A}x + \boldsymbol{B}u \tag{2.120}$$

Where;

$$\boldsymbol{A} = \begin{bmatrix} 0 & 0 & K_B & -K_B & 0 & 0 \\ 0 & 0 & 0 & K_S & -K_S & 0 \\ -\frac{1}{M_B} & 0 & -\frac{B_B}{M_B} & \frac{B_B}{M_B} & 0 & 0 \\ 0 & -\frac{1}{M_S} & \frac{B_B}{M_S} & \frac{-B_B - B_S}{M_S} & \frac{B_S}{M_S} & 0 \\ 0 & \frac{1}{M_{Pt}} & 0 & \frac{B_S}{M_{Pt}} & -\frac{B_S}{M_{Pt}} & \frac{A_P}{M_{Pt}} \\ 0 & 0 & 0 & 0 & \frac{2A_P}{C} & \frac{(2 - RK_{pf})}{RC} \end{bmatrix} \tag{2.121}$$

$$x^T = [F_{KB} \quad F_{KS} \quad V_B \quad V_S \quad V_{Pt} \quad P_C] \tag{2.122}$$

$$\boldsymbol{B}^T = \begin{bmatrix} 0 & 0 & \dfrac{1}{M_B} & 0 & 0 & 0 \\ 0 & 0 & 0 & 0 & 0 & \dfrac{2K_{vf}}{C} \end{bmatrix} \tag{2.123}$$

$$u^T = [F_F \quad x_v] \tag{2.124}$$

2.3.2 Closed Loop Linear Equivalent Rotor-Actuator Model

Open loop state space representation can be converted into closed loop system by using the same methodology given in (2.83). As the valve input determines the response of the system by only influencing the 6th state equation, methodology of closed loop is to be applied to only 6th state equation. However, displacement of the cylinder cannot be converted as represented in terms of state variables because cylinder is not directly connected a ground point. For that reason, an additional state variables of cylinder output are to be defined to acquire cylinder displacement which is an analytical component of valve input. Using (2.83) by retaining X_P as it is and by adding a state variable of X_P, 8th state equation is converted to following;

$$\dot{P}_C = \frac{1}{C}\left(-2A_P V_{M1} + \frac{2}{R}P_C - \frac{2K_{vf}K_{ls}b}{(a+b)}x_i - \frac{2K_{vf}K_{ls}a}{(a+b)}X_P + K_{pf}P_C - K_{pf}P_S\right) \tag{2.125}$$

7th state equation is a simple representation which is given in (2.126).

$$\dot{X}_{Pt} = V_{Pt} \tag{2.126}$$

After necessary implementations; state matrix, states, input matrix and inputs are modified to get closed loop system as follows;

$$\boldsymbol{A} = \begin{bmatrix} 0 & 0 & K_B & -K_B & 0 & 0 & 0 \\ 0 & 0 & 0 & K_S & -K_S & 0 & 0 \\ -\frac{1}{M_B} & 0 & -\frac{B_B}{M_B} & \frac{B_B}{M_B} & 0 & 0 & 0 \\ 0 & -\frac{1}{M_S} & \frac{B_B}{M_S} & \frac{-B_B - B_S}{M_S} & \frac{B_S}{M_S} & 0 & 0 \\ 0 & \frac{1}{M_P} & 0 & \frac{B_S}{M_P} & -\frac{B_S}{M_P} & \frac{A_P}{M_P} & 0 \\ 0 & 0 & 0 & 0 & \frac{2A_P}{C} & -\frac{(2 - RK_{pf})}{RC} & -\frac{2K_{ls}K_{vf}a}{C(a+b)} \\ 0 & 0 & 0 & 0 & 1 & 0 & 0 \end{bmatrix} \quad (2.127)$$

$$x^T = [F_{KB} \quad F_{KS} \quad V_B \quad V_S \quad V_{Pt} \quad P_C \quad X_{Pt}] \quad (2.128)$$

$$\boldsymbol{B}^T = \begin{bmatrix} 0 & 0 & \frac{1}{M_B} & 0 & 0 & 0 & 0 \\ 0 & 0 & 0 & 0 & 0 & -\frac{2K_{vf}K_{ls}b}{C(a+b)} & 0 \end{bmatrix} \quad (2.129)$$

$$u^T = [F_F \quad x_i] \quad (2.130)$$

Bode plot representation that demonstrates the relationship between pilot input and cylinder output is obtained and given in Figure 2.12 Bode Plot of Closed Loop System, Pilot Input (m) and Cylinder Output (m).

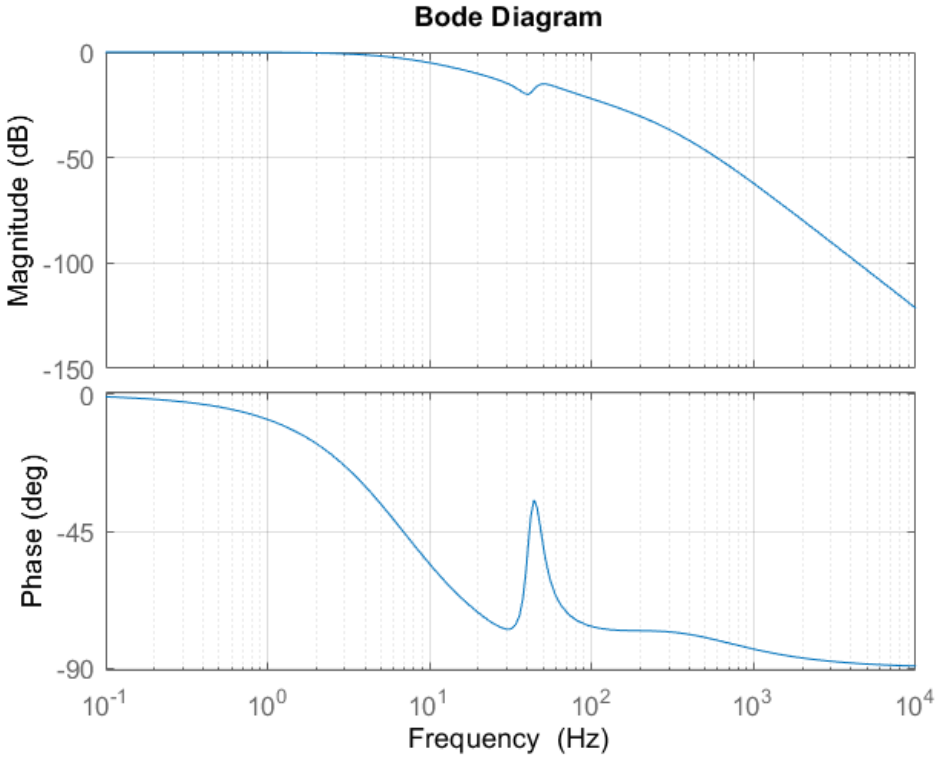

Figure 2.12 Bode Plot of Closed Loop System, Pilot Input (m) and Cylinder Output (m)

2.4 Design Parameters

2.4.1 Fluid Parameters

Bulk Modulus is the most significant fluid parameter that determines the natural frequency of the hydraulic system. It refers to the compressibility of hydraulic oil under a particular pressure that is applied to the liquid. In fact, it refers to capacitance of the hydraulic fluid that operates within the system. Basically, hydraulic oil with a high capacitance value is preferred due to get rapid dynamic responses. Likewise, capacitance of common hydraulic oils that are used in aircraft applications such as MIL-H-5606 or SAE-AS-83282 are significantly high. Furthermore, their capacitance value increases even higher levels under high temperature conditions. As a fundamental definition, bulk modulus β can be defined as volumetric strain of

the fluid under volumetric stress caused by application of pressure. Definition of bulk modulus is given in (2.131).

$$\beta = -V\frac{dP}{dV} \tag{2.131}$$

Sign convention is to be taken in the other way around as negative in the formula because it represents the "compressibility" of the fluid. In research that is executed to determine bulk modulus of two types of hydraulic fluid as air entrapped and purged from air [26], several coefficients are determined. By taking the purged hydraulic oil, a reference bulk modulus coefficient can be found overall as $1.4*10^9$ Pa. For linear simulations, bulk modulus is considered as a capacitance coefficient of C instead of an independent coefficient. Having knowledge of reference bulk modulus value and total volume of the chamber provides determination of the capacitance coefficient, as it is found as follows;

$$C = \frac{A_P x}{\beta} \tag{…}$$

$$C = \frac{7 * 10^{-4} * 0.1}{1{,}4 * 10^{-9}} = 5 * 10^{-13}\frac{m^4 s^2}{kg} \tag{2.132}$$

2.4.2 Leakage Parameters

Leakage is a significant parameter that affects mainly the overall damping of FCA. There are two types of significant leakage may occur during operation of the system, these are valve leakage and cylinder leakage. For the simulation of linear system, valve leakage is not included independently as it is evaluated that examination of contribution of the leakage is not necessary. Instead, MCV orifice width and length is arranged in a way that it demonstrates the effect of leakage by not allowing a predetermined amount of fluid to pass the actuator chamber.

Second type of leakage is cylinder leakage that occurs because of including a clearance between cylinder and actuator inside surface. Having a dynamic seal between external flange of the cylinder body and inside surface of actuator body

prevents huge amount of the leakage between chambers. This type of seal accompanies cylinder through its complete stroke. Despite using such seals, there is always an internal leakage between two chambers of the actuator due to have a more damped characteristic. Allowing such an arranged leakage value significantly decreases load acting to dynamic system by cylinder for rapid inputs given to the system. Besides, allowing a leakage flow rate is provided with design gap that is called clearance.

For selecting an appropriate leakage coefficient to provide accurateness of the model, similar investigations are inspected. According to Dransfield and Bruce [25], leakage flowrate coefficient is investigated for several design gap that is left between cylinder and internal surface of actuator cylinder. Different design gaps are investigated because of production sensitivity, in fact provided tolerance. A rough design gap is selected, which 0.04 mm between two components, and approximately under 3000 psi hydraulic pressure level, leakage rate is observed. According to Figure 2.13, leakage coefficient can be determined under 3000 psi.

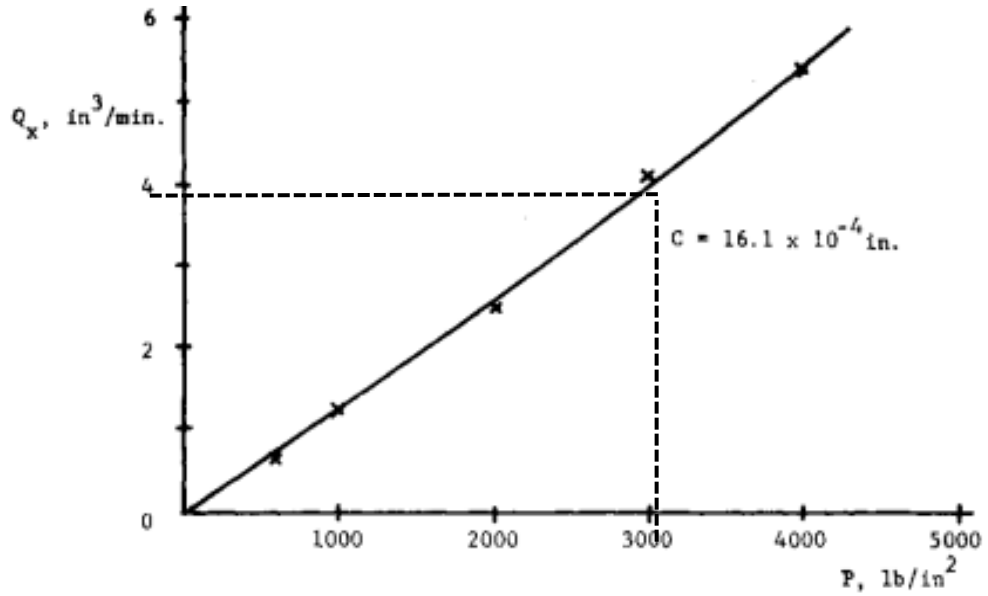

Figure 2.13 Leakage under 3000 psi Pressure [25]

According to Figure 2.13, it is observed 4 in^3/min leakage is observed. Leakage coefficient *R* can be found as follows;

$$R = \frac{20.7\ MPa}{65.5\ mm^3/_{min}} = \frac{20.7 * 10^6\ Pa}{1.1 * 10^{-6}\ m^3/_s} \quad (\ldots)$$

$$R = \frac{20.7 * 10^6\ Pa}{1.1 * 10^{-6}\ m^3/_s} = 1.91 * 10^{-13}\ \frac{kg}{m^4 s} \quad (2.133)$$

It is demonstrated in results that leakage coefficient is selected highly consistent with real design of FCA.

2.5 Nonlinear Dynamics of Equivalent Actuator Rotor Model

Having the nonlinear model of a hydraulic system brings several benefits compared to linear model. Initially, states of model are easier to control and observe because states can be gathered and used in any part of the simulation. Furthermore, hydraulic valves in nonlinear system demonstrates more proper characteristics as they are inherently nonlinear components. Model is not only valid within a vicinity that restricts the usability of the system, but also valid in wide ranges. Finally, controller design and adding servo valve function to the system is easier while using a nonlinear system. Considering these advantages, a nonlinear system of equivalent actuator-rotor model is obtained. Equivalent actuator-rotor model is given in Figure 2.14.

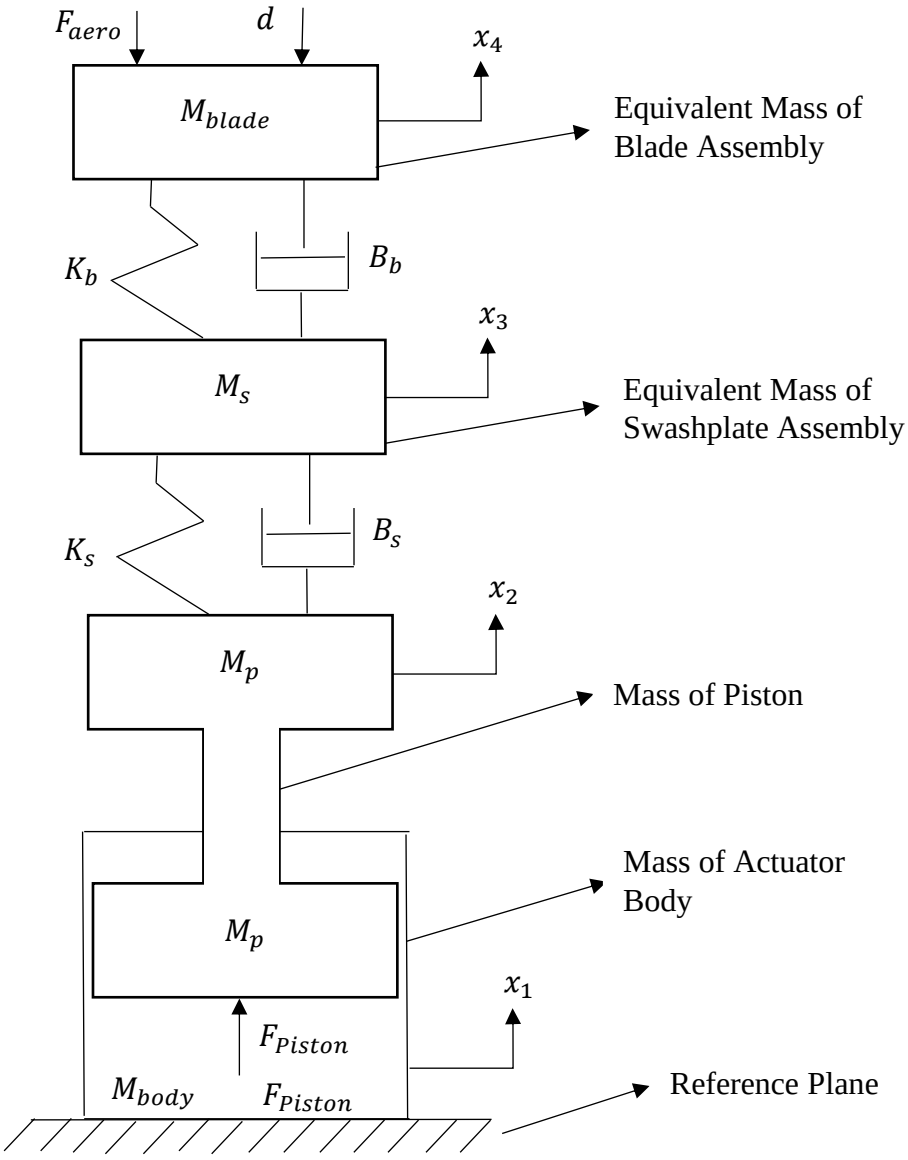

Figure 2.14 Equivalent Rotor-Actuator Model

In the Equivalent model, 3 degrees of freedom system is considered. Represented masses and equivalent masses are described in the figure as well as can be seen more clearly in Figure 2.8. Likewise in linear model, three masses are selected as cylinder mass (M_P), swashplate assembly equivalent mass (M_S) and blade assembly equivalent mass (M_B). Cylinder mass is selected based on real design of the FCA. On the other hand, blade and swashplate assembly masses are determined

considering inertial effects acting on the rotor system. In addition to linear rotor model with 2 masses, cylinder-rod assembly of a single FCA is represented as 1 degrees of freedom model likewise rotor dynamic model. Eventually, overall dynamic system become a 3 degrees of freedom system. Although actuator body is represented by M_{Body}, it does not have a dynamic contribution to the system as it is taken stationary by having a zero acceleration. Thus, actuator body becomes that reference plane of motion for other masses by having x_1 always zero. Aerodynamic loads and environmental disturbances are considered as force inputs to blades equivalent mass.

2.5.1 Swashplate Kinematics from Inputs via Actuators

As it is described, 3 FCAs are installed on the helicopter separated by 120°. Cylinder outputs of actuators are determined by three different types of pilot input. For the nonlinear model, displacements of actuators are considered as D_1, D_2, D_3 for forward, left and right FCA; respectively. Linearized version of Cylinder displacement rates determined by inputs has already been produced in (2.35). From these rates, displacements are obtained as follows as independent equations.

$$D_1 = -RC_{y1}y_1 + C_{x1}x_1 \tag{2.134}$$

$$D_2 = \frac{RC_{y1}y_1}{2} + \frac{\sqrt{3}RC_{y2}y_2}{2} + C_{x1}x_1 \tag{2.135}$$

$$D_3 = \frac{RC_{y1}y_1}{2} - \frac{\sqrt{3}RC_{y2}y_2}{2} + C_{x1}x_1 \tag{2.136}$$

Rates of FCAs have already been developed. Kinematic relations between pilot input and combined output values are to be taken as a reference of steady state response of the system. Mechanism proportions of C_{x1}, C_{y1}, C_{y2} are affecting the force acts backwards to the input levers. However, they are not into consideration, and it is assumed that inputs can be given to Actuator via a force that can be given in any magnitude. Ends of the cylinder rods are attached with a single lug at each corner of stationary swashplate equilateral triangle. For that reason, pitch angle of the

swashplate is directly determined by using D_1, D_2 and D_3; on the other hand, roll angle is directly determined by D_2 and D_3. Note that lug position is not only changing in the vertical direction but also changing in the horizontal directions especially in the higher angles, to eliminate geometrical singularity. However, it is assumed that actuators are moving only along on a single z-axis in same reference frame, assumption reason are described in 1.1.3.4.

Pitch Tilting angle of the SSP itself is represented with α. Inherently, value of α is between $-\pi/2$ and $\pi/2$. Regarding the necessary assumptions, rate of α can be gathered using (2.137) by means of D_1, D_2, D_3 and R.

$$\alpha = \arcsin\left(\frac{2\left|D_1 - \frac{(D_2 + D_3)}{2}\right|}{3R}\right) \cdot \begin{cases} -1, & D_{coef,1} < 0 \\ 1, & D_{coef,1} \geq 0 \end{cases} \tag{2.137}$$

Roll Tilting angle of the SSP itself is represented with β. Similarly, value of β is between $-\pi/2$ and $\pi/2$. Additionally, it is expressed in terms of D_2 and D_3 as the forward FCA does not move while giving y_2 input which result roll tilting angle of the Swashplate. Rate of α can be gathered using (2.138) by means of D_2, D_3 and R.

$$\beta = \arcsin\left(\frac{2|D_2 - D_3|}{\sqrt{3}R}\right) \cdot \begin{cases} -1, & D_{coef,2} < 0 \\ 1, & D_{coef,2} \geq 0 \end{cases} \tag{2.138}$$

In these equations, sign criterion of related Tilting Angle is decided with coefficients of $D_{coef,1}$ and $D_{coef,2}$ for pitch and roll tilting angles, consequently. Definitions of these coefficients are given in (2.139) and (2.140).

$$D_{coef,1} = D_1 - \frac{(D_2 + D_3)}{2} \tag{2.139}$$

$$D_{coef,2} = D_2 - D_3 \tag{2.140}$$

Using the kinematic relationships, displacements of FCAs and both tilting angles are obtained, and they can be considered as the steady state value of the given input if they are considered only as analytical relationships without any hydraulic interface. To get a capability of competing with higher loads, hydraulic system is to be

integrated. In a hydraulic control system, parameters of hydraulic mathematical model undertake a significant role while determining the performance of control system as inputs are transmitted through rotor components via hydraulic control system. Nonlinear mathematical is obtained to analyze influences of hydraulic parameters precisely; in the end; to obtain sensible results.

2.5.2 Nonlinear Hydraulic System

Hydraulic system that is used for transmitting pilot input to stationary swashplate is mainly consist of three identical hydraulic FCAs. Each actuator has an MCV, a cylinder rod assembly and a mechanical controller, in fact a feedback lever, that arranges feedback taking by main control valve. Pilot input is transmitted to main control valve with a reduction ratio that is defined as $K_{Layshaft}$ described as mechanical linkage in 1.1.2. Valve input takes mechanical feedback from the position of the cylinder. Closed loop feedback control of hydraulic actuator is completed with a $K_{P,Layshaft}$ constant for nonlinear hydraulic system. Elements of closed loop control system are given in Figure 2.15.

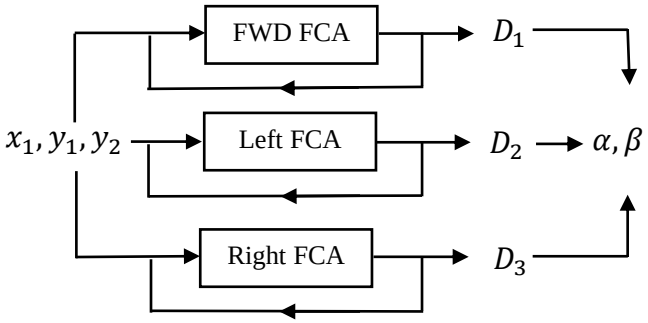

Figure 2.15 Input-Output Relationship of Closed Loop System

Nonlinear hydraulic system takes feedback from mechanical feedback lever. Feedback is calculated by difference between reference cylinder position and actual cylinder Output at the given timestep. Definition of cylinder error of regarded actuator and its related valve input caused by the error are provided in (2.141) and (2.142).

$$e(t) = D - D_{ref} \tag{2.141}$$

$$x_{v,Pilot} = K_{ls} e(t) \tag{2.142}$$

Control valve input directly changes the width of orifices in the main control valve. Eventually, one side of the chamber is fed from high pressure side while other one is being pressurized by low pressure side.

2.5.2.1 Main Control Valve

Main control valve consists of a sleeve spool mechanism that is used to arrange width of the orifices that connects either side of the chamber to the high-pressure source while connecting others side of the chamber to low pressure tank. Null position of main control valve is zero and, in these conditions, valve only allows internal leakage and does not connect any system to high- or low-pressure side. Input of MCV can be given either in positive or in negative direction. Considering two different chambers as A and B, depending on the position of main control valve spool, either chamber A of the cylinder is pressurized while chamber B is being connected to low pressure side, or chamber B is pressurized as chamber A is connected to low pressure side. There can be three types of different lapping in the design of MCV which are underlapping, critical lapping and overlapping. Lapping conditions and valve response in terms of creation of the load flow are demonstrated below [27].

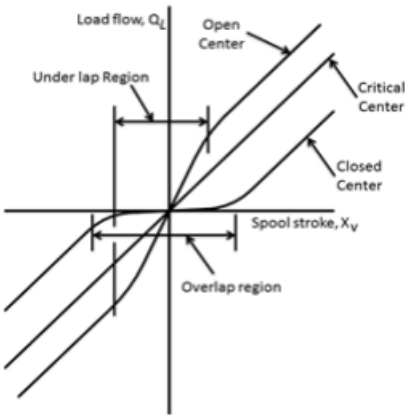

Figure 2.16 Graphical Demonstration of Different Lapping [27]

Different lapping conditions can be applied to operate system as intended. In aircraft applications, overlapping is widely used in switching valves. However, it is not preferred in adjustable control valves because hydraulic actuator does not respond small inputs in overlapped valves. It is not desired especially flight conditions under which pilot sensitively adjusts the orientation of the helicopter such as sea missions or mountain missions. Underlapped valves are also not as desirable although they allow sensitive control in most cases, it causes huge amount of leakage during steady state conditions. In aircraft applications, critical sizing is significant and such leakage causes oversizing of the power components such as hydraulic pumps and transmission as driver of mechanical pumps. Thus, critically lapped MCVs are widely used in aircraft applications with slight amount of leakage that allows capability of movement faster than exactly critically lapped MCV. However, effect of leakage is considerable low during inspection of system responses Thus, derivations of nonlinear system is started with consideration of no leakage inside MCV; in fact, neglecting the slight underlapping. There are four nodes of MCV which pressure source P_S, chamber A pressure P_A, chamber B pressure P_B and return (tank) pressure P_R. Representative circuit of MCV is provided in Figure 2.17.

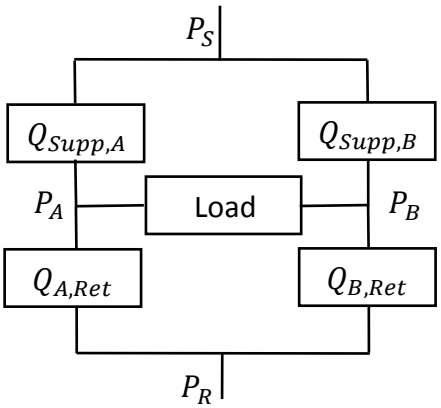

Figure 2.17 Representative Circuit of Main Control Valve

Due to the pressure difference between supply port, chamber A, chamber B and return port; flow occurs from higher pressure to lower pressure. If x_v is positive, then the pressure of chamber A will be greater than the chamber B. If x_v is negative, then

the pressure of chamber B will be greater than the chamber A in steady state conditions. Besides, x_0 can be described as the leakage coefficient that refers to shift value when it is intended to keep valve at neutral position. Sign convention is decided by looking flow direction at the load. Flow from P_A to P_B is taken as positive. Thus, if Pressure of chamber is higher than A, flow occurs on the opposite direction of what is selected as positive on load side. For that reason, Pressure equation of chamber B and return equation of chamber A are multiplied with -1. Flow equations among pressure sinks and sources are given from (2.143) to (2.146).

$$Q_{Supp,A} = C_D h \sqrt{\frac{2(|P_S - P_A|)}{\rho}} . \begin{cases} x_v + x_0, & x_v \geq 0 \\ 0, & x_v < 0 \end{cases} \tag{2.143}$$

$$Q_{Supp,B} = -C_D h \sqrt{\frac{2(|P_S - P_B|)}{\rho}} . \begin{cases} 0, & x_v \geq 0 \\ x_v + x_0, & x_v < 0 \end{cases} \tag{2.144}$$

$$Q_{A,Ret} = -C_D h \sqrt{\frac{2(|P_A - P_R|)}{\rho}} . \begin{cases} 0, & x_v \geq 0 \\ x_v + x_0, & x_v < 0 \end{cases} \tag{2.145}$$

$$Q_{B,Ret} = C_D h \sqrt{\frac{2(|P_B - P_R|)}{\rho}} . \begin{cases} x_v + x_0, & x_v \geq 0 \\ 0, & x_v < 0 \end{cases} \tag{2.146}$$

Valve width is taken as 0 if it is intended to close the corresponding port, which emphasizes that no leakage occurs while closing either supply of chamber A flow or chamber B flow. Simulink models of equations from (2.143) to (2.146) are provided from Figure 2.18 to Figure 2.21.

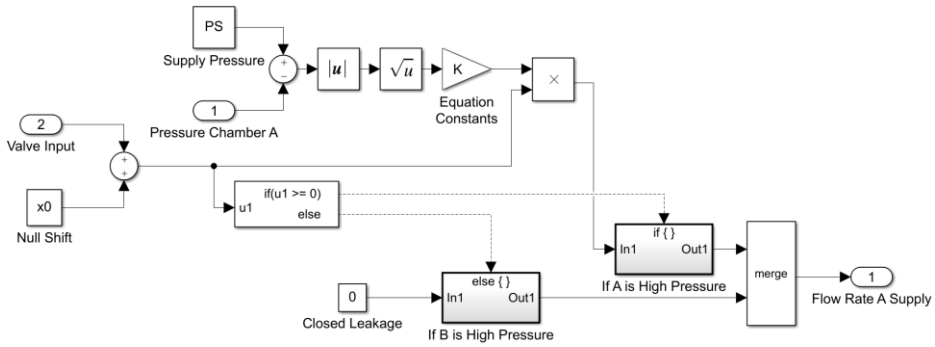

Figure 2.18 Pressure Source to Chamber A Flow Equation

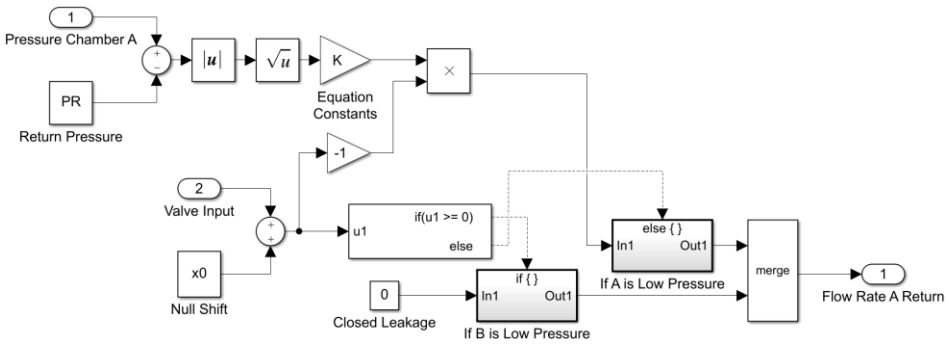

Figure 2.19 Chamber A to Return Tank Flow Equation

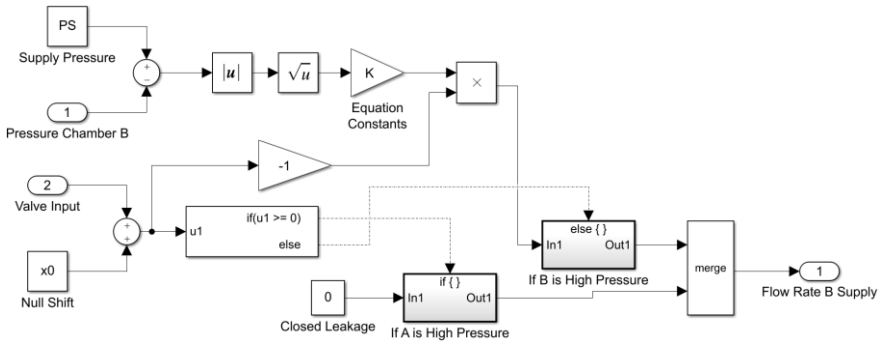

Figure 2.20 Pressure Source to Chamber B Flow Equation

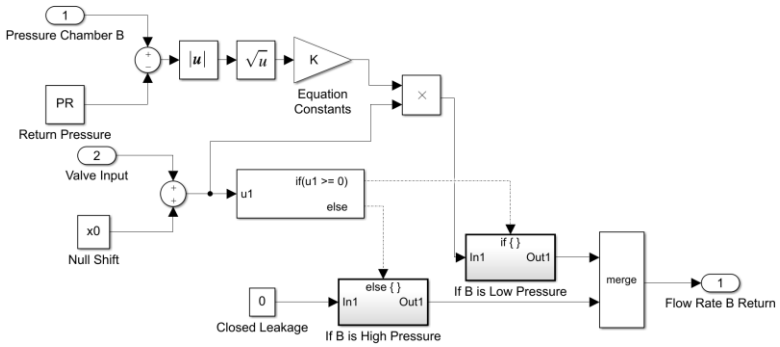

Figure 2.21 Chamber B to Return Tank Flow Equation

2.5.2.2 Pressures of Chambers

Calculation of pressures are sensitively important to obtain precise results because force arises within the system because of pressure difference between chamber A and chamber B. Conversely to the linear system, pressure at different sides of the

hydraulic cylinder can be obtained as P_A and P_B instead of compound pressure value. Fluid is pressurized fundamentally for its compressible characteristic. Compressibility mainly refers to the energy storage capacity of the fluid and compressibility coefficient of a fluid is defined as Bulk Modulus (β). To obtain the pressures of both chambers independent from each other, compressibility equations are written as (2.147) and (2.148).

$$\frac{dV_A}{dt} = \frac{V_A}{\beta}\frac{dP_A}{dt} \tag{2.147}$$

$$\frac{dV_B}{dt} = \frac{V_B}{\beta}\frac{dP_B}{dt} \tag{2.148}$$

Simulink® model of (2.147) and (2.148) is provided in Figure 2.24 and Figure 2.23, respectively.

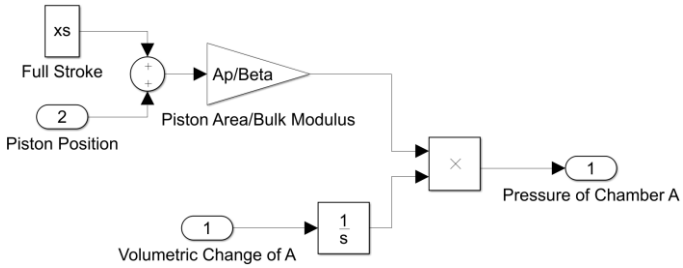

Figure 2.22 Pressure Calculation of Chamber A

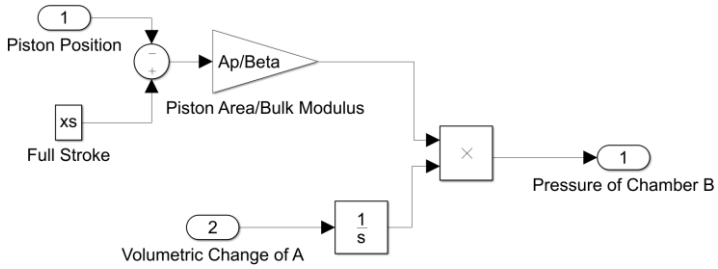

Figure 2.23 Pressure Calculation of Chamber B

2.5.2.3 Flow Rate of Chambers

Flow rate of the hydraulic ram can be determined by taking the volumetric difference between two successive time steps. Thus, either of the chamber has a positive flow rate while other chamber having a negative flow rate. Inlet and outlet flow are the same except having inverse signs, and compression is also an exception. Flow rate of each chamber can be defined as follows;

$$Q_A = \frac{dV_A}{dt} = \frac{V_{A,t_i} - V_{A,t_{i-1}}}{t_i - t_{i-1}} \tag{2.149}$$

$$Q_B = \frac{dV_B}{dt} = \frac{V_{B,t_i} - V_{B,t_{i-1}}}{t_i - t_{i-1}} \tag{2.150}$$

For adding impact of fluid compressibility to flow rate, (2.147) and (2.148) are to be integrated within flow relations. By making the implementation and after necessary arrangements, P_A and P_B are found as (2.151) and (2.152).

$$P_A = \frac{\beta}{V_A} \int_0^t Q_A dt \tag{2.151}$$

$$P_B = \frac{\beta}{V_B} \int_0^t Q_B dt \tag{2.152}$$

Where;

$$V_A = A_A(x_t + x_p) \tag{2.153}$$

$$V_B = A_B(x_t - x_p) \tag{2.154}$$

In the analysis, a balanced actuator is designed and A_A and A_B are equal, which are written as A_P. However, mathematical model is open for any unbalanced actuator implementation thanks to (2.153) and (2.154). Flow equations are rewritten in terms of cylinder displacement x_p in (2.155) and (2.156).

$$Q_A = \frac{dV_A}{dt} = A_P \frac{dx_p}{\partial t} = A_P \frac{x_{p,t_i} - x_{p,t_{i-1}}}{t_i - t_{i-1}} \tag{2.155}$$

$$Q_B = \frac{dV_B}{dt} = -A_P \frac{dx_p}{\partial t} = -A_P \frac{x_{p,t_i} - x_{p,t_{i-1}}}{t_i - t_{i-1}} \quad (2.156)$$

Simulink® model of (2.155) and (2.156) is provided in Figure 2.24.

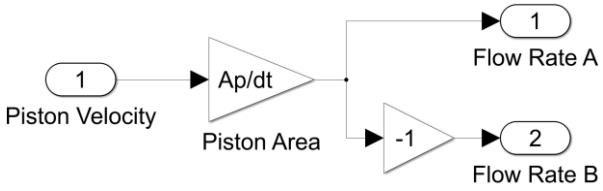

Figure 2.24 Simulink Model of Flow Rate Calculation

2.5.2.4 Force Calculation

Pressure values of each chamber are calculated independently for any time step. It brings a further step which is force calculation. Calculated force is directly applied to driven system, in fact rotor assembly. In addition to applied forces, there are also environmental and frictional forces that are to be modeled and evaluated. Initially, as long as the actuator moves in either direction, there is a frictional force arises because of friction in the cylinder. Friction can be modeled either as a velocity dependent linear function or only amplified with a constant dependent to velocity of cylinder, and added to mathematical model as $F_{friction}$. Secondly, there is a disturbance acting to blades as a dynamic force caused by changing air density through flight profile. Disturbance can become entangled in the system with various frequency ranges. These frequency ranges are to be investigated in a mathematical model to get rid of any drawback during flight operation. Disturbance is demonstrated by d. Additionally, there are external forces that can be demonstrated as F_{ext} that represents the force acting on rotor blades statically. It diverges from disturbance by being a static force bounded to angle of attack of each rotor blade, acting to rotor components and SSP as a compound of each aerodynamic force. However, F_{ext} and d are evaluated as an input of blade equivalent mass and not considered as compound force of actuator. Thus, force acting to the dynamic system via FCA is given in (2.157.

$$F_{FCA} = (P_A - P_B)A_P + F_{friction} \tag{2.157}$$

Simulink® model of (2.157) is provided in Figure 2.25.

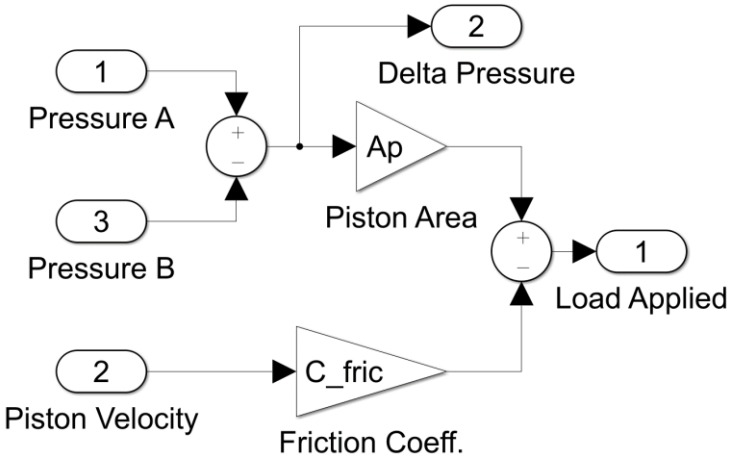

Figure 2.25 Simulink Model of Force Calculation

2.5.3 Dynamic System Equations of Motion

Helicopter rotor dynamics are to be fundamentally modeled to comprehend if there is any frequency mode that effects the stability of FCA. A resonant frequency mode causes huge amount displacement to change of rotor blades in a narrow frequency range that creates unbearable forces for the structure of the helicopter body and its components. For the investigation, helicopter rotor and actuator assembly is divided into four different masses as given in Figure 2.14. Representation of these masses have already been mentioned in 2.5.1. Analytical equations of motion to implement the mathematical model are found as given from (2.158) through (2.160), successively given for mass of the actuator body (M_{body}), cylinder-rod assembly (M_P), Swashplate assembly (M_S) and blade assembly (M_{blade}).

$$M_P \frac{d^2x_2}{dt^2} = F_{piston} - K_s x_{23} - B_s \frac{dx_{23}}{dt} \tag{2.158}$$

$$M_S \frac{d^2x_3}{dt^2} = K_s x_{23} + B_s \frac{dx_{23}}{dt} - K_B x_{34} - B_B \frac{dx_{34}}{dt} \tag{2.159}$$

$$M_B \frac{d^2 x_4}{dt^2} = K_B x_{34} + B_B \frac{\partial x_{34}}{\partial t} - F_{aero} - d \tag{2.160}$$

Definitions of states and derivatives of the states are given as (2.161) through (2.164).

$$x_{23} = x_2 - x_3 \tag{2.161}$$

$$x_{34} = x_3 - x_4 \tag{2.162}$$

$$\frac{\partial x_{23}}{\partial t} = \frac{\partial x_2}{\partial t} - \frac{\partial x_3}{\partial t} \tag{2.163}$$

$$\frac{\partial x_{34}}{\partial t} = \frac{\partial x_3}{\partial t} - \frac{\partial x_4}{\partial t} \tag{2.164}$$

By making the analysis, equivalent mass-spring-damper characteristics of swashplate and blade assemblies are to be easily investigated because of the easiness of manipulation. Two different modes of frequency are expected as dynamic system in motion are consist of two equivalent masses. Simulink® model of dynamic system is given in Figure 2.26.

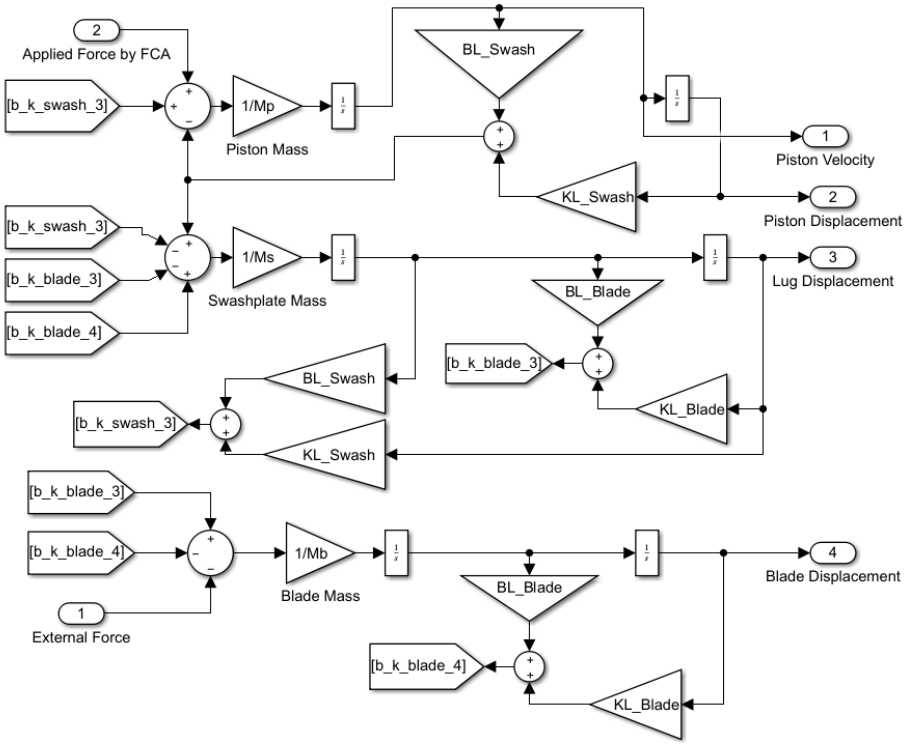

Figure 2.26 Four Degrees of Freedom Dynamic System

CHAPTER 3

EXPERIMENTAL SETUP AND TESTS

In this chapter, a developed test system for the system characterization of rotor hydraulic control system is introduced. By using the experimental test setup, both rotor control model and actuator behavior under various conditions can be examined and verified comparing with simulations. Using the test system, behavior of hydraulic actuator for pilot input is verified. Besides, helicopter SSP motion is verified by cyclic and collective inputs which involve combined motion of each actuator. Additional components that are used to construct and create necessary hydraulic pressure under safe conditions are described.

3.1 Test Setup

Experimental test setup is constructed as 1:1 exact scale of real helicopter rotor control system. Three main rotor FCAs are installed in exactly same configuration and separated from each other as 120° by the same distance. In real helicopter, each actuator is connected to one corner of the SSP triangle. Instead of real helicopter model, FCAs are connected to actuator ends of an opposite actuator without having any SSP component. Opposite actuator are used to make external loading of each actuator which are called External Load Actuator (ELA). ELAs can be separately controlled testing control system and they operate by the principle of force control. Inputs for each FCA are applied by an electrohydraulic actuator which is called Pilot Input Actuator (PIA). PIA's can also be separately controlled from each other. Relation between any pilot input and ratios of PIAs are controlled by testing control system, but arranges as same as derived kinematic ratios in 2.1. There are several Hydraulic Power System (HPS) components are used to supply necessary hydraulic pressure and flow during testiffng. Hydraulic Pump (HP) is a crucial component of

HPS as it creates and regulates hydraulic pressure without any instability under 20.7 MPa. As long as it is assumed in mathematical system that pressure is constant under 20.7 MPa, it is significant to verify retaining pressure level constant during test activity. Stability criterion of HP are defined in 3.1.2.4. There is a filter installed on the inlet of MCV pressure line which is used to prevent contamination of equipment because of hydraulic fluid that is used within the system. Preventing from contamination is significant because huge particles especially greater than 100 μm can cause severe damage and influence the performance of hydraulic actuator in a negative manner. Installed filter is capable of filtering particles higher than 5 μm referring to minimum size of the critical particle defined in SAE contamination standard [29]. There is a hydraulic tank that is used to retain necessary fluid that provides safe operation of the system. Tank is a critical component because during testing, there is a slight temperature increase and volume of the fluid increases. Thus, fluid surplus under higher temperature levels are retained in hydraulic tank. A spare amount of hydraulic fluid is kept in the tank in case of any leakage condition, preventing immediate loss of pressure and damaging FCA under external loads. Space fluid level is kept approximately at 1 L, despite capacity of the tank is much higher. There is a safety valve incorporated within the system at the pressure line to be used in case of any decrease in the pressure due to prevention of FCAs. Components and used number of them are given in Table 3.1.

Table 3.1 Equipment and Their Counts on Experimental Setup

Equipment Number	Equipment Name	# of Components
1	Hydraulic Pump (HP)	1
2	Safety Valve (SV)	1
3	Filter	1
4	Tank	1
5	Flight Control Actuator (FCA)	3
6	Pilot Input Actuator (PIA)	3
7	External Load Actuator (ELA)	3

Experimental setup is started to be constructed initially from HPS equipment to verify if necessary power, in fact pressure and flow rate, can be supplied or not. A demonstration of base construction that includes equipment that are numbered from 1 to 4 are given in Figure 3.1.

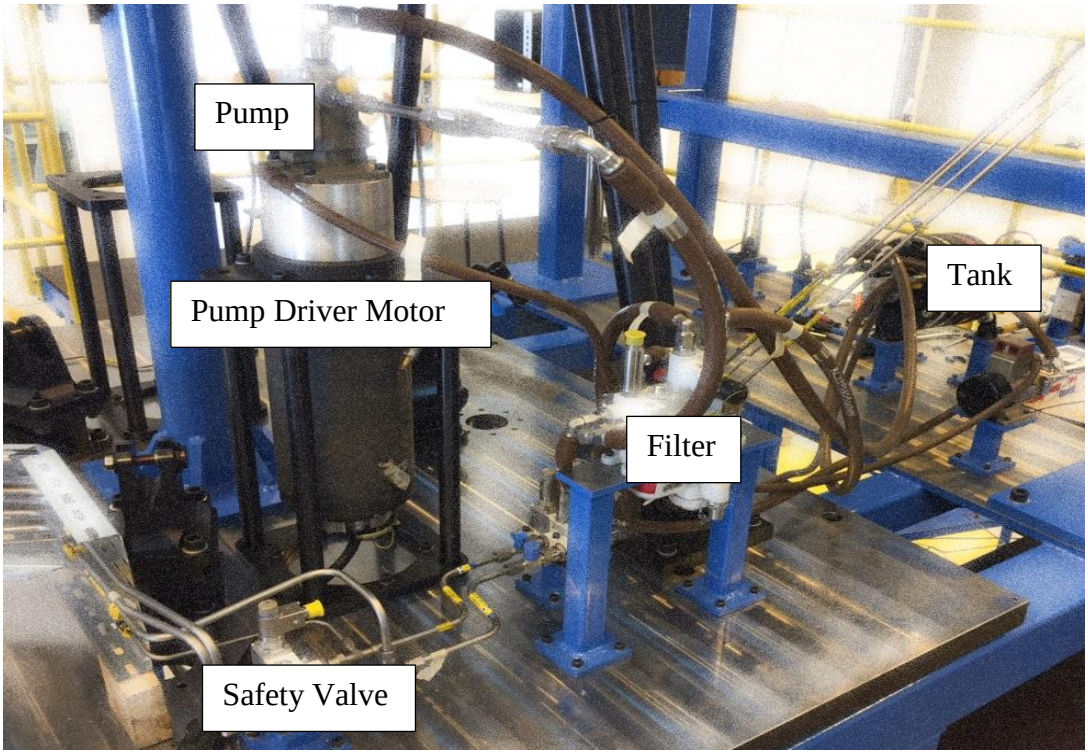

Figure 3.1 HPS Components for Necessary Pressure and Flow Rate

After installation of fundamental HPS components, FCAs are installed regarding real helicopter configuration. Input lever of FCA is driven by a PIA which is also installed and cylinder of PIA is connected to pilot input point of input lever. After that, ELA is installed and cylinder end of ELA is connected with cylinder output end of FCA. Force, pressure, displacement sensors are installed between necessary points on the hydraulic or mechanical circuit. ELA/PIA and their connections to Right FCA cylinder output are demonstrated in Figure 3.2 and Figure 3.3 [30].

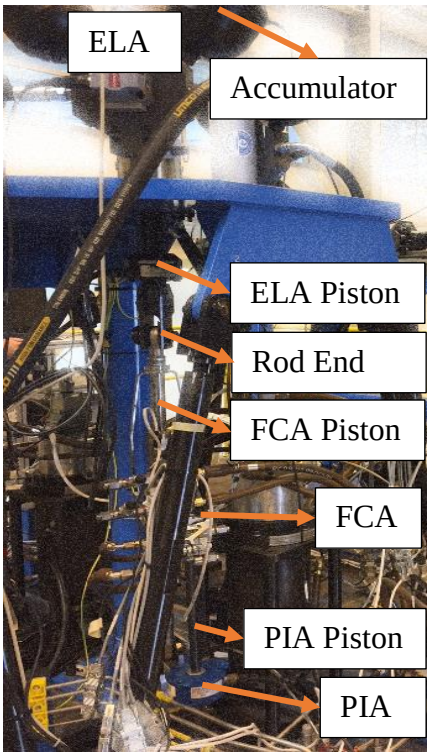

Figure 3.2 ELA/PIA and Their Connections to Right FCA [30]

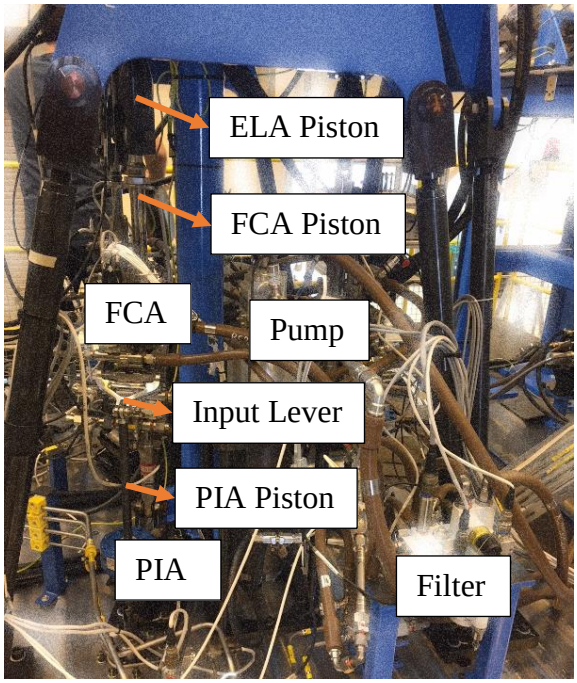

Figure 3.3 Additional View: ELA/PIA and Their Connections to Right FCA [30]

To demonstrate the exactness of mechanical and hydraulic connections that are applied to Left FCA, installation of Left FCA is given in Figure 3.4 [30].

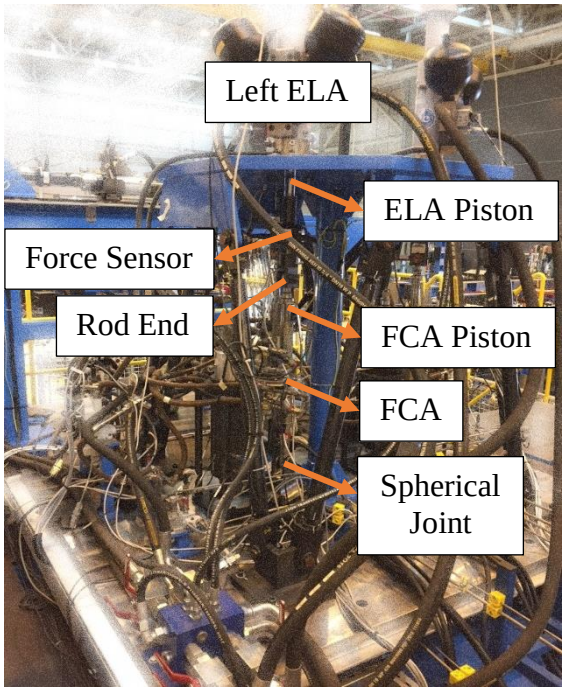

Figure 3.4 ELA and Its Connections to Left FCA [30]

3.1.1 Schematic Representation and Operation Principle

Input of FCAs is given by using PIAs instead of pilot via mechanically connected rod and bell crank assemblies. Instead, all PIAs are controlled and for the given amount of pilot input, they are displaced with an adjusted ratio which is equal to actual helicopter pilot input/input lever ratio. Despite lack of loads transmitted from rotor components, ELA actuator is put to simulate static and dynamic loads acting on each actuator separately. ELAs are operated by force control principle in case of arising excessive loads that instantaneously acting on FCA cylinder. FCA, ELA and PIA are fixed to a structure of test setup. Schematic representation for the clear comprehension of test setup is demonstrated in Figure 3.5 for a single actuator.

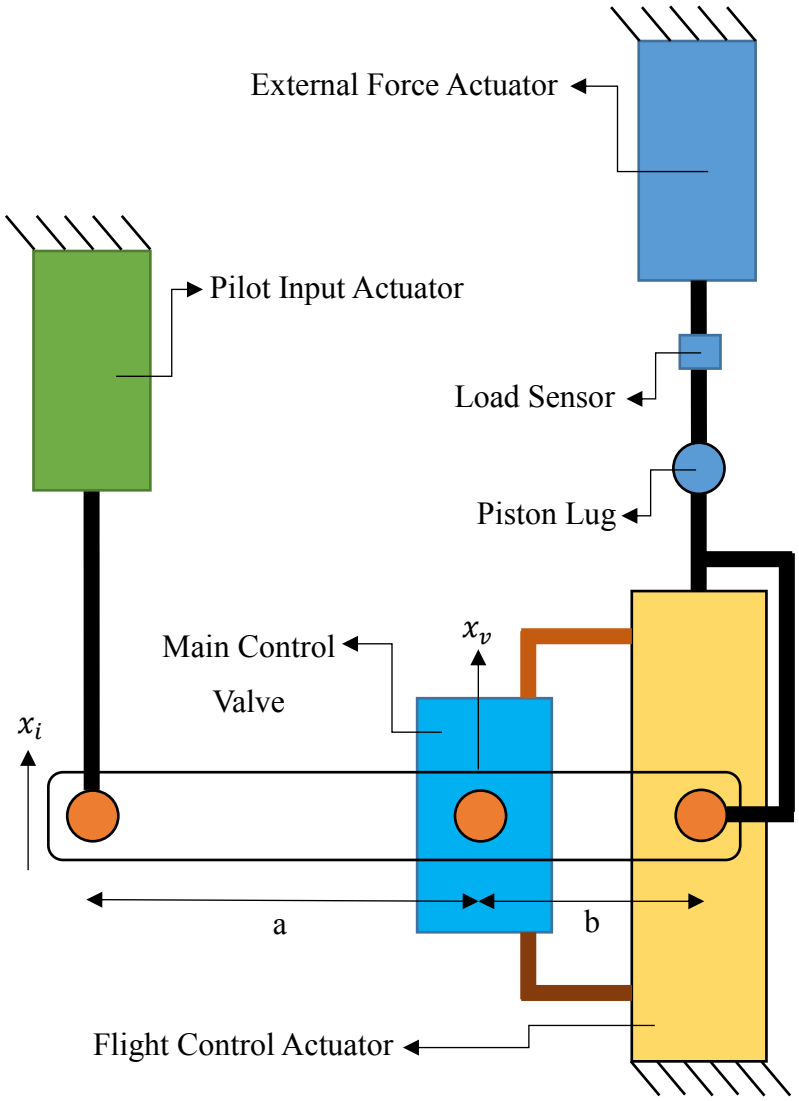

Figure 3.5 Schematic Representation of Test Setup for a Single FCA

For each FCA, several sensors are used to obtain system characterization. Displacement, force and pressure values are obtained from these locations in certain frequencies. Due to be confident of constant pressure supply, pressure data is taken in high resolution (>1000 Hz). Displacement and Load data are taken in low resolution, but it is sufficient to observe peak load, load trend and peak displacement values. (>100 Hz). Measurement locations and frequency ranges are given in the Appendix A.

3.1.2 Components of Test Setup

Test Setup consist of several main components that are used to create necessary simulation parameters and sustain test setup with ideal condition. Especially in a test rig that requires huge forces and sensitive control of them, significance of sub-components is more significant. Information is provided in following chapters about properties of sub-components.

3.1.2.1 Hydraulic Fluid:

Selection of hydraulic fluid is significant for obtaining healthy test data because mathematical model of hydraulic fluid is constructed as compressible fluid. Thus, compressibility of the fluid plays a critical role in any time step during tests. In aircraft applications, there are several common hydraulic fluids are to be used regarding the design standards. Among these hydraulic fluids [31][32][33], MIL-H-87257 is selected in all test runs. Value of Bulk Modulus (β) is also taken from the specification of the fluid. Bulk Modulus is given for 40°C in the specification; however, as hydraulic fluids behave linear characteristic in narrow ranges and tests are executed between 25-45°C conditions, Bulk Modulus is taken as constant as this value in mathematical model. Properties of the hydraulic fluid are given in Table 3.2.

Table 3.2 Properties of Hydraulic Fluid

Fluid Property	Specification
Reference Specification	MIL-H-87257
Kinematic Viscosity (mm^2/s)	6.7 @ 40°C
Bulk Modulus (Pa)	1.379×10^9
Flash Point (°C)	160
Fire Point (°C)	170
Pour Point (°C)	-60

3.1.2.2 External Load Actuator (ELA):

ELAs are installed on opposite of each actuator. They are used to apply external loads on FCAs axially. They have several qualities which enables to simulate flight conditions. Initially, they can be used to demonstrate the inertial effects of rotor components in a realistic way by using an adjustable force controller. Owing to forces controller, transient forces coming from rotor components can be considered. Additionally, they can be used to apply static forces on FCA to simulate aerodynamic loads coming from rotor blades caused by pitch angle of rotor blades. Besides, dynamic loads can also be simulated which refers to varying loads on FCA because of rotation of swashplate in non-zero pitch and roll angles as well as disturbances tat are acting on rotor components. Properties of ELAs are given in Table 3.3.

Table 3.3 Properties of External Load Actuator (ELA)

ELA Property	Specification
Effective Area (m^2)	7.85×10^{-4}
Stroke (m)	0.08
Load Capacity (N)	16250
Power Source	Hydraulic
Operation Pressure (Pa)	20.7×10^{6}
Maximum Rate (m/s)	0.22

3.1.2.3 Pilot Input Actuator (PIA):

PIAs are installed at the input lever of each actuator to simulate pilot inputs. They can give inputs up to 4 Hz frequency. As they compete with the lever force only does not take any flight loads, their load capacity is comparably smaller than ELAs and FCAs. Command of PIA is also processed with transfer function of PIA before applying it to input lever as in input to FCA. Thus, divergence between ideal command and actual applied command via PIA is clearly defined. Properties of PIA are given in Table 3.4.

Table 3.4 Properties of Pilot Input Actuator (PIA)

PIA Property	Specification
Effective Area (m^2)	4.83×10^{-5}
Stroke (m)	0.06
Load Capacity (N)	1000
Power Source	Hydraulic
Operation Pressure (Pa)	20.7×10^6
Maximum Rate (m/s)	0.35

3.1.2.4 Hydraulic Pump (HP):

HP is used to sustain overall pressure of HPS in any input condition and enable system to perform necessary flight conditions as HP feeds all FCAs, PIAs and ELAs simultaneously. It includes a pressure regulator inside the pump which retains pressure level constant independent from instantaneous rpm value. Pressure of the HP can be evaluated as stable and constant as it compensates, and pressure decrease under 20.7 Pa within 50 ms. In all test conditions, this criterion is provided; thus, proposal of constant system pressure for the exact simulation of the mathematical model is provided. Properties of PIA are given in Table 3.5.

Table 3.5 Properties of Hydraulic Pump (HP)

HP Property	Specification
Flow Capacity (L/min)	59.2
Pressure (Pa)	21.2×10^6 @ zero flow
Pressure (Pa)	20.1×10^6 @ full flow
Mechanical Efficiency	0.85
Revolutionary Range (rpm)	5500-11500

3.1.2.5 Tank:

Tank is used to retain necessary amount of fluid during testing activity. In case of any leakage condition, it protects instantaneously damaging of equipment. Besides, it compensates fluid diminution during temperature decrement. For any temperature increment, surplus fluid is delivered to hydraulic tank. Properties of Tank are given in Table 3.6.

Table 3.6 Properties of Tank

Tank Property	Specification
Fluid Capacity (L)	1.2 L
Pressure (Pa)	4.2×10^5
Type	Cylinder Type

3.1.2.6 Safety Valve (SV):

Safety valve is as three-way two position mechanically activated valve operating with the pilot pressure of high-pressure line. In case of any pressure drop, safety valve cuts the flow to the al consumers for the protection of equipment.

3.1.3 Test Configuration

There are two different types of test activity executed to comprehend the behavior of the system. Tests can be divided as Step Input and Sinusoidal Input tests. During all test activities, temperature is maintained around 25°C; thus, temperature does not have any effect on system behavior of any independent test. Test results are evaluated in terms of compatibility of path tracking and frequency response domain.

3.1.3.1 Step Input Tests

In the test activity, 6 different types of step input are given via 3 types of input to main rotor. Step inputs can be listed as Forward Cyclic (FWD_CYC), Backward Cyclic, (AFT_CYC), Leftwards Cyclic (LEFT_CYC), Rightwards Cyclic (RIGHT_CYC), Upwards Collective (UP_COL) and Downwards Collective (DOWN_COL). Step inputs are given several times for each test and input is bring to neutral position afterwards. It can be evaluated that step inputs are very similar among each other. Executed tests are listed in Table 3.7.

Table 3.7 Executed Tests with Step Input

Test Name	x_i^F(cm)	x_i^R(cm)	x_i^L(cm)	t_{step}
FWD_CYC	+2	-1	-1	0.3
AFT_CYC	-2	+1	+1	0.3
LEFT_CYC	0	+1	-1	0.3
RIGHT_CYC	0	-1	+1	0.3
UP_COL	-1	-1	-1	0.3
DOWN_COL	+1	+1	+1	0.3

Mathematical formula for the step input is provided in (3.1), where A_{step} represents the amplitude of the response arranged manually for any step input and t_d represents delay time of the step input.

$$x_i(t) = \frac{A_{step} \tanh(24(t - t_d) + 1)}{2} \tag{3.1}$$

3.1.3.2 Sinusoidal Input Tests

Sinusoidal Input tests are executed to understand the frequency response behavior of the control system and compare it to theoretical results. To search for the frequency

band, frequencies from 0.25 Hz up to 4 Hz are given via PIA ad cylinder output response is tracked. Executed tests are listed in Table 3.8.

Table 3.8 Executed Tests with Sinusoidal Input

Test Name	x_i^F(cm)	f_i	t_{sin}
LOW_F	-1 / +1	0.217	30
LOWMID_F	-1 / +1	0.434	30
MID_F	-1 / +1	0.868	30
MIDHIGH_F	-1 / +1	3.472	10
HIGH_F	-1 / +1	6.944	5

3.1.4 Test Results

It is required to evaluate step and sinusoidal input test results from different perspectives; therefore, test results are obtained for step inputs and sinusoidal inputs separately and provided in independent sections.

3.1.4.1 Step Inputs

There are six different types of step input that can be given to SSP to change pitch angles of the blades of main rotor. Thus; six different step inputs are inspected under divergent sections.

3.1.4.1.1 Forward Cyclic (FWD_CYC)

In FWD_CYC test, a forward cyclic input is given that results in 3 cm negative displacement in Forward FCA and simultaneously, 1.5 cm positive displacements of left and right FCAs. Opposite force that is applied on FCAs is selected as 5 kN static± 1 kN dynamic. Input command and actual inputs of FCAs for FWD_CYC test is provided in Figure 3.6.

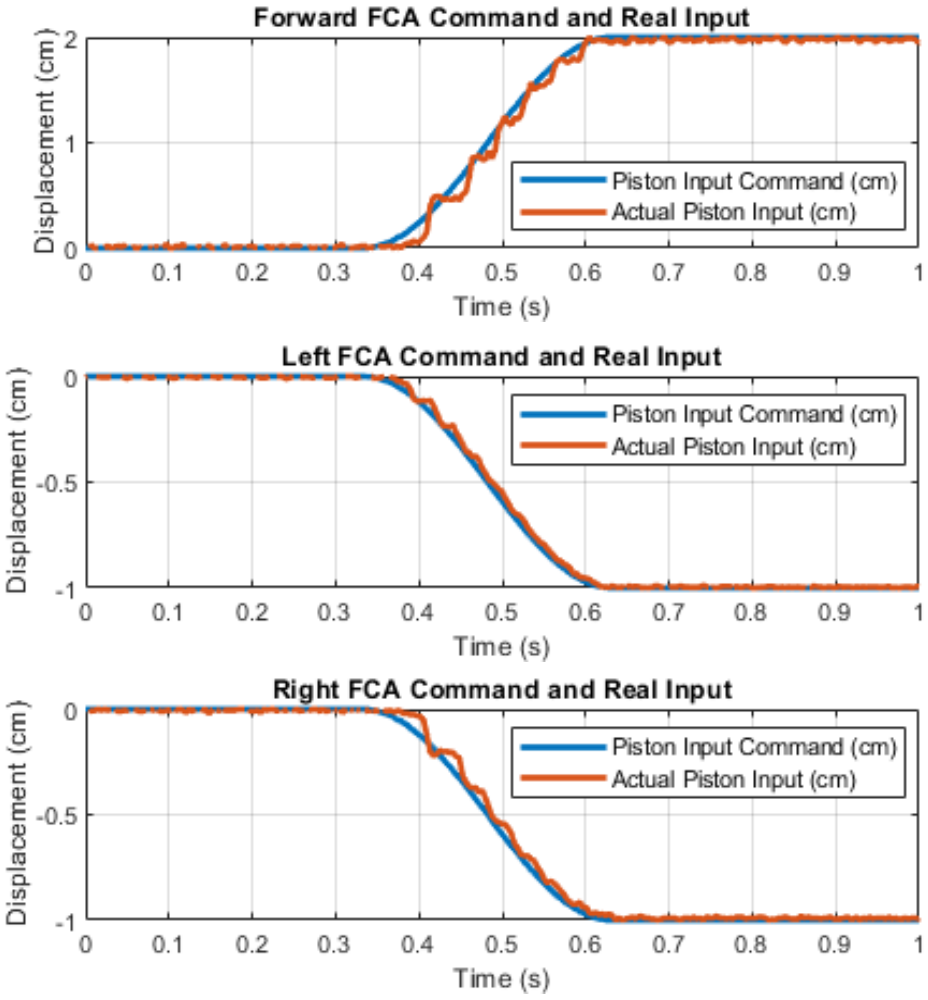

Figure 3.6 Experimental Forward, Left and Right FCA Pilot Input Command (FWD_CYC)

By the given inputs, obtained outputs and desired outputs derived from actual cylinder input for each individual actuator for FWD_CYC test are provided in Figure 3.7.

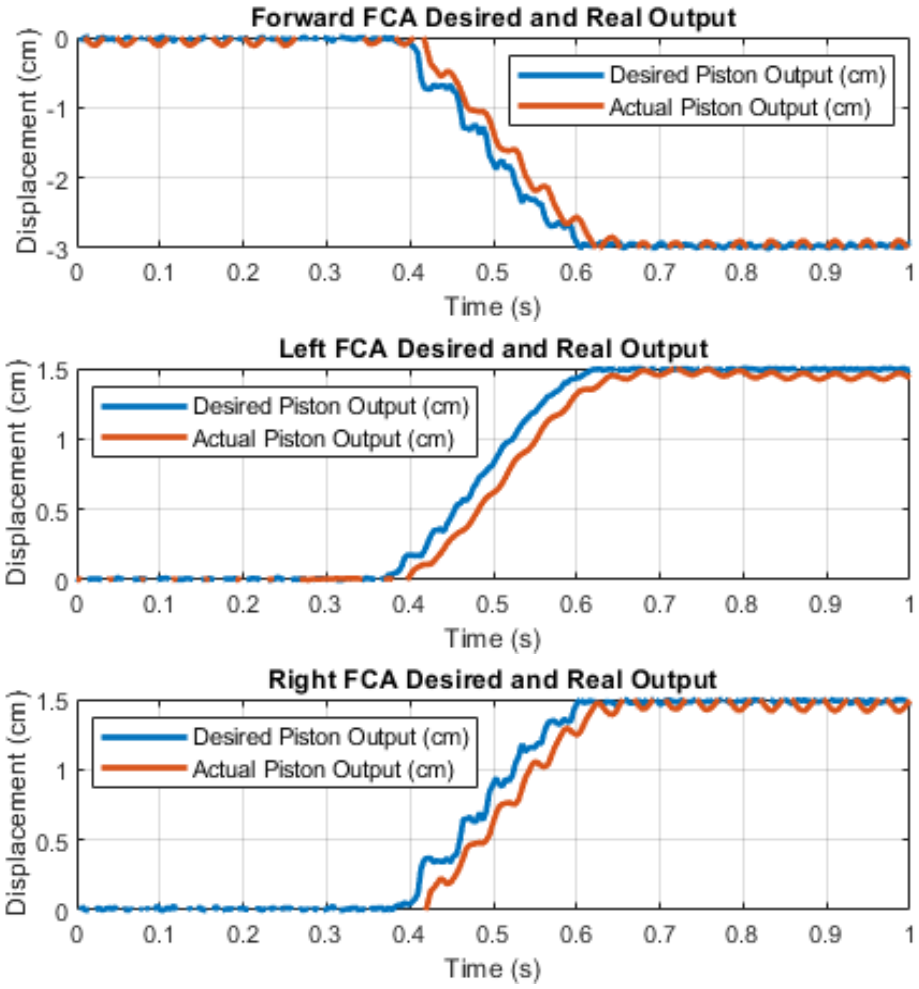

Figure 3.7 Experimental Forward, Left and Right FCA Cylinder Output (FWD_CYC)

Pressures of each FCA inlet are demonstrated for FWD_CYC test in Figure 3.8.

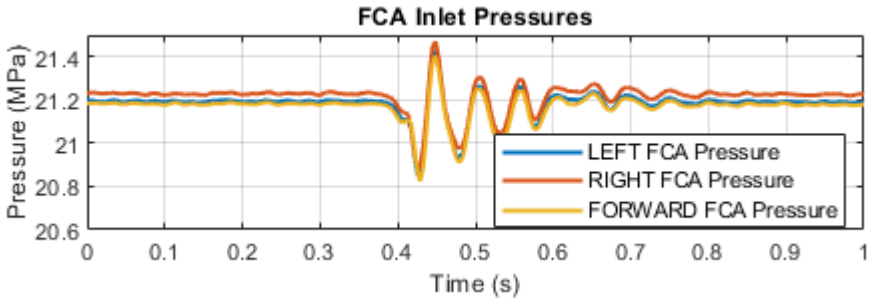

Figure 3.8 Inlet Pressures During Test Activity (FWD_CYC)

3.1.4.1.2 Backward Cyclic (AFT_CYC)

In AFT_CYC test, a backward cyclic input is given that results in 3 cm positive displacement in Forward FCA and simultaneously, 1.5 cm negative displacements of left and right FCAs. Opposite force that is applied on FCAs is selected as 5 kN static ± 1 kN dynamic. Input command and actual inputs of FCAs for AFT_CYC test is provided in Figure 3.9.

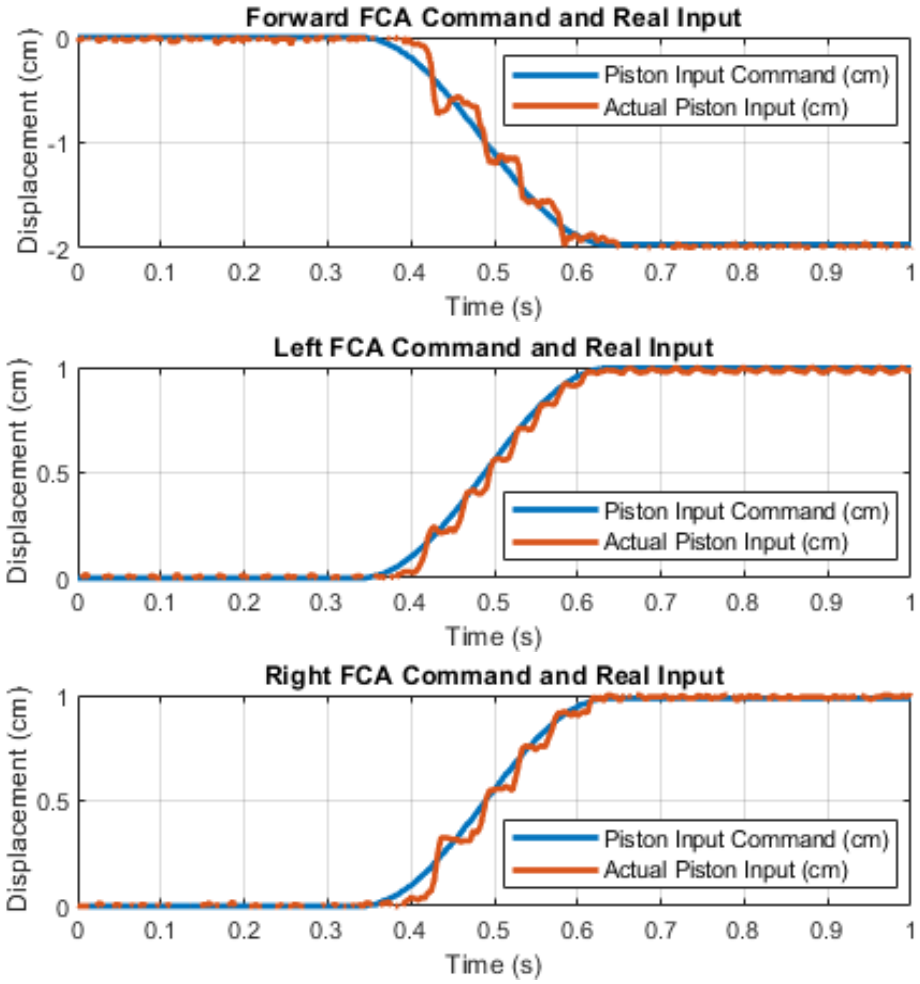

Figure 3.9 Experimental Forward, Left and Right FCA Pilot Input Command (AFT_CYC)

By the given inputs, obtained outputs and desired outputs derived from actual cylinder input for each individual actuator for AFT_CYC test are provided in Figure 3.10,

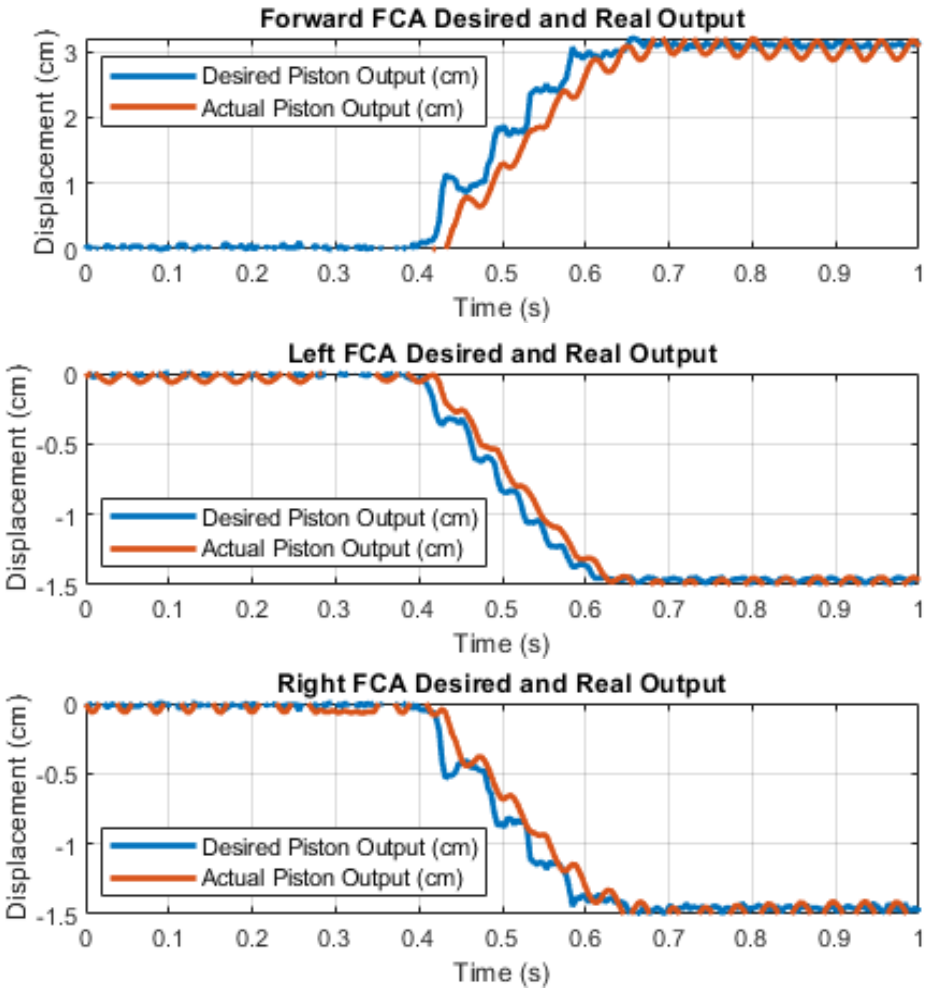

Figure 3.10 Experimental Forward, Left and Right FCA Cylinder Output (AFT_CYC)

Pressures of each FCA inlet are demonstrated for AFT_CYC test in Figure 3.11.

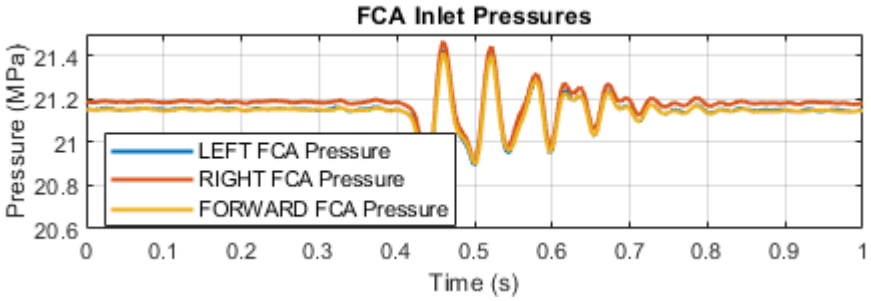

Figure 3.11 Inlet Pressures during Test Activity (AFT_CYC)

3.1.4.1.3 Leftwards Cyclic (LEFT_CYC)

In LEFT_CYC test, a forward cyclic input is given that results in no displacement in Forward FCA and simultaneously, 1.5 cm negative displacement of left and 1.5 cm positive displacement of right FCAs. Opposite force that is applied on FCAs is

selected as 5 kN static± 1 kN dynamic. Input command and actual inputs of FCAs for LEFT_CYC test is provided in Figure 3.12.

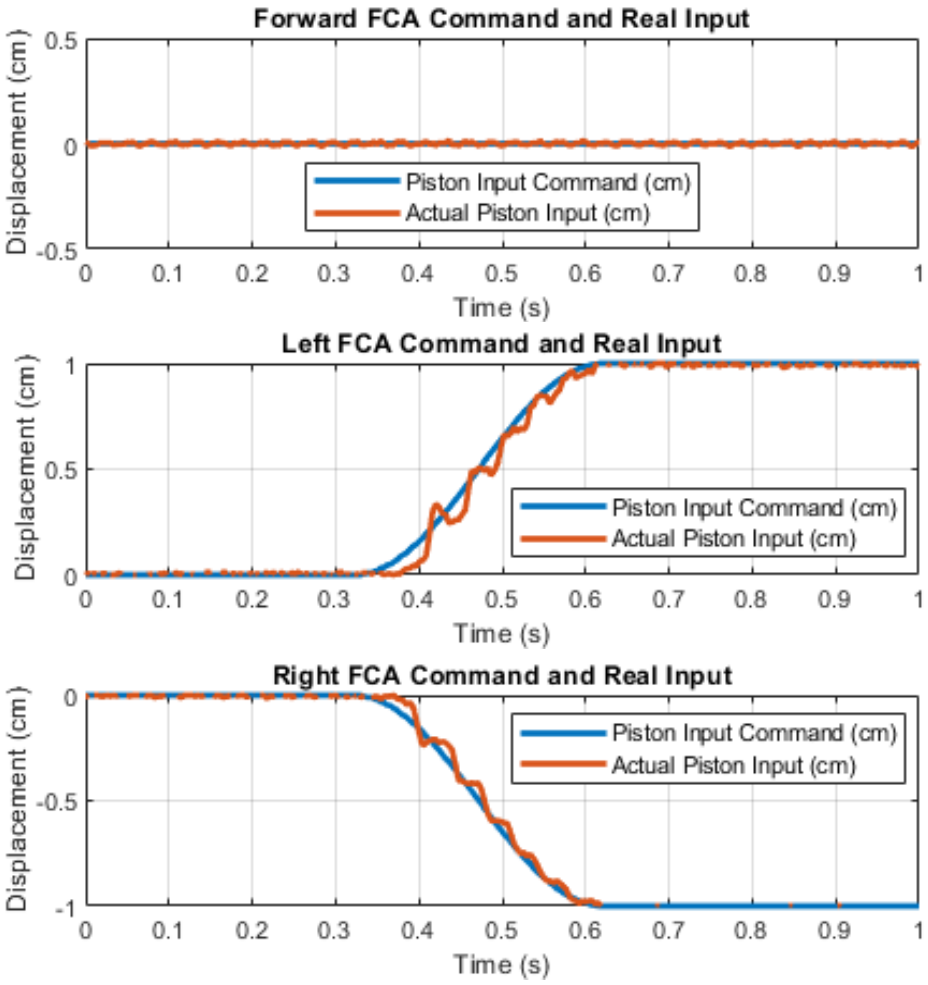

Figure 3.12 Experimental Forward, Left and Right FCA Pilot Input Command (LEFT_CYC)

By the given inputs, obtained outputs and desired outputs derived from actual cylinder input for each individual actuator for LEFT_CYC test are provided in Figure 3.13,

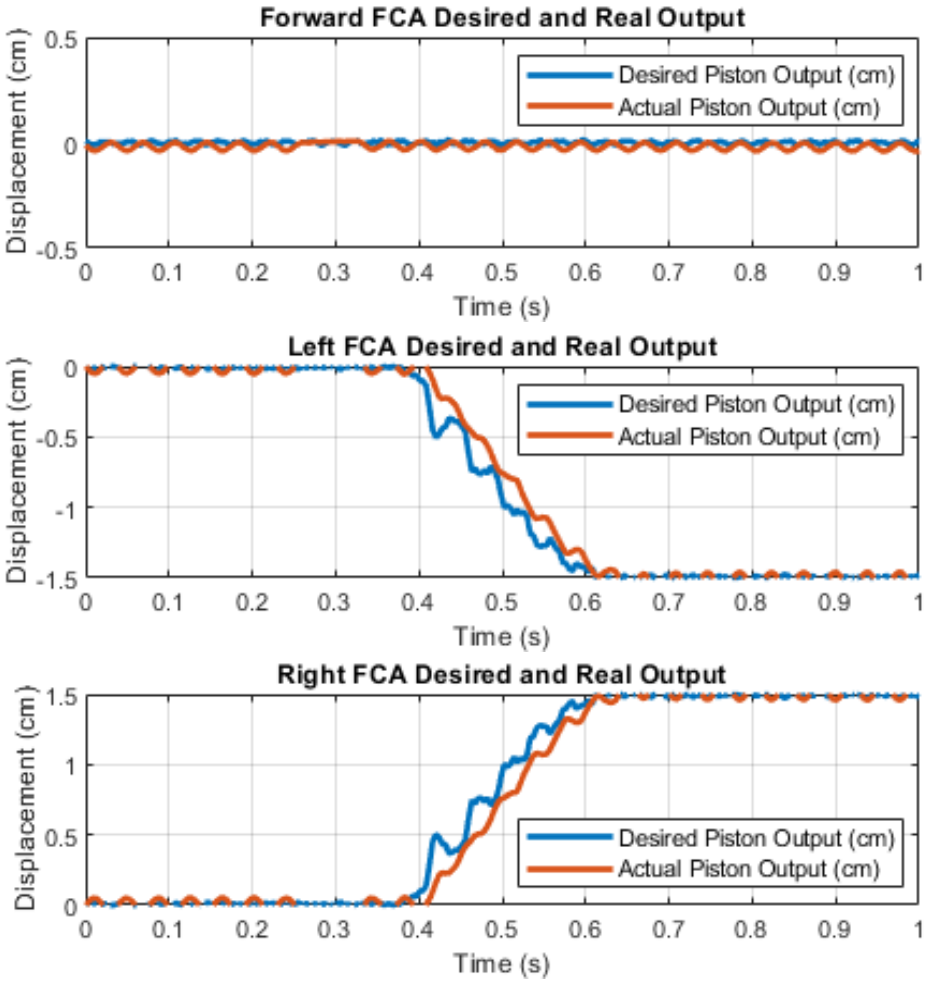

Figure 3.13 Experimental Forward FCA Cylinder Output (LEFT_CYC)

Pressures of each FCA inlet are demonstrated for LEFT_CYC test in Figure 3.14.

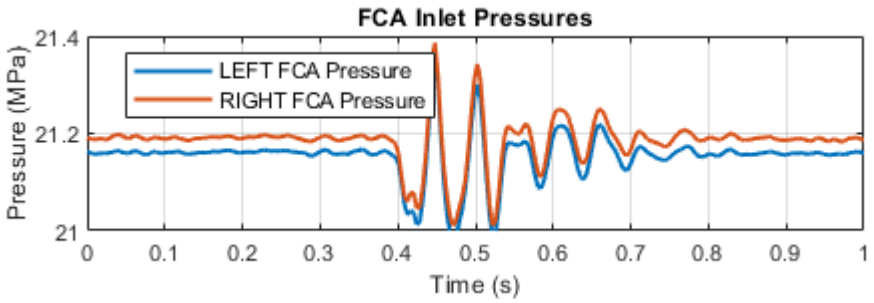

Figure 3.14 Inlet Pressures During Test Activity (LEFT_CYC)

3.1.4.1.4 Rightwards Cyclic (RIGHT_CYC)

In RIGHT_CYC test, positive lateral cyclic input is given to the system that results in 1.5 cm negative displacement of Right FCA and 1.5 cm positive displacement in Left FCA in steady state condition. Opposite force that is applied on FCAs is selected as 5 kN static± 1 kN dynamic. Input command and actual inputs of FCAs for RIGHT_CYC test is provided in Figure 3.15.

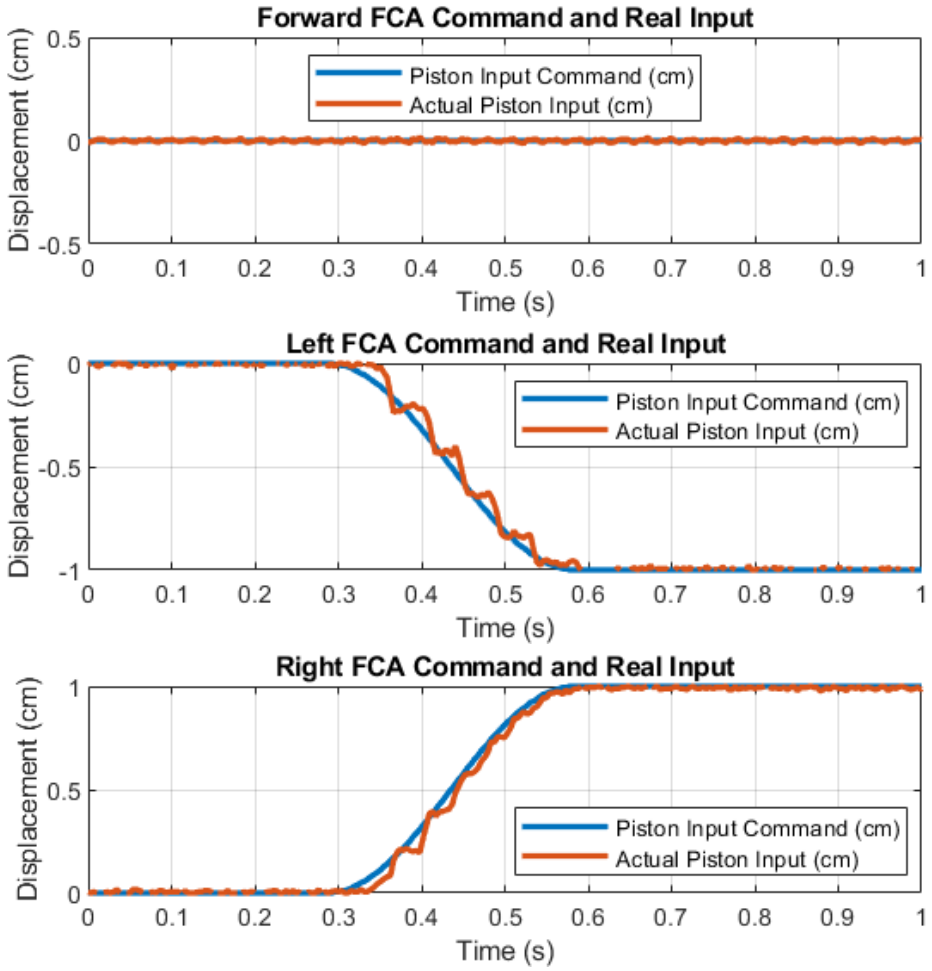

Figure 3.15 Experimental Forward, Left and Right FCA Pilot Input Command (RIGHT_CYC)

By the given inputs, obtained outputs and desired outputs derived from actual cylinder input for each individual actuator are provided in Figure 3.16.

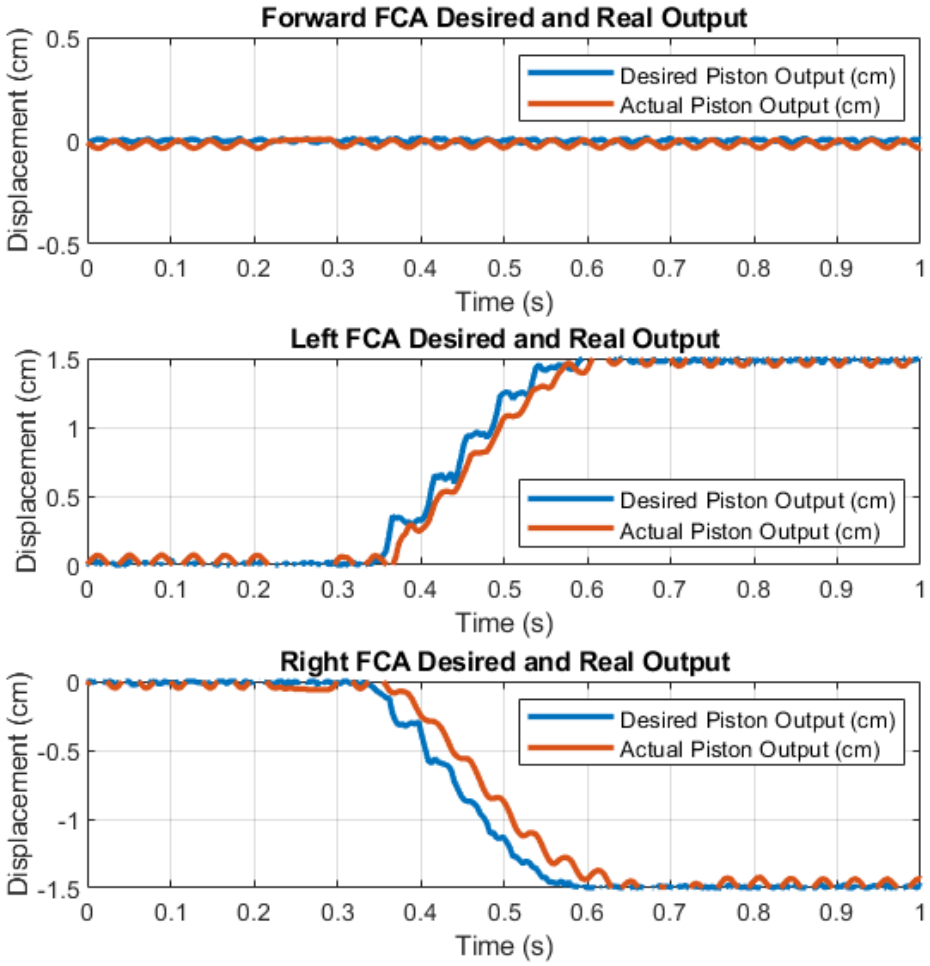

Figure 3.16 Experimental Forward FCA Cylinder Output (RIGHT_CYC)

Pressures of each FCA inlet are demonstrated in Figure 3.17.

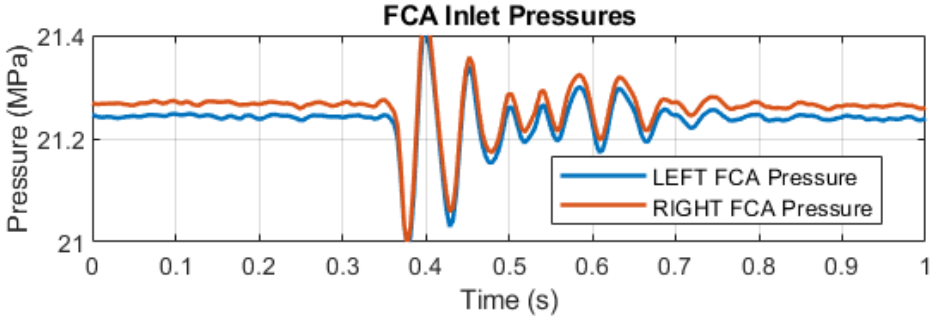

Figure 3.17 Inlet Pressures During Test Activity (RIGHT_CYC)

3.1.4.1.5 Upwards Collective (UP_COL)

In UP_COL test, a Collective input is given which results in -1 cm displacement of pilot input (x_i) each FCA simultaneously. That results in 1.5 cm steady state displacement of each FCA. Besides, 5 kN static ± 1 kN dynamic force is applied on each FCA by ELAs as opposite force. Input command and actual inputs of FCAs for UP_COL test is provided in Figure 3.18.

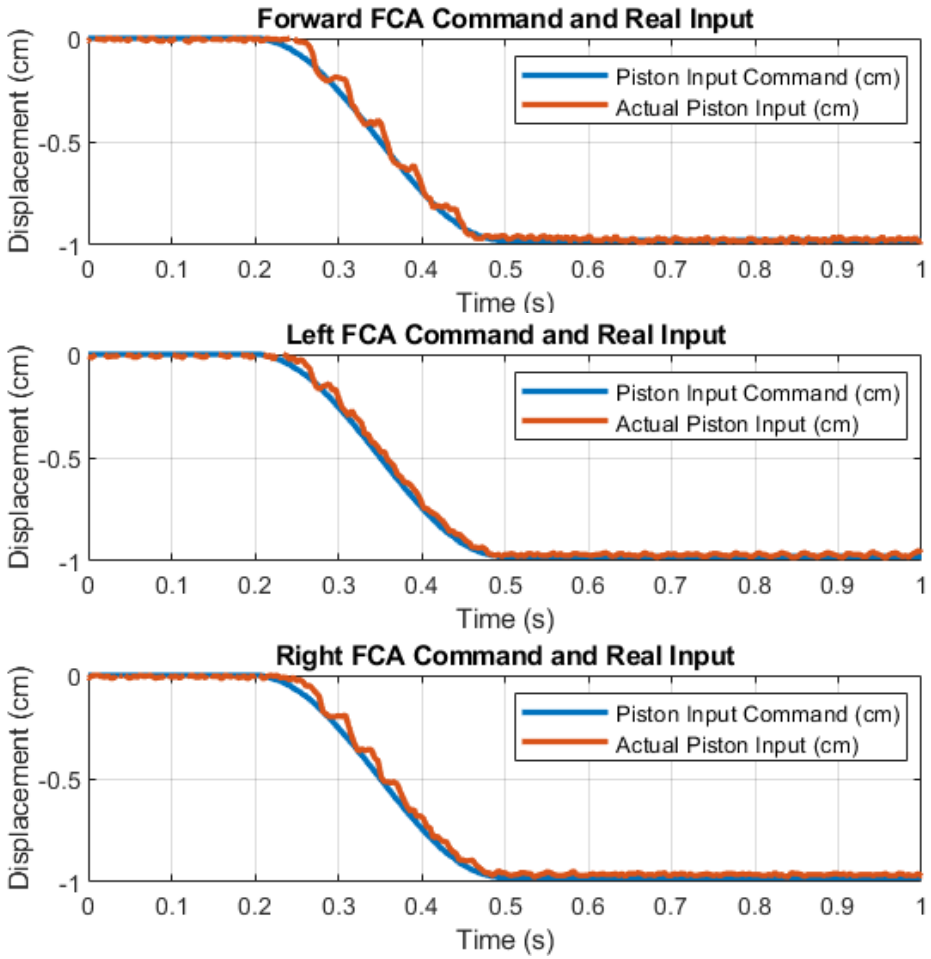

Figure 3.18 Experimental Forward, Left and Right FCA Pilot Input Command (UP_COL)

By the given inputs, obtained outputs and desired outputs derived from actual cylinder input for each individual actuator are provided in Figure 3.19.

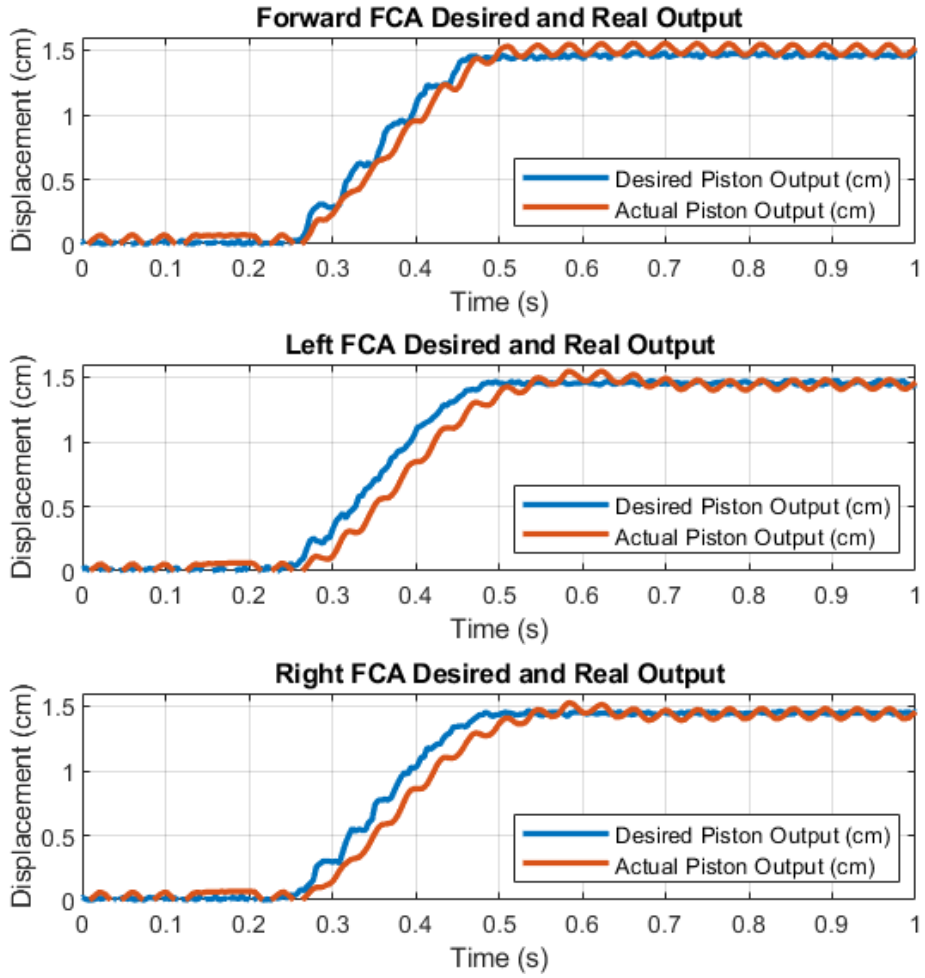

Figure 3.19 Experimental Forward, Left and Right FCA Cylinder Output (UP_COL)

During test activities, inlet pressures of FCAs are sustained higher than 21 MPa and transient cases are recovered within the limits. Inlet pressures for UP_COL are given in Figure 3.20.

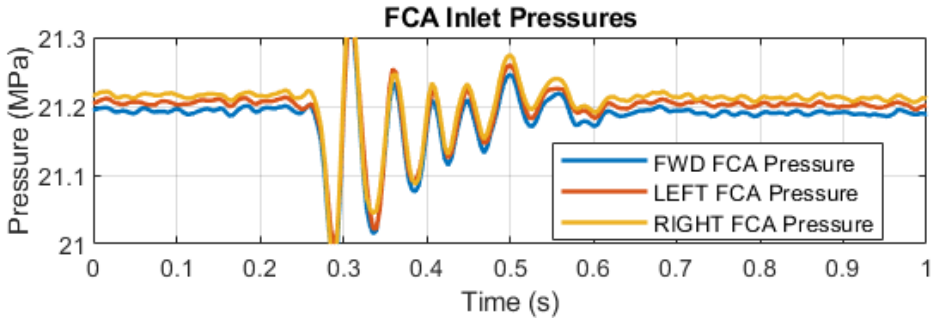

Figure 3.20 Inlet Pressures during Test Activity (UP_COL)

3.1.4.1.6 Downwards Collective (DOWN_COL)

In DOWN_COL test, a Collective input is given which results in 1 cm displacement of pilot input (x_i) each FCA simultaneously. That results in -1.5 cm steady state displacement of each FCA. Likewise, in 3.1.4.1.5, kN static ± 1 kN dynamic force is applied on each FCA by ELAs as opposite force, command and actual inputs of FCAs for DOWN_COL test is provided in Figure 3.21.

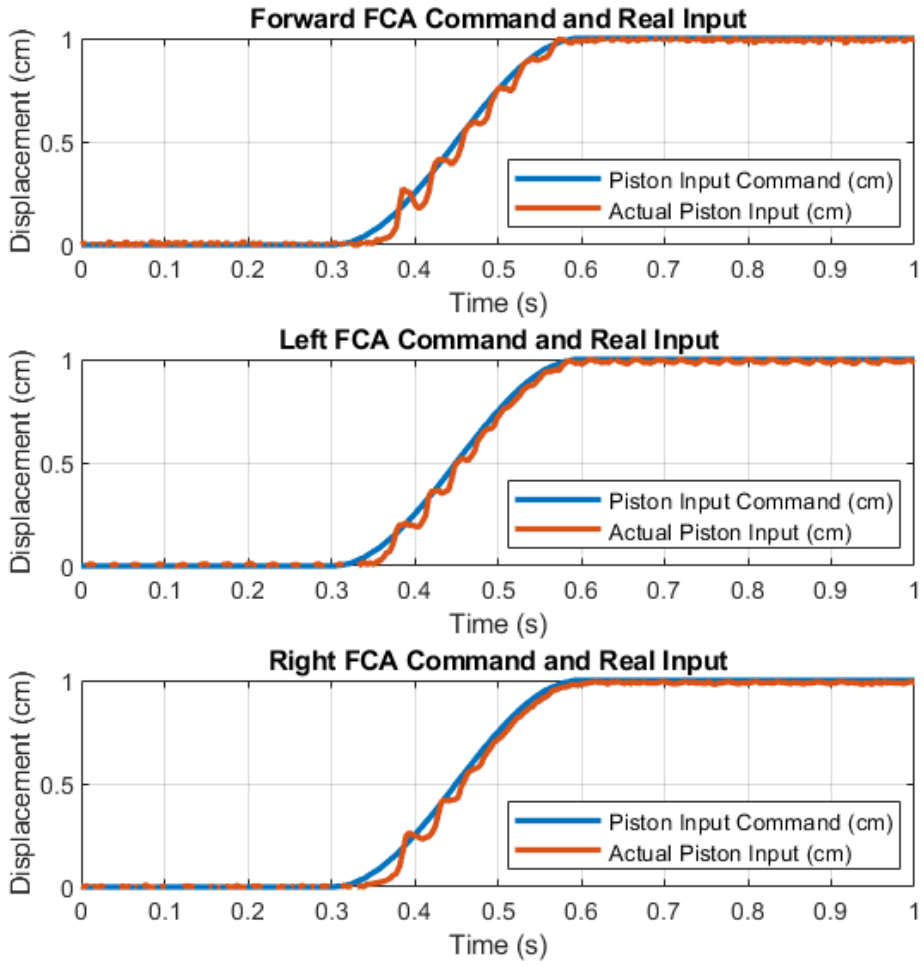

Figure 3.21 Experimental Forward, Left and Right FCA Pilot Input Command (DOWN_COL)

Again, output of the cylinder is tracked comparison between desired output derived from given real input to FCA is made. Thus, output of each actuator are given in Figure 3.22.

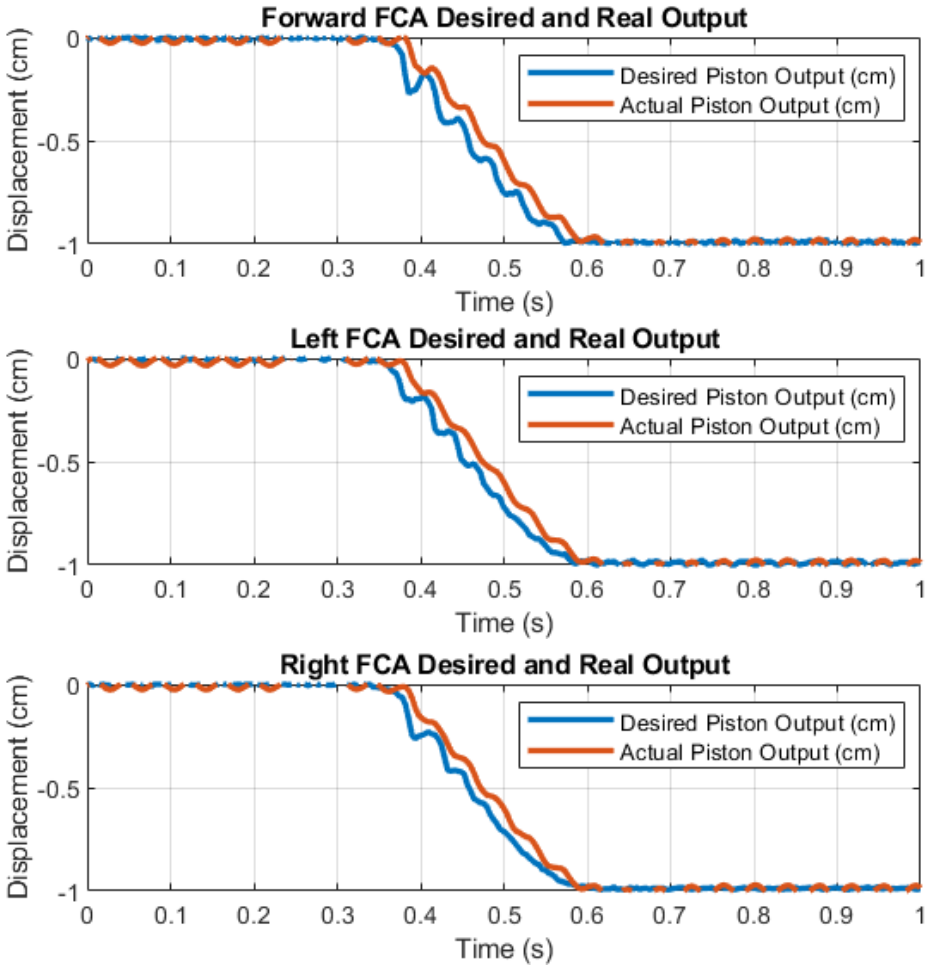

Figure 3.22 Experimental Forward, Left and Right FCA Cylinder Output (DOWN_COL)

Pressures of each FCA inlet are demonstrated in Figure 3.23.

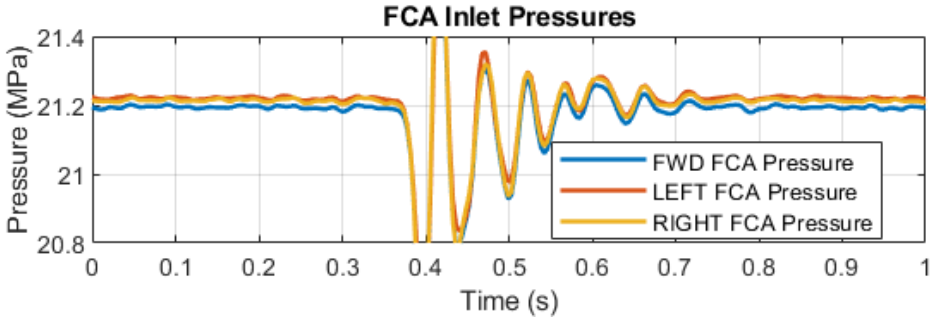

Figure 3.23 Inlet Pressures During Test Activity (DOWN_COL)

3.1.4.2 Sinusoidal Inputs

Purpose of the sinusoidal input test is to determine the frequency response range of the FCA. All along the test, system response is tracked in terms of amplitude and phase lag. Testing inputs are given to a single FCA instead of tracking the performance of all actuators because they are identical actuator and frequency response characteristic of these actuators are also identical. During test activity, position of pilot input point and cylinder output point in the input lever is tracked as well as pressure variation of the actuator and external load that is applied during test activity. Besides, external load is applied with a dynamic oscillation due to inspect if there is any excitation on high frequencies up to 20 Hz. On the other hand, test inputs are given to the system from 0.29 Hz up to 9.2 Hz separately. During test activity, amplitude gain and phase lag of each cycle in independent test activities are measured and recorded. An overall value from the recorded data is obtained in case of minimizing the error of the test. For each cycle, a local peak founder is used to determine each peak separately. After that, overall value is obtained by summing all positive peaks and absolute of negative peaks, dividing them into the two times of the number of cycles. Phase lag is found by setting the zero of each cycle as reference and extracting the time difference of each cycle when the displacement goes exactly on the reference. Then, overall value of these time differences are divided into a length of cycle.

3.1.4.2.1 Low Frequency Test (LOW_F)

Low frequency test is named as LOW_F in which a 0.217 Hz sinusoidal input is given to the pilot input point of the FCA via PIA. Input and output displacements, magnified view of output displacement and desired position, inlet pressure and external load applied via ELA are given from Figure 3.24 to Figure 3.28, successively.

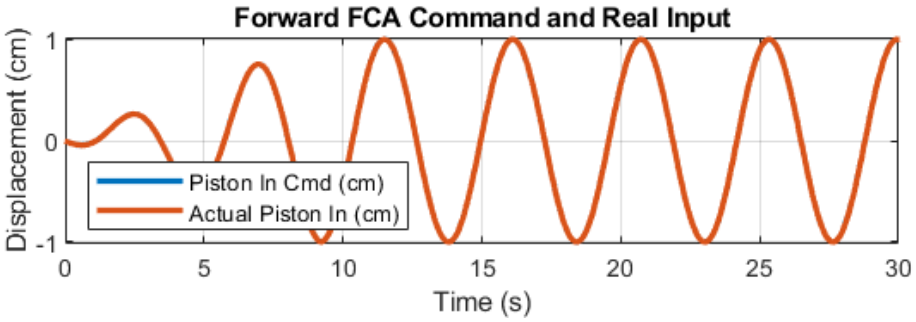

Figure 3.24 Experimental FCA Pilot Input Command (LOW_F)

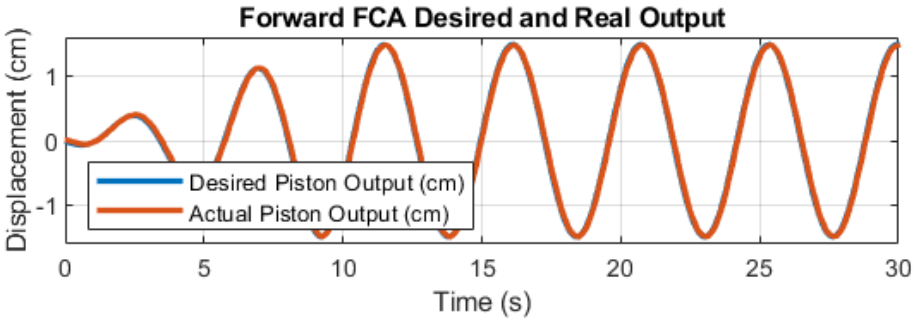

Figure 3.25 Experimental FCA Cylinder Output (LOW_F)

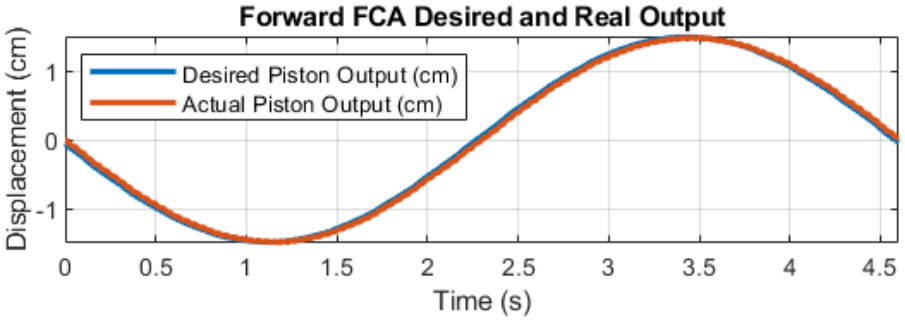

Figure 3.26 Magnified FCA Cylinder Output (LOW_F)

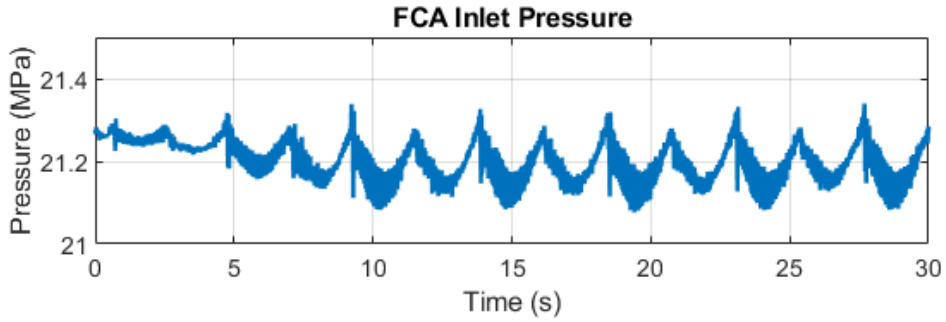

Figure 3.27 Inlet Pressure of FCA during Test

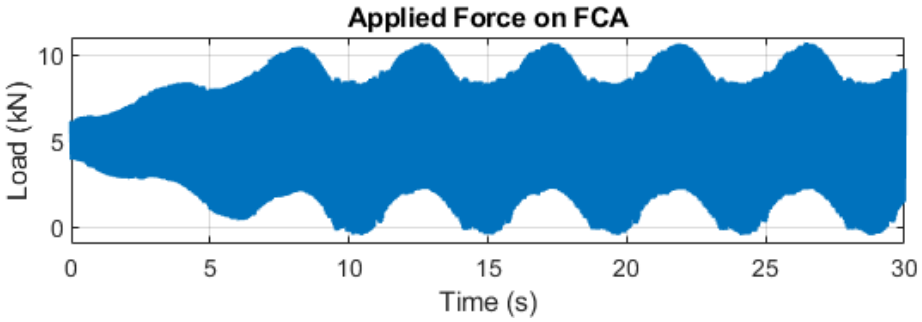

Figure 3.28 External Load Applied on FCA during Test

During low frequency tests, amplitude is calculated as -0.05 dB from the recorded data and phase lag is calculated as 1.96°.

3.1.4.2.2 Low-Mid Frequency Test (LOWMID_F)

Low-Medium frequency test is named as LOWMID_F in which a 0.434 Hz sinusoidal input is given to the pilot input point of the FCA via PIA. Input and output displacements, magnified view of output displacement and desired position, inlet pressure and external load applied via ELA are given from Figure 3.29 to Figure 3.33, successively.

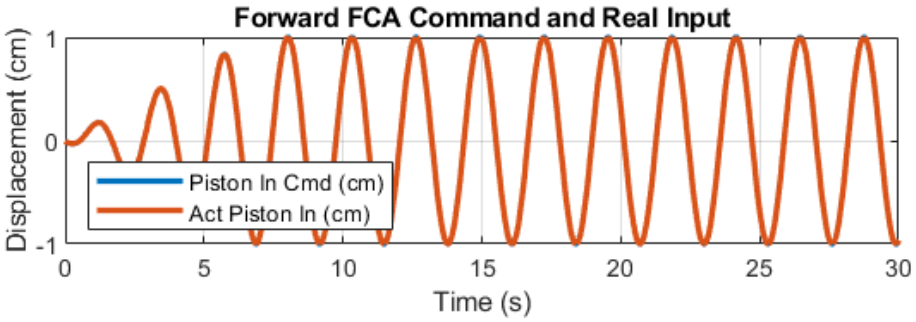

Figure 3.29 Experimental FCA Pilot Input Command (LOWMID_F)

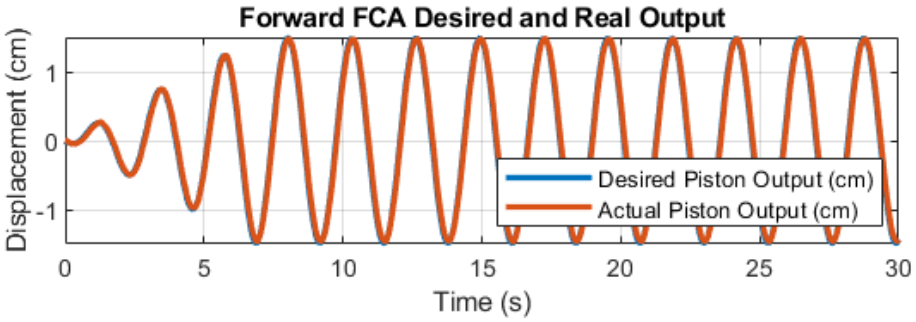

Figure 3.30 Experimental FCA Cylinder Output (LOWMID_F)

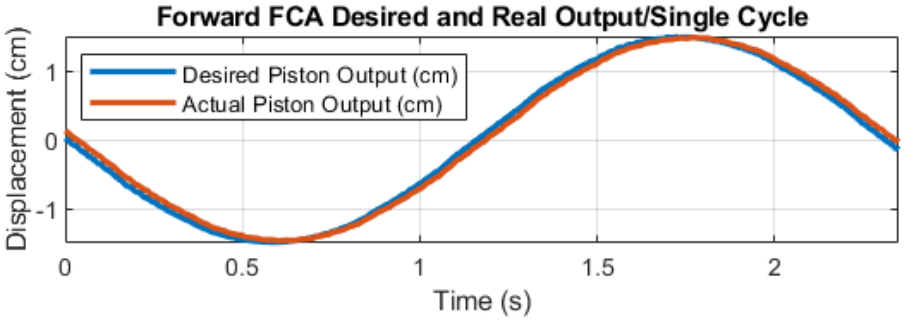

Figure 3.31 Magnified FCA Cylinder Output (LOWMID_F)

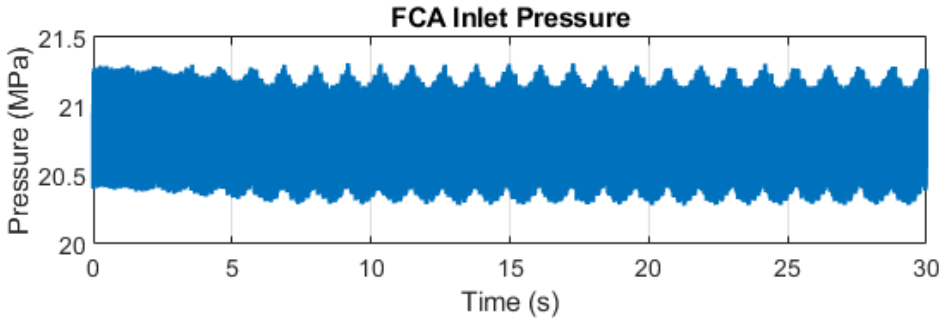

Figure 3.32 Inlet Pressure of FCA during Test (LOWMID_F)

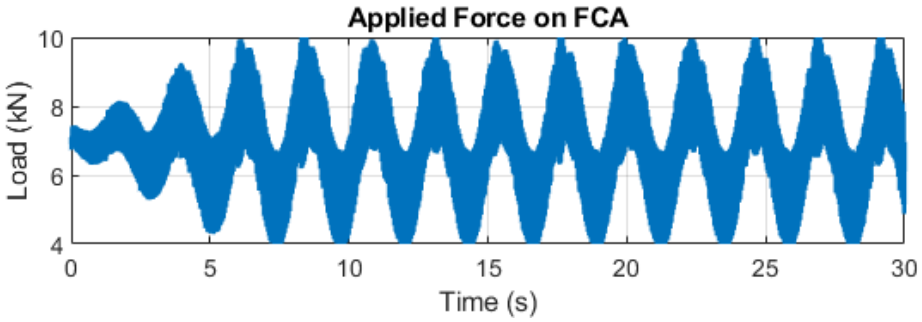

Figure 3.33 External Load Applied on FCA during Test (LOWMID_F)

During low-mid frequency tests, amplitude is calculated as -0.11 dB from the recorded data and phase lag is calculated as 4.07°.

3.1.4.2.3 Mid Frequency Test (MID_F)

Medium frequency test is named as MID_F in which a 0.868 Hz sinusoidal input is given to the pilot input point of the FCA via PIA. Input and output displacements, magnified view of output displacement and desired position, inlet pressure and external load applied via ELA are given from Figure 3.34 to Figure 3.38, successively.

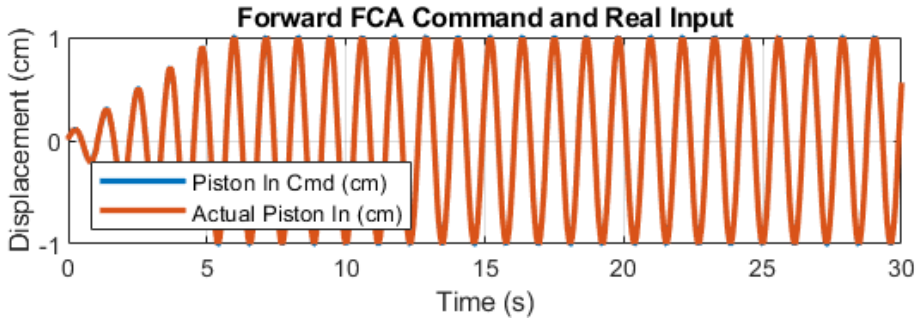

Figure 3.34 Experimental FCA Pilot Input Command (MID_F)

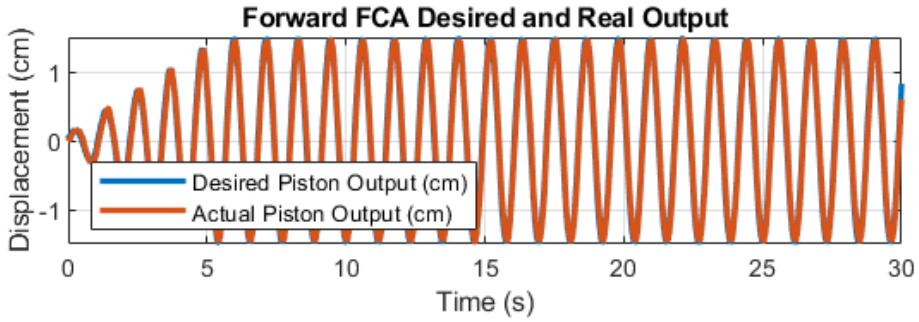

Figure 3.35 Experimental FCA Cylinder Output (MID_F)

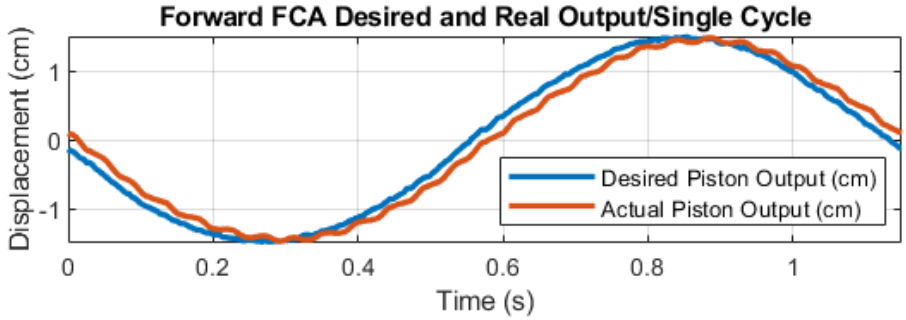

Figure 3.36 Magnified FCA Cylinder Output (MID_F)

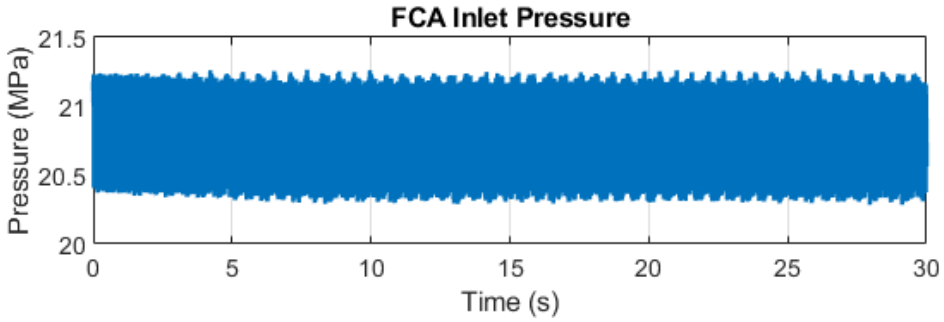

Figure 3.37 Inlet Pressure of FCA During Test (MID_F)

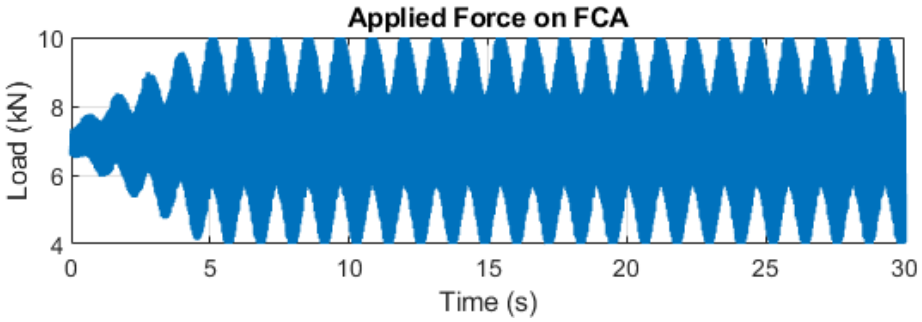

Figure 3.38 External Load Applied on FCA During Test (MID_F)

During mid frequency tests, amplitude is calculated as -0.19 dB from the recorded data and phase lag is calculated as 7.51°.

3.1.4.2.4 Mid-High Frequency Test (MIDHIGH_F)

Medium-High frequency test is named as MIDHIGH_F in which a 3.472 Hz sinusoidal input is given to the pilot input point of the FCA via PIA. Input and output displacements, magnified view of output displacement and desired position, inlet pressure and external load applied via ELA are given from Figure 3.39 to Figure 3.43, successively.

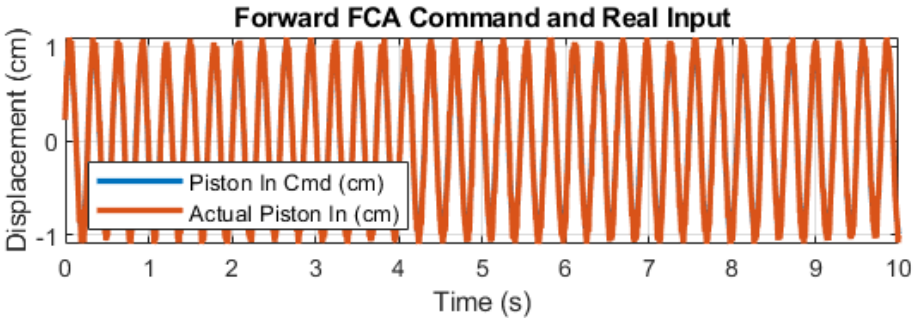

Figure 3.39 Experimental FCA Pilot Input Command (MIDHIGH_F)

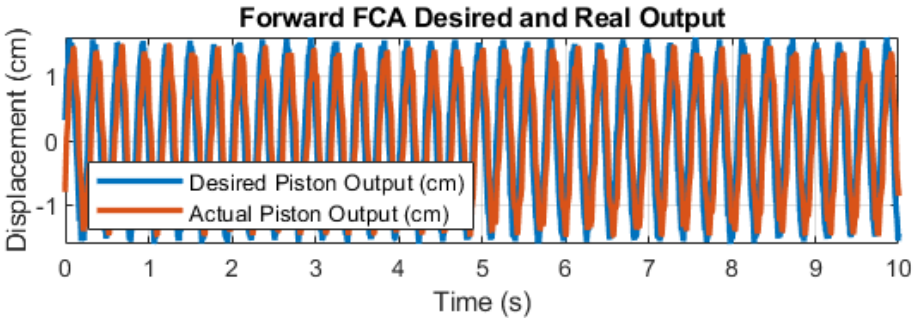

Figure 3.40 Experimental FCA Cylinder Output (MIDHIGH_F)

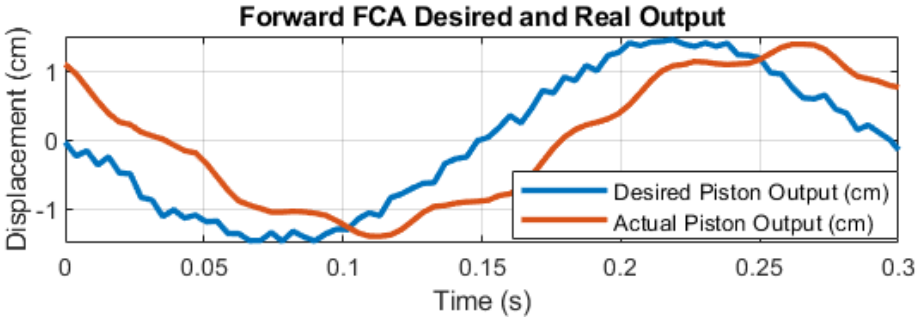

Figure 3.41 Magnified FCA Cylinder Output (MIDHIGH_F)

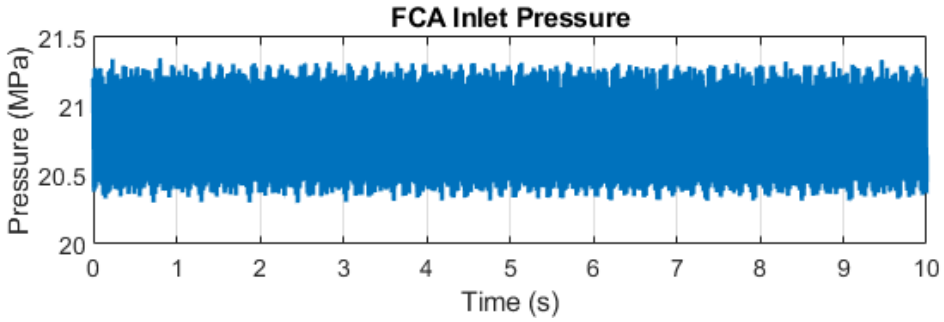

Figure 3.42 Inlet Pressure of FCA during Test (MIDHIGH_F)

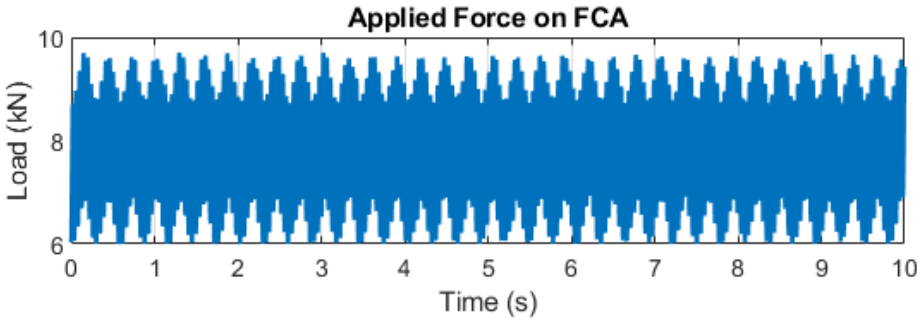

Figure 3.43 External Load Applied on FCA during Test (MIDHIGH_F)

During mid frequency tests, amplitude is calculated as -0.66 dB from the recorded data and phase lag is calculated as 37.89°.

3.1.4.2.5 High Frequency Test (HIGH_F)

High frequency test is named as HIGH_F in which a 6.944 Hz sinusoidal input is given to the pilot input point of the FCA via PIA. Input and output displacements, magnified view of output displacement and desired position, inlet pressure and external load applied via ELA are given from Figure 3.44 to Figure 3.48, successively.

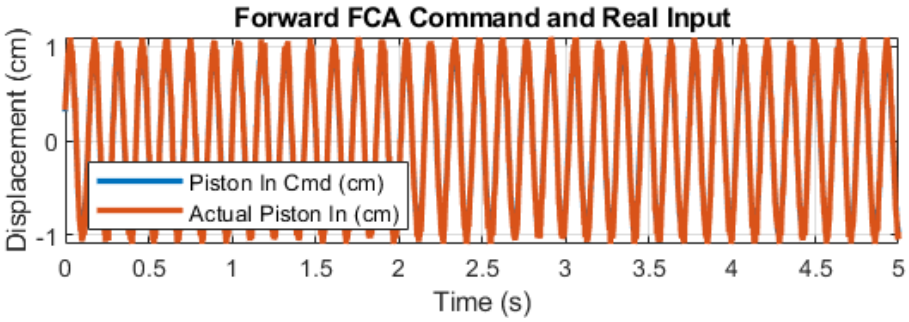

Figure 3.44 Experimental FCA Pilot Input Command (HIGH_F)

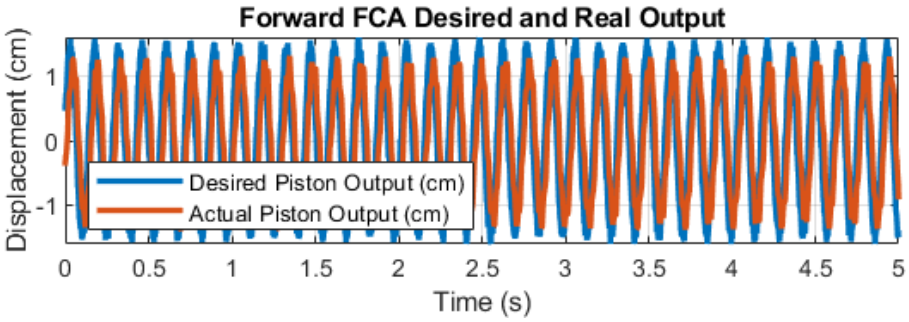

Figure 3.45 Experimental FCA Cylinder Output (HIGH_F)

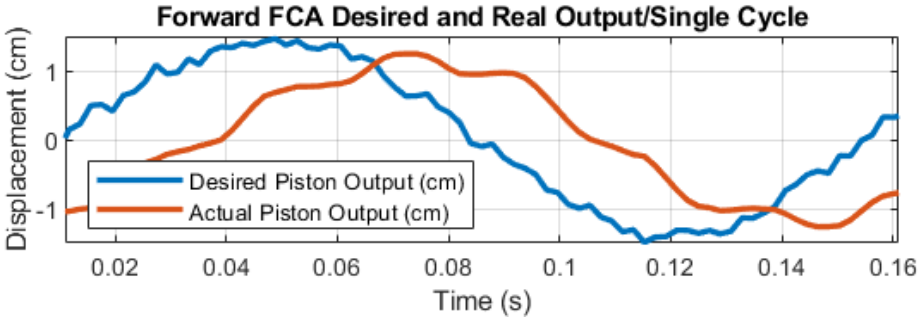

Figure 3.46 Magnified FCA Cylinder Output (HIGH_F)

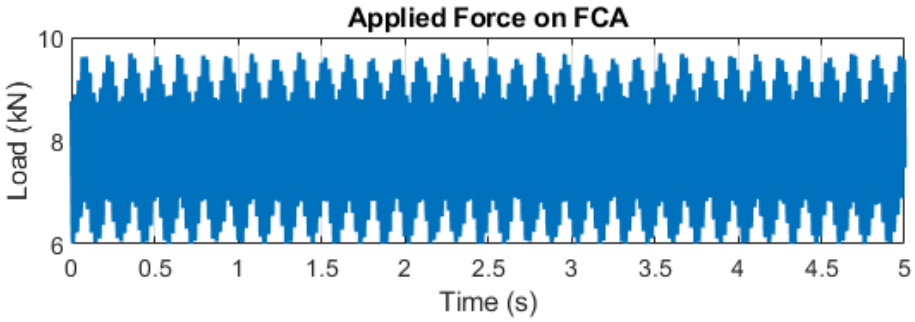

Figure 3.47 Inlet Pressure of FCA During Test (HIGH_F)

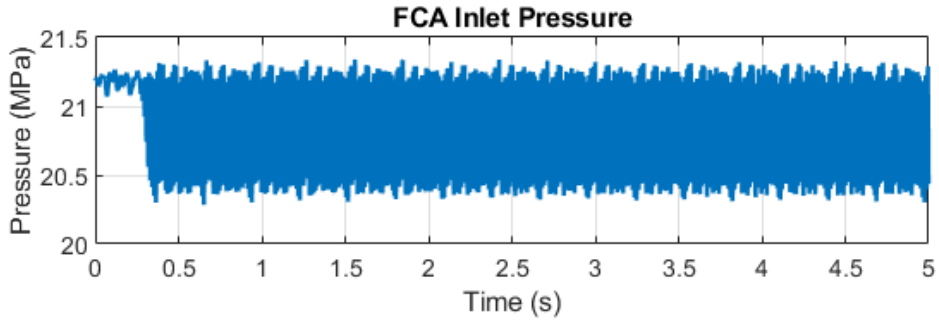

Figure 3.48 External Load Applied on FCA During Test (HIGH_F)

During mid frequency tests, amplitude is calculated as -1.28 dB from the recorded data and phase lag is calculated as 63.64°.

3.1.5 Comparison with Mathematical Model

In chapter 3.1.4, test inputs between 0.217 Hz and 6.944 Hz are applied as pilot inputs to demonstrate operation of a single FCA. Besides, there are several inputs is given as step inputs by amplitude of 1 cm on the input lever side to observe system behavior during application of roll and pitch inputs In this chapter, these inputs are given identically on the simulation including static and dynamic loads that are caused by helicopter main rotor natural frequency. By means of simulation results, behavior is system can be verified and mathematically modeled FCA on Simulink® environment can be further used in controller design applications without hesitation of correctness of the hydro mechanical system behavior.

3.1.5.1 Sinusoidal Inputs Simulation

At the simulation environment, frequencies from 0.217 Hz up to 6.944 Hz are applied to control system purposing the control the motion of the swashplate. Besides, externally applied loads in test setup by ELAs are also simulated to acquire more reliable results. As a general comment on test results, phase of the profiles is matching throughout the simulation. However, considering the amplitudes and profile of the cylinder output, external loads that are applied via helicopter main rotor frequencies are naturally passes through a low-pass filter because of the assumption of rotor components and actuator as an equivalent mass-spring and damper system. Thus, test results that are obtained and to be compared are also low pass filtered for a meaningful comparison. Thus, phase shift and peak amplitudes are compared between simulation and test. Besides, pilot input profile can be directly applied to mathematical model instead of having a transfer function of PIA in the mathematical model. In the real helicopter control system, pilot input is directly given by pilot using internal bell crank and rod assemblies. Thus, a motion which is provided by PIA due to internal controller of PIA system is not to be given while controlling the helicopter. Applied low pass filter is given in Figure 3.49.

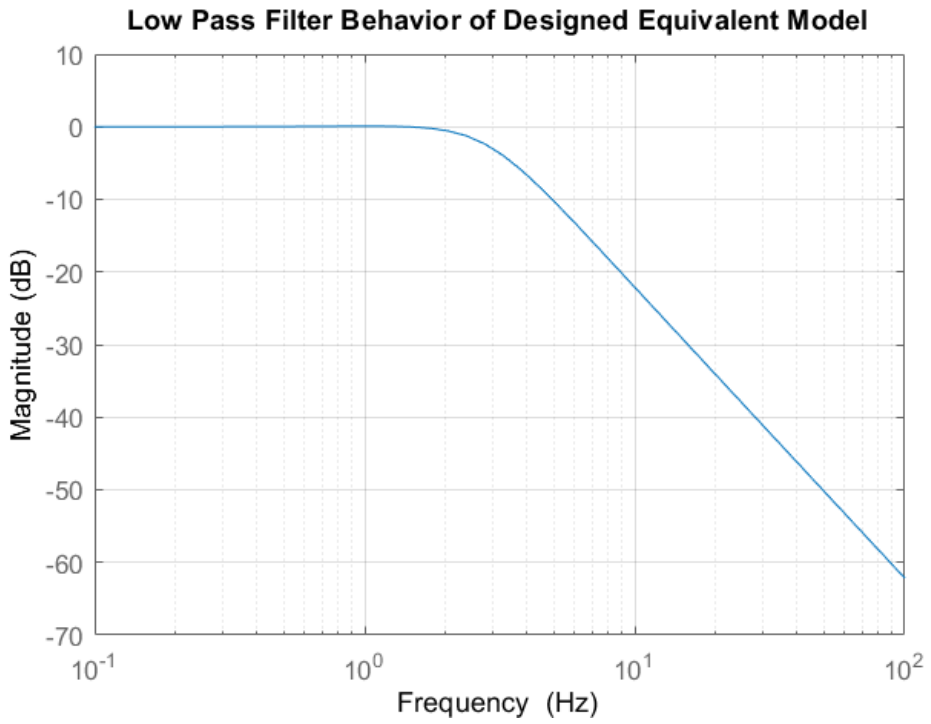

Figure 3.49 Low Pass Filter Behavior of Equivalent Blass Mass in Modeled FCA

Natural frequency of swashplate assembly (ω_s) is much higher than natural frequency of blade assembly (ω_b). For that reason, considering blade assembly only is sufficient for acquiring reliable results. Duration of the simulation is selected the same as duration of the test for the purpose of comparing them more accurately and being sure that system characteristic demonstrates a steady state behavior independent from operation time as well as in the simulation. As an additional note, sinusoidal inputs are applied to a single actuator in the simulation likewise in testing system.

3.1.5.1.1 Low Frequency Simulation and Test Comparison

Low frequency test is executed with frequency of 0.217 Hz sinusoidal input with amplitude of 1 cm. As the modeled system demonstrates more accurate results on low frequencies, results of low frequency simulation are highly compatible with test

results. Comparison between test and simulation results are provided in Figure 3.50 and magnified to a single cycle in Figure 3.51.

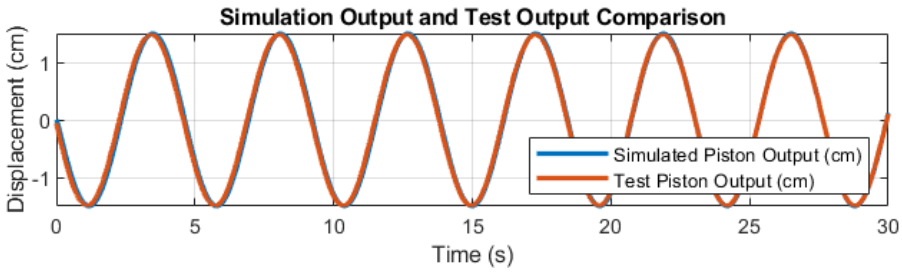

Figure 3.50 Low Frequency Comparison Between Simulated and Tested Cylinder Output

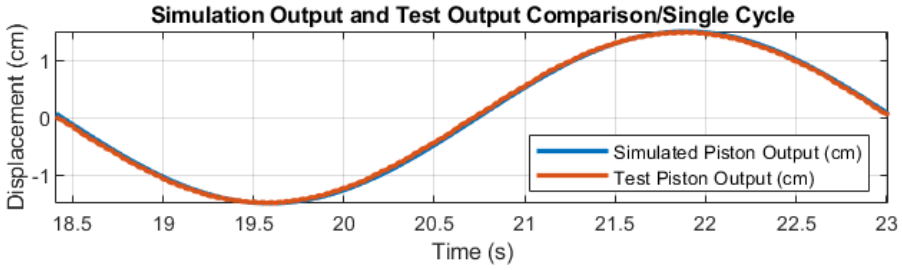

Figure 3.51 Low Frequency Comparison of Cylinder Outputs in a Single Cycle

Difference between desired and actual cylinder outputs for the simulated input and outputs is given in Figure 3.52 and filtered test data for the corresponding simulation is given in Figure 3.53 which is the filtered version of what is tested in Figure 3.26.

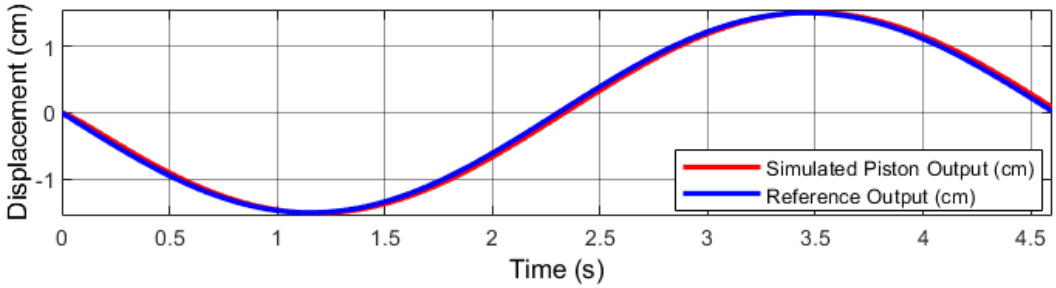

Figure 3.52 Low Frequency Simulated Cylinder Output to Reference Output

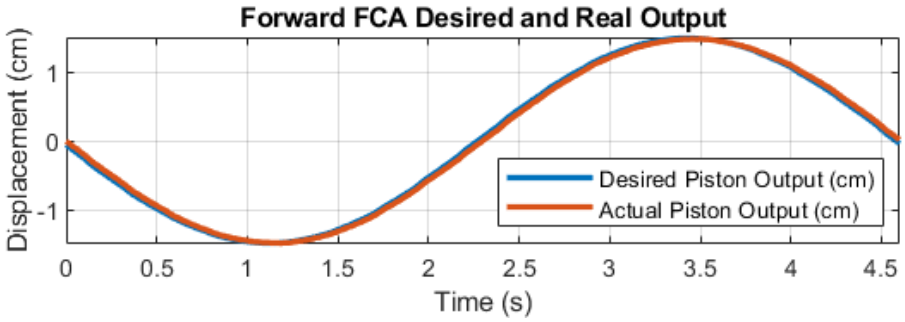

Figure 3.53 Filtered Data of Low Frequency Test

3.1.5.1.2 Low- Mid Frequency Simulation and Test Comparison

Low frequency test is executed with frequency of 0.434 Hz sinusoidal input with amplitude of 1 cm. Like low frequency, these simulation results are quite compatible compared to test results. Comparison between test and simulation results are provided and magnified to a single cycle in Figure 3.54 and Figure 3.55, respectively.

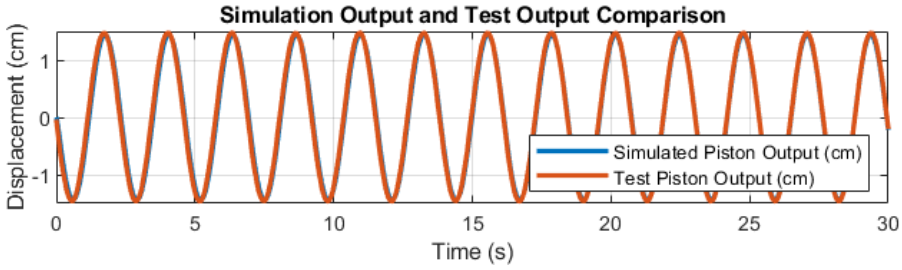

Figure 3.54 Low-Mid Frequency Comparison Between Simulated and Tested Cylinder Output

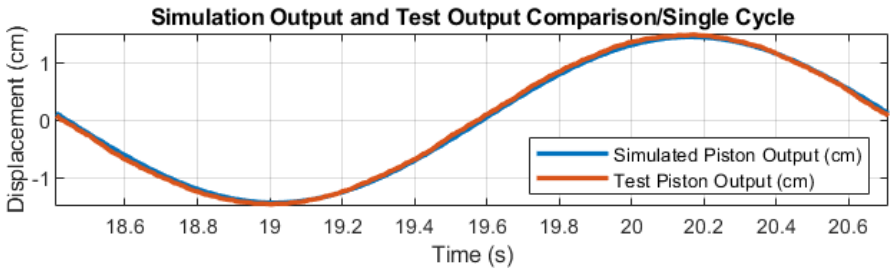

Figure 3.55 Low-Mid Frequency Comparison of Cylinder Outputs in a Single Cycle

Difference between desired and actual cylinder outputs for the simulated input and outputs is given in Figure 3.56 and filtered test data for the corresponding simulation is given in Figure 3.57 which is the filtered version of what is tested in Figure 3.31.

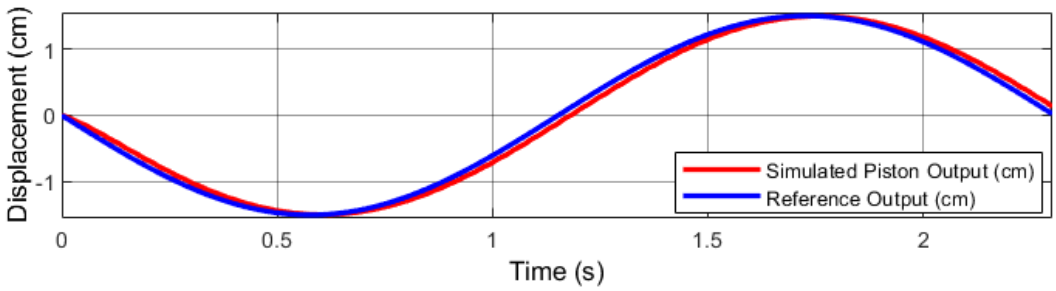

Figure 3.56 Low-Mid Frequency Simulated Cylinder Output to Reference Output

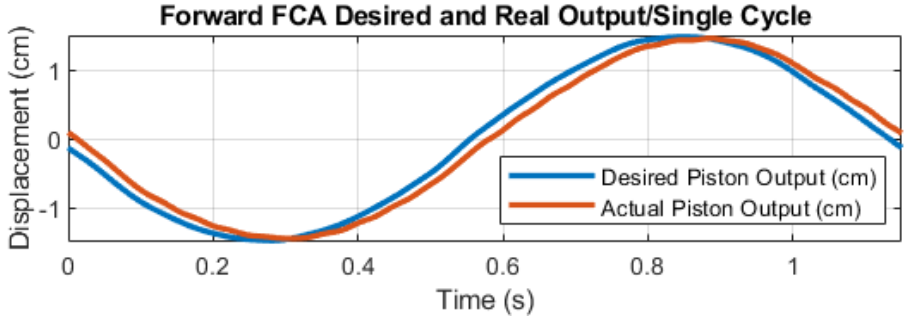

Figure 3.57 Filtered Data of Low-Mid Frequency Test

3.1.5.1.3 Mid Frequency Simulation and Test Comparison

Mid frequency test is executed with frequency of 0.868 Hz sinusoidal input with amplitude of 1 cm. Comparison between test and simulation results are provided and magnified to a single cycle in Figure 3.58 and Figure 3.59, respectively.

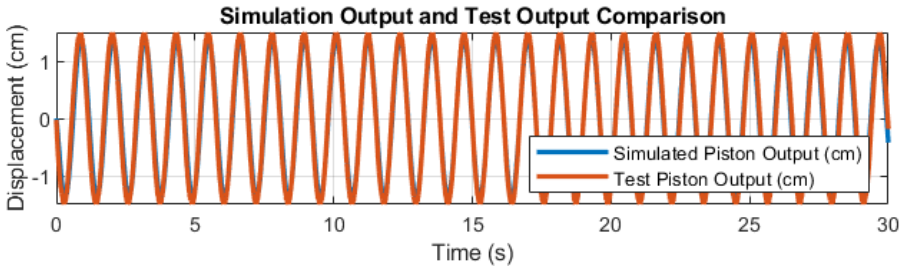

Figure 3.58 Mid Frequency Comparison Between Simulated and Tested Cylinder Output

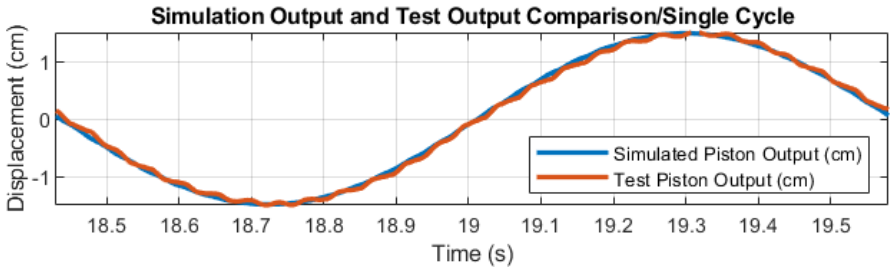

Figure 3.59 Mid Frequency Comparison of Cylinder Outputs in a Single Cycle

Difference between desired and actual cylinder outputs for the simulated input and outputs is given in Figure 3.60 and filtered test data for the corresponding simulation is given in Figure 3.61 which is the filtered version of what is tested in Figure 3.36.

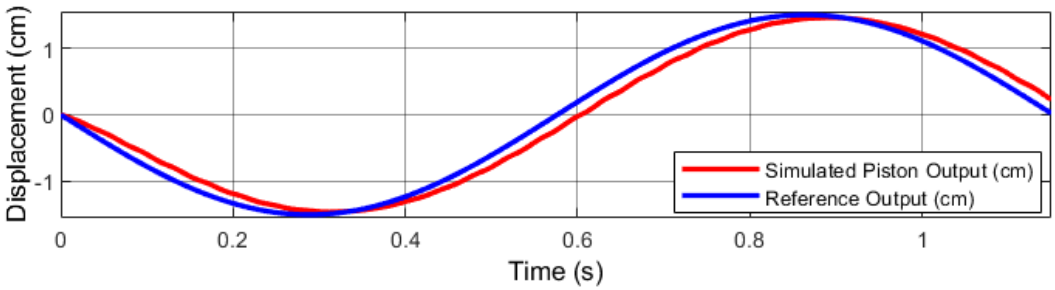

Figure 3.60 Mid Frequency Simulated Cylinder Output to Reference Output

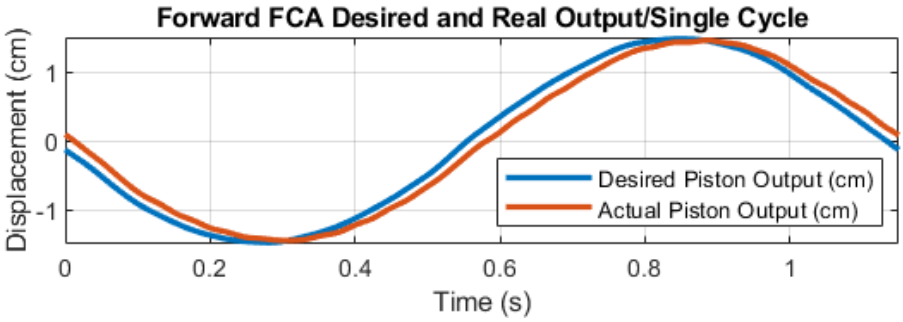

Figure 3.61 Filtered Data of Mid Frequency Test

3.1.5.1.4 Mid-High Frequency Simulation and Test Comparison

Mid-High frequency test is executed with frequency of 3.472 Hz sinusoidal input with amplitude of 1 cm. Comparison between test and simulation results are provided and magnified to a single cycle in Figure 3.62 and Figure 3.63, respectively.

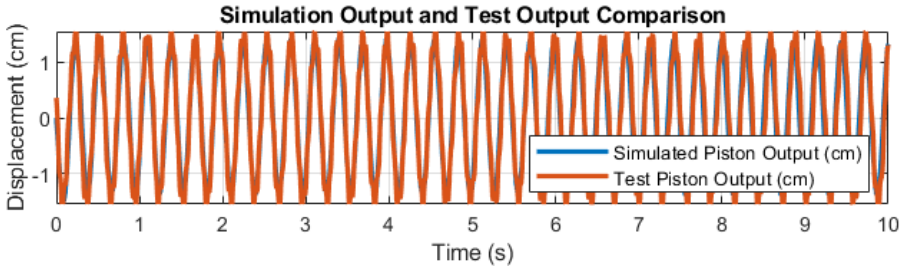

Figure 3.62 Mid-High Frequency Comparison Between Simulated and Tested Cylinder Output

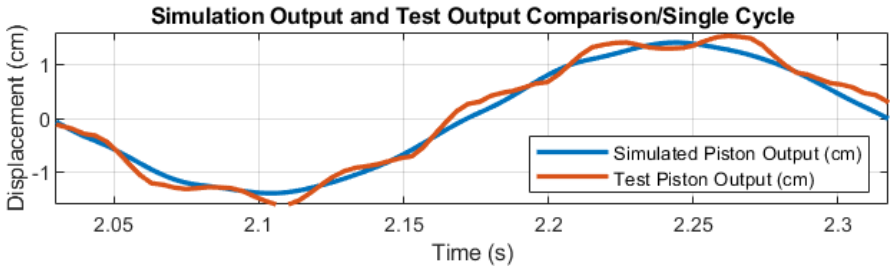

Figure 3.63 Mid-High Frequency Comparison of Cylinder Outputs in a Single Cycle

Difference between desired and actual cylinder outputs for the simulated input and outputs is given in Figure 3.64 and filtered test data for the corresponding simulation is given in Figure 3.65 which is the filtered version of what is tested in Figure 3.41.

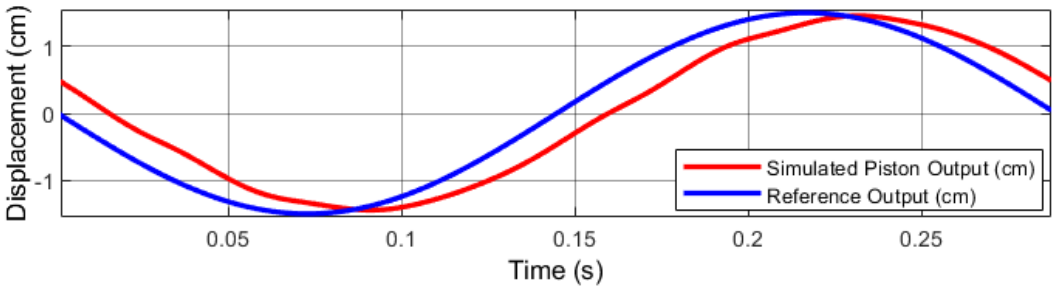

Figure 3.64 Mid-High Frequency Simulated Cylinder Output to Reference Output

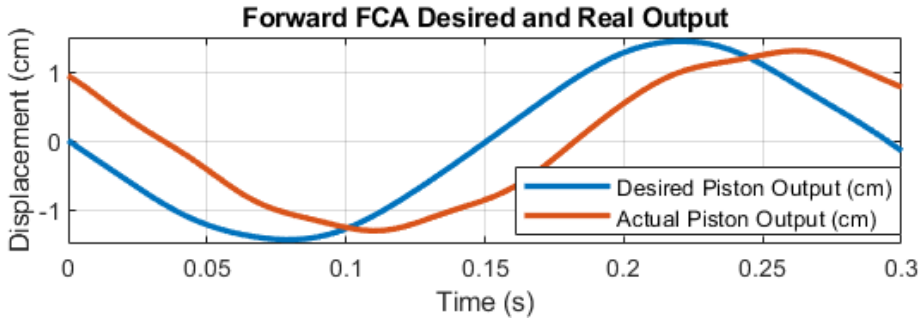

Figure 3.65 Filtered Data of Mid-High Frequency Test

3.1.5.1.5 High Frequency Simulation and Test Comparison

High frequency test is executed with frequency of 6.944 Hz sinusoidal input with amplitude of 1 cm. Comparison between test and simulation results are provided and magnified to a single cycle in Figure 3.66 and Figure 3.67, respectively.

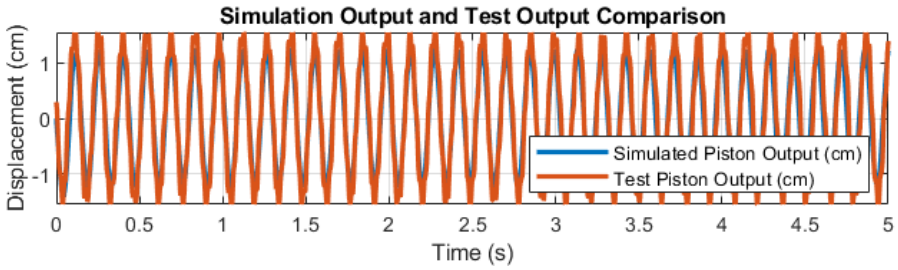

Figure 3.66 High Frequency Comparison Between Simulated and Tested Cylinder Output (Raw Data)

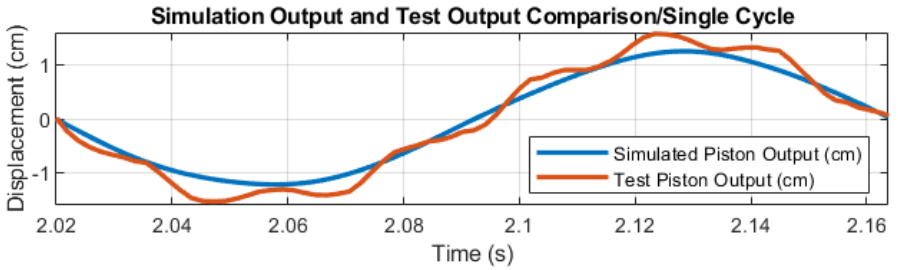

Figure 3.67 High Frequency Comparison of Cylinder Outputs in a Single Cycle

Difference between desired and actual cylinder outputs for the simulated input and outputs is given in Figure 3.68 and filtered test data for the corresponding simulation is given in Figure 3.69 which is the filtered version of what is tested in Figure 3.46.

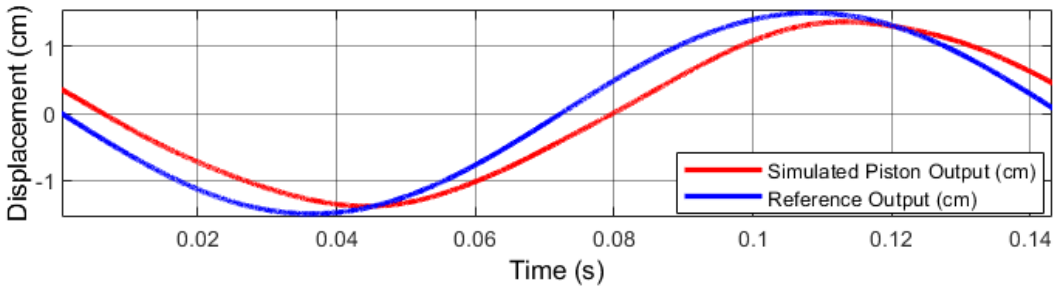

Figure 3.68 High Frequency Simulated Cylinder Output to Reference Output

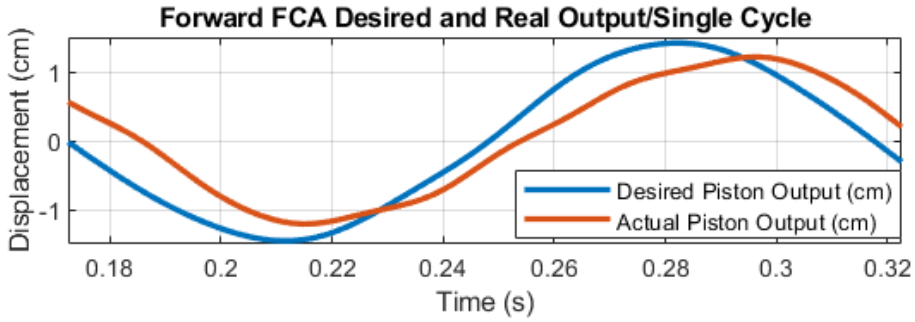

Figure 3.69 Filtered Data of High Frequency Test

3.1.5.2 Step Inputs Simulation

Step inputs are simulated in two parts for comparison. Initially, a positive lateral cyclic input is given with the same amplitude as in the test and roll angle (β) is obtained; after that, it is brought to null position. Next, a positive longitudinal cyclic input is given again in the same amplitude of what has been given in the test activity and pitch tilting angle (α) is obtained. Note that external load that is applied on FCAs are filtered with respect to Figure 3.49 likewise in previous simulations.

3.1.5.2.1 Positive Lateral Cyclic Simulation

In this simulation, an input is given to the system that results in +15 mm displacement in left FCA, -15 mm displacement in Right FCA and no displacement in Forward FCA as expected. Steady state value of the expected roll degree is calculated in (3.2), taking the side length of SSP triangle as 600 mm.

$$\beta = \arctan\left(\frac{15}{(600/2)}\right) = 2{,}86° \tag{3.2}$$

Positive Lateral Cyclic input from null position to reference position are inspected both in simulation and test results as they are demonstrated in Figure 3.70 and Figure 3.71, respectively.

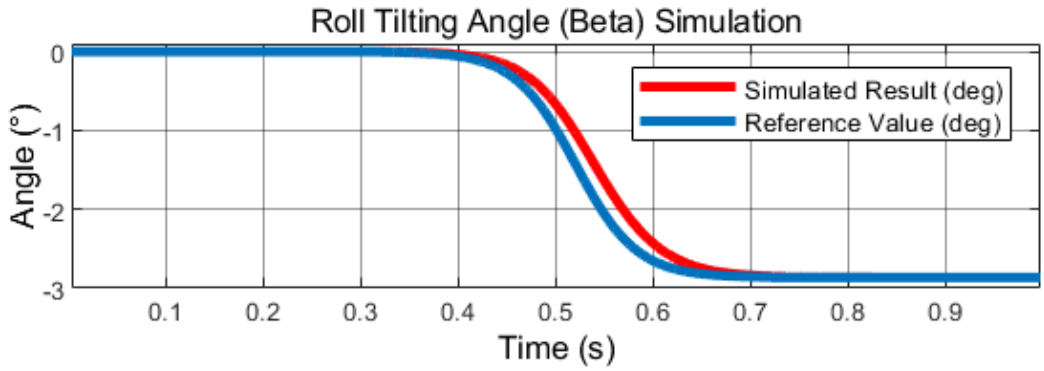

Figure 3.70 Right Cyclic Null to Reference Simulation Results

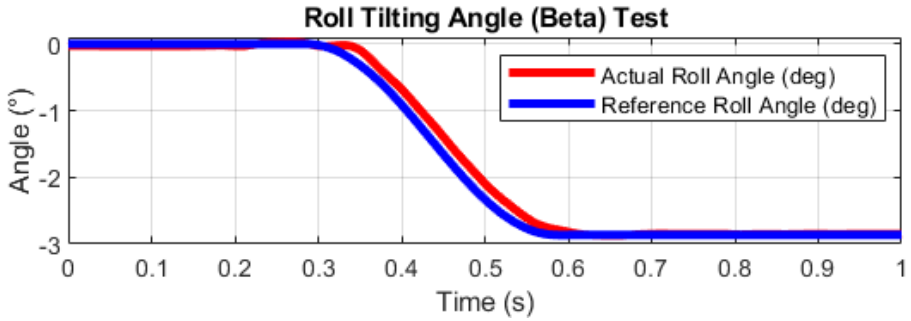

Figure 3.71 Right Cyclic Null to Reference Test Results

Results are also inspected that are starting from steady state reference value and ending at the null position of the input for simulation and test that are provided in Figure 3.72 and Figure 3.73, respectively.

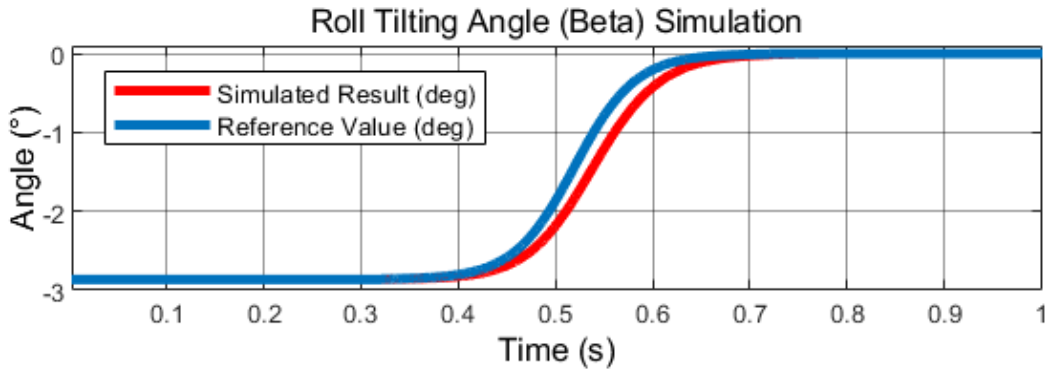

Figure 3.72 Right Cyclic Reference to Null Simulation Results

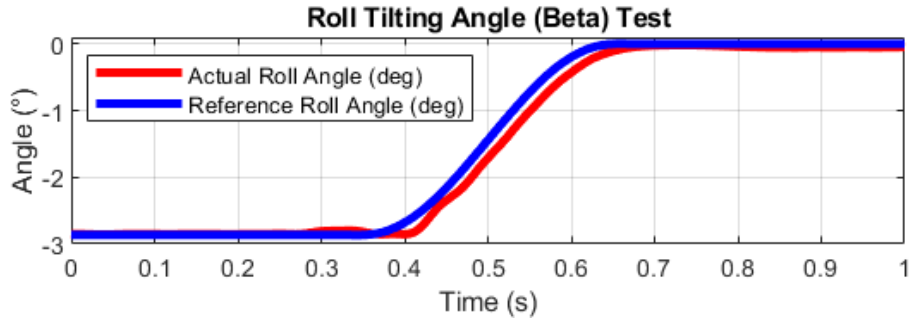

Figure 3.73 Right Cyclic Reference to Null Test Results

It can be observed that there is a slight increase in the actual response of the angle before beginning of step input although there is no stimuli given at that time. It is evaluated as the calculation error of independent FCAs as they have independent controllers that result in a displacement in any FCA because they work with force control principle. It is also evaluated that this slight increase has no effect on the response to the step input that is applied to control system.

3.1.5.2.2 Positive Longitudinal Cyclic Simulation

In the simulation, a reference positive longitudinal input is given to the system that results in positive pitch angle. In the simulation, Forward FCA output cylinder moves downwards with an amplitude of 30 mm at the same time Left and Right FCAs move upwards as 15 mm. Steady state value of the expected pitch degree is calculated in (3.3), taking the side length of SSP triangle as 600 mm.

$$\alpha = \arctan\left(\frac{D1 + D2}{a\sqrt{3}}\right) = \arctan\left(\frac{45}{300\sqrt{3}}\right) = 4{,}95° \qquad (3.3)$$

Positive Longitudinal Cyclic input from null position to reference position are inspected both in simulation and test results as they are demonstrated in Figure 3.74 and Figure 3.75, respectively.

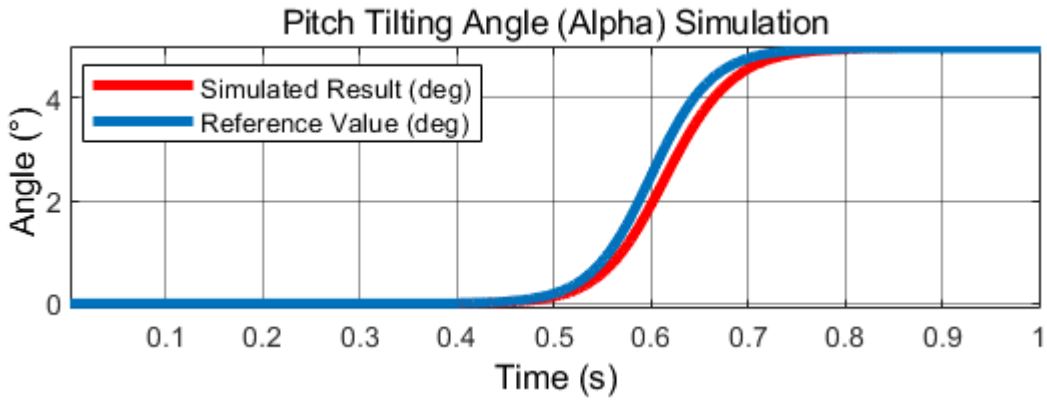

Figure 3.74 Forward Cyclic Null to Reference Simulation Results

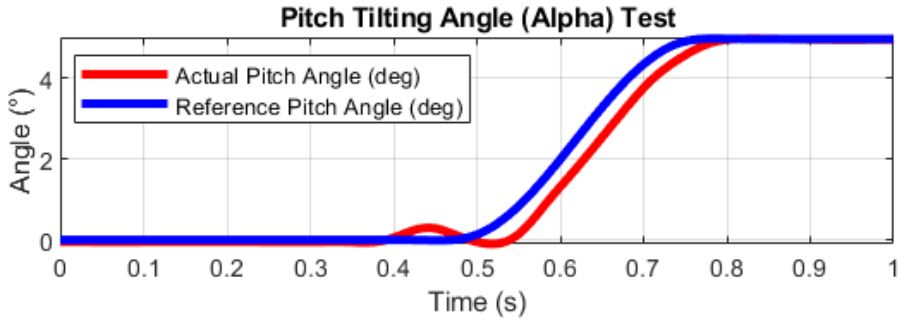

Figure 3.75 Forward Cyclic Null to Reference Test Results

Results are also inspected from reference to null position, and they are provided in Figure 3.76 and Figure 3.77 for simulation and test results, respectively.

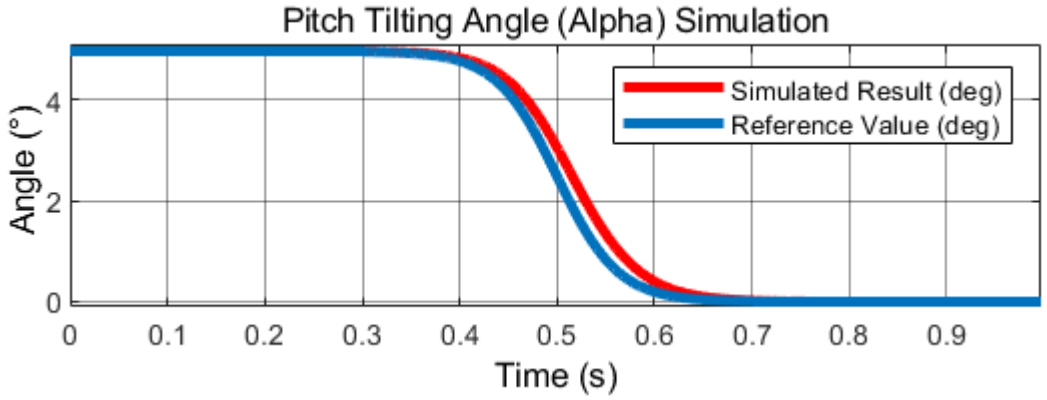

Figure 3.76 Forward Cyclic from Reference to Null Simulation Results

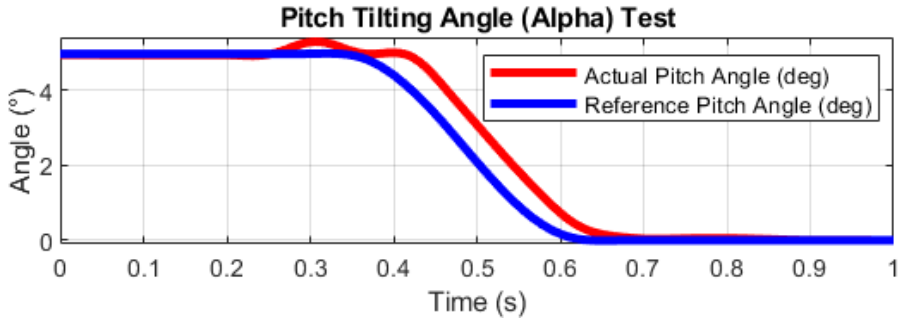

Figure 3.77 Forward Cyclic from Reference to Null Test Results

As it can be clearly seen in test figures of Figure 3.75 and Figure 3.77, there is a slight increase before application of step input, to which a pilot input is not a reference. Thus, they can be evaluated as unintentional response of FCAs as they are providing a force control. It can be stated that these unintentional movements do not affect the rise time and peak value at the end of the profile. However, Peak values are affected at the beginning of the test activities which are to be filtered while analyzing these results.

3.1.6 Compatibility Assessment of Mathematical Model

Mathematically modeled FCA is tested and analysed from now on. Based on the results that are obtained in 3.1.4 and 3.1.5, a compatibility assesment is to be given in order for using the model in control applications for the further chapters. Beyond small differences that are to be stated as limitations, mathematically modeled FCA is suitable to be used in conroller design. Compatibility comments can be performed based on summary of all responses of the FCA during test and simulation activities.

Initially, amplitude and phase lag diagrams of real system, linear system (1-Mass) and non-linear system (3-Mass) are obtained and compared. Based on the comparison, profiles are close to each each other in low frequencies (<10 Hz). It is sufficient to make interpretation of comptability because neither pilot nor aand automatic controller can not give inputs above 10 Hz. Cut-off frequency of real system is higher than linear and nonlinear system; however, it is closeer to nonlinear

model. On the other hand, phase lag profile is slightly different from both linear and nonlinear system as real test setup tends to have a higher phase lag in low frequencies. In overall evaluation, profiles of nonlinear system and real system are close to each other in terms of amplitudes. Bode comparison is provided in Figure 3.78 for amplitude and Figure 3.79 for phase lag between 0.01-10 Hz frequncies which represents the frequency range of control input given by manual and automatic control systems.

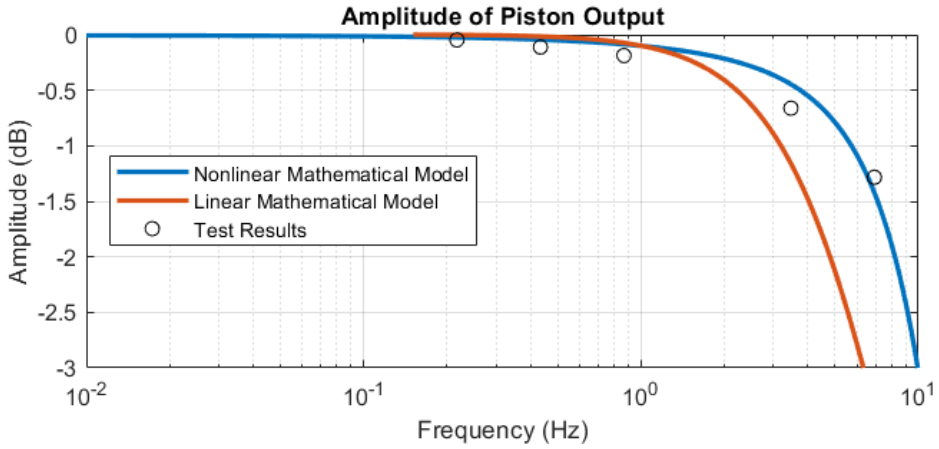

Figure 3.78 Comparison of Modeled Systems and Real System (Amplitude)

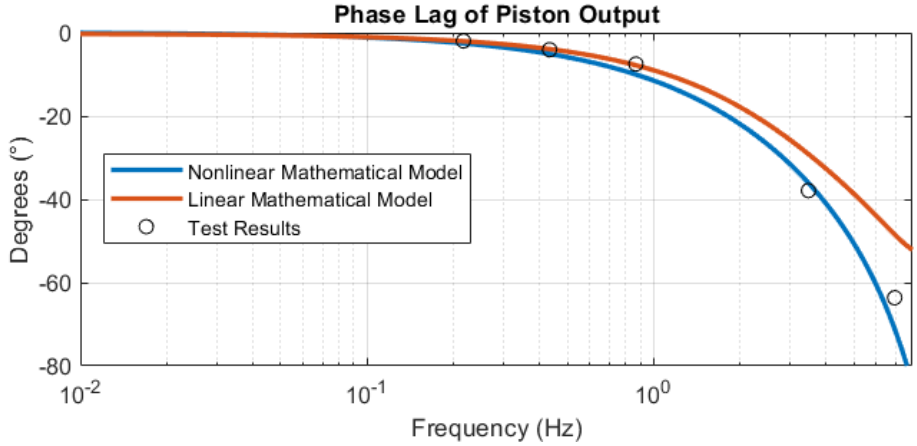

Figure 3.79 Comparison of Modeled Systems and Real System (Phase)

In addition to frequency response, it can be stated that peak values and rise times are quite compatible within simulation and test while applying different types of step inputs. Rise time of nonlinear simulation is slightly higher than test system. It is

because test system does not actually have a mass that is acting by the applied force from actuator. As long as ELAs are not moving, only moving mass become the cylinder mass of ELA. As it can be predicted, it is much more smaller compared to mass of rotor system components. Besides, ELAs are not simulating any inertial force as inertial effects are included in nonlinear simulation. Considering these interpretations, nonlinear model can is said to be fully compatible with tested FCAs. For the linear system, compatiblity is given as partially because cut-off frequency is considerably low around 6 Hz, which is lower than control input frequency of both pilot and automatic controller.

CHAPTER 4

CONTROLLER DESIGN

In this chapter, two different controllers are introduced that are integrated to FCA and cooperates with FCA in a sequence for particular purposes. Stability Actuator is used to correct the orientation of the helicopter body in pitch, roll and yaw degrees of freedom. Swashplate Control Actuator (SCA) instead, is used to enhance the overall performance of SSP instead of correcting complete helicopter motions. Performance of SCA is measured by certain performance parameters. These actuators transmits their inputs to MCV via linkage mechanisms that are designed with transmission ratios inside FCA. SCA, Stability Actuator and pilot inputs are controlling the piston displacement and velocity in a coordinated way. Both of these actuators have separate component of the shelf servo valves which have common transfer functions that can be implemeted into mathematical equations.

4.1 Reduction of 3 DoF into 2 DoF System

SSP controller can be designated via any strategy that benefits the response of the SSP. In this chapter, two types of control strategy are applied to improve the behavior of the system, which are PID control and model-based control. However, due to not having an additional natural frequency by adding rotor blades as an independent mass of the system, system is reduced to a 2-mass system in linear scenario and 3 mass system in nonlinear scenario. Linear system derivation with 2-mass system, which are piston mass (M_P) rotor mass (M_R) that includes equivalent mass of rotor blades and swashplate together, is given in Appendix B. After making necessary derivations, bode plot of 2-Mass system is obtained and given in Figure 4.1.

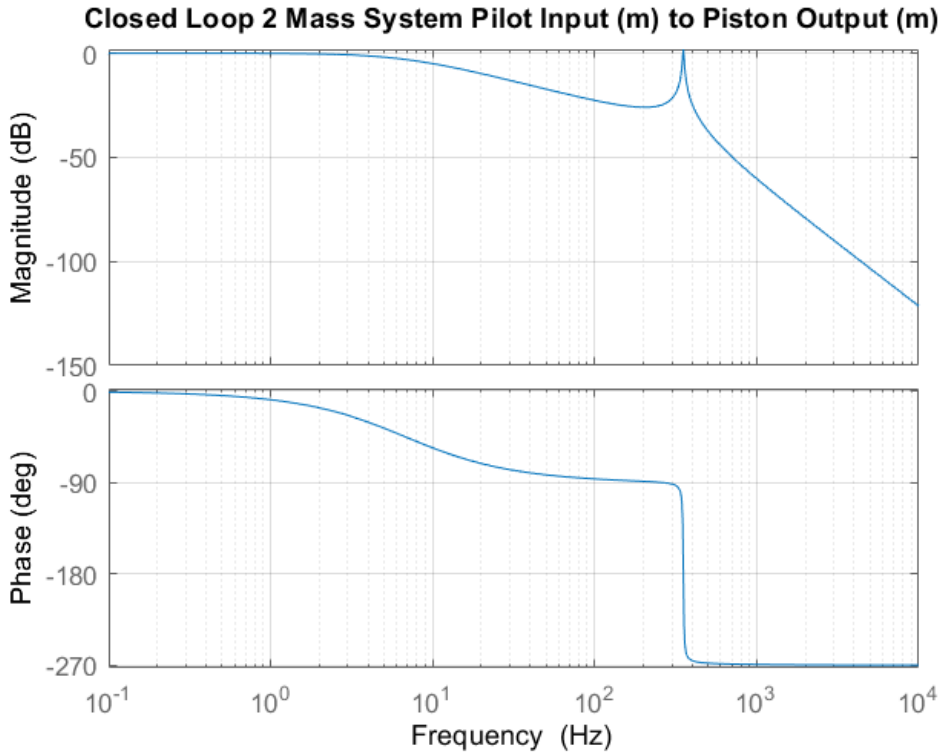

Figure 4.1 Bode Plot of Closed Loop 2-Mass System, Pilot Input (m) and Cylinder Output (m)

It is assumed that both pilot and controller input can be applied to the overall control system up to 10 Hz frequency. Thus, it is required to make a comparison starting from a small frequency and goes up to 10 Hz. Comparison between frequency responses of 2-Mass and 3-Mass systems are given in Figure 4.2 for amplitude and Figure 4.3 for phase lag respectively.

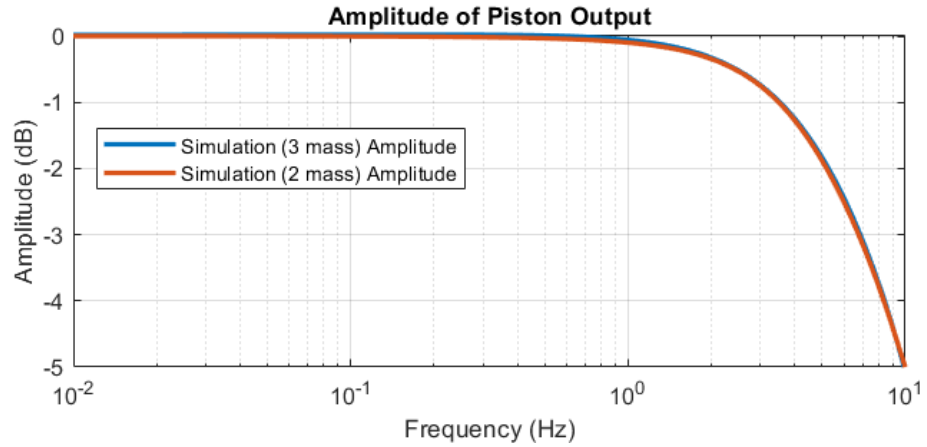

Figure 4.2 Amplitude Comparison of 2-Mass and 3-Mass System

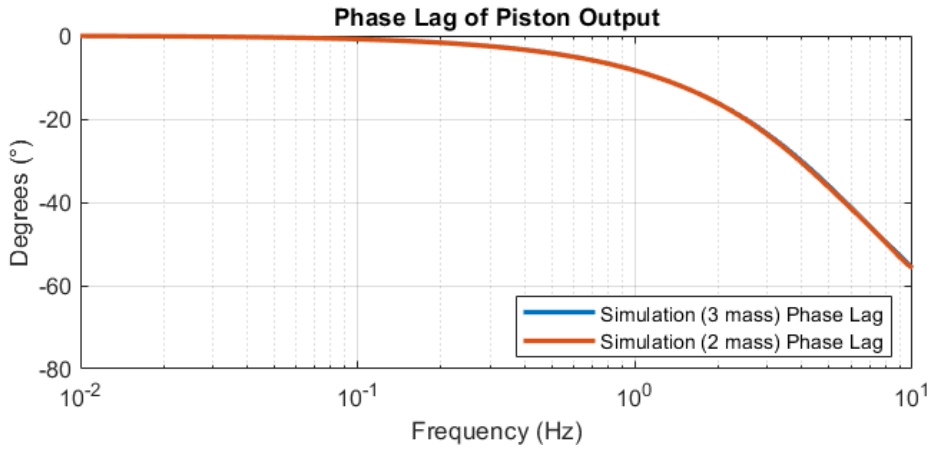

Figure 4.3 Phase Lag Comparison of 2-Mass and 3-Mass System

It can be clearly stated that amplitude and phase characteristics of 2-Mass and 3-Mass system are almost equal. Thus, 2-Mass system can be used for controller design instead of 3-Mass system without any assumption except input frequencies are limited with 10 Hz. Up to 10 Hz, a slight difference between two systems are arises; however, it does not affect the controller. Besides, helicopter main rotor natural frequency (usually up to 20 Hz) does not bring any resonant output that cause instability.

4.2 Mathematical Model with Stability Actuator

Mathematical model of helicopter Hydraulic control system has already been derived in previous chapters. This derivation is based on only for mechanical inputs and response of the system to these inputs. In this chapter, first of the two hydro mechanical control actuators are introduced which is called "Stability Actuator". Stability actuator is used to control and correct orientation and rates of complete helicopter body in terms of its pitch, roll and yaw axis; which are sequentially defined as α_{hc}, β_{hc} and r_{hc}. Considering effect of the main rotor to overall helicopter orientation, only α_{hc} and β_{hc} can be determined by main rotor. Stability actuator cooperates with a computer that detects the current orientation of the helicopter and calculates error between current and ideal orientation of the helicopter which is called "Stability Computer". Additionally, control algorithm is developed within Stability computer and desired inputs are transmitted as electrical current to servo valve that drives stability actuator. In this study, close loop control is not provided with stability actuator as helicopter body and corresponding motions of the body is not modeled and represented. Overall control principle of stability actuator is given in Figure 4.4.

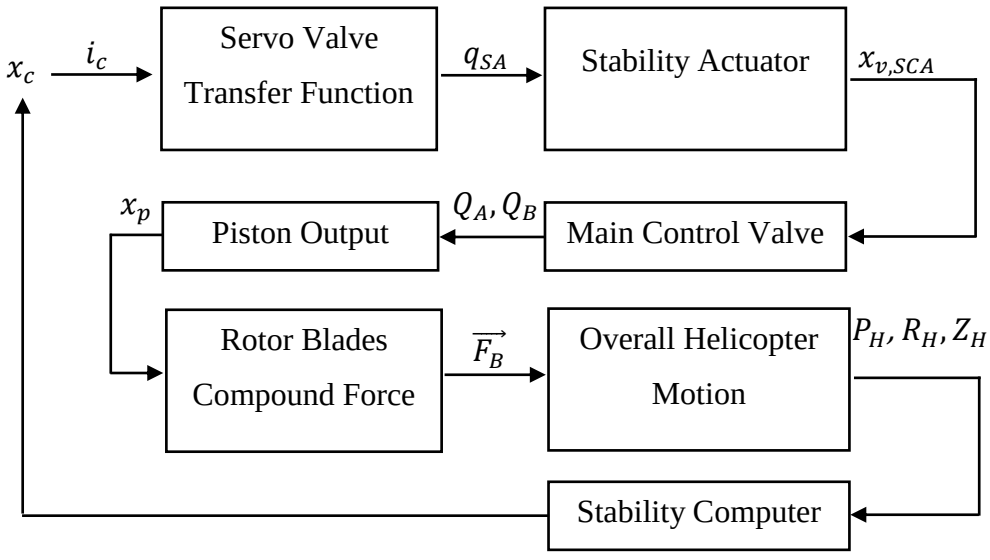

Figure 4.4 General Control Principle of Stability Actuator

Fundamental operation principle of Stability Actuator is defined as follows. Initially, there should be a difference between current and desired orientation of the helicopter. Desired orientation of the helicopter is calculated by given pilot inputs at momentarily during flight. Combination of pilot inputs refers to a particular position of air vehicle that is calculated via stability computer. Furthermore, current orientation is tracked via angular position transducer. Errors between these two orientations are defined for pitch and roll degrees of freedom of helicopter body as follows;

$$e_{pitch} = \alpha_{hc,desired} - \alpha_{hc,current} \tag{4.1}$$

$$e_{roll} = \beta_{hc,desired} - \beta_{hc,current} \tag{4.2}$$

For the correction of defined error values, specified computer inputs additional to pilot inputs are defined. Collective, longitudinal cyclic and lateral cyclic of computer inputs are defined as $x_{1,c}$, $y_{1,c}$ and $y_{2,c}$; successively. These inputs are to convert null position of the cylinder from zero to any desired value due to compensate disturbances caused by environmental effects. Inputs are transmitted as currencies of i_c to a servo valve. Dur to the similarities of properties among servo valves used for stability purposes, transfer function of the servo valve is assumed and directly implemented to the mathematical model. Servo valve transfer function of stability actuator is constructed between input current and output position of the stability actuator. The servo valve converts current value to flow rate and feeding either side of stability actuator with this flow. It is a closed loop transfer function and closed loop is completed via an LVDT that is used to measure displacement of stability actuator. Closed loop representation of stability actuator is given in Figure 4.5.

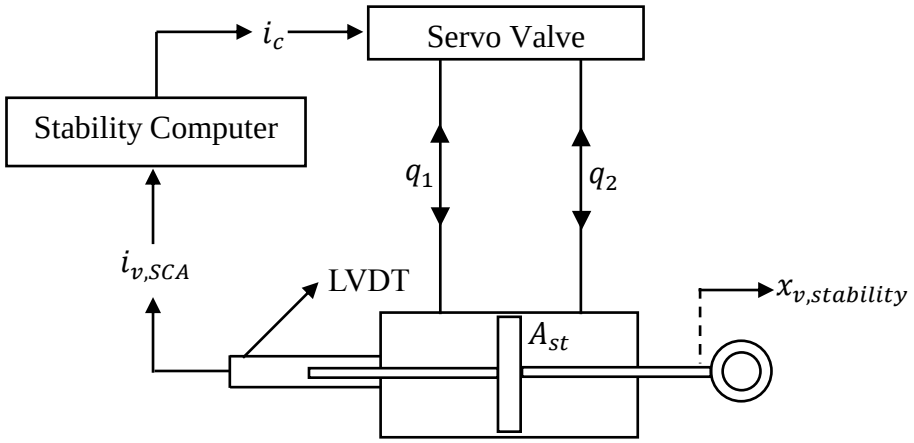

Figure 4.5 Closed Loop Control of Stability Actuator Itself

Note that Figure 4.5 only represents control of stability actuator and control of helicopter body orientation is to be represented with another closed loop system. However, stability computer is a common input source that is a crucial component of both closed loop systems. For stability actuator, cylinder area A_{st} exhibit a significance as the component is required to create forces that is greater than static friction force of MCV and linkages. Feedback of stability actuator is transmitted through an LVDT as electrical signal. By varying current values, either q_1 or q_2 is filling the chamber while other one is discharging. For that reason, flow can arise in both directions according to the electrical signal. A similar servo valve is selected in the design of FCA, which is proven by using in a velocity control application by adding a free state to denominator of the transfer function [28]. For the stability actuator, complete closed loop system can be represented via a transfer function that is given in (4.3).

$$\frac{x_{v,stability}(s)}{i_c(s)} = \frac{1}{\left(\frac{1}{340}\right)^2 s^2 + \left(\frac{14}{340}\right) s + 1} \tag{4.3}$$

Original configuration of FCA involves mechanical control loop and control loop of stability actuator. This configuration is to be modified in 4.3 and 4.4. Non-modified (original) configuration of FCA internal control loops and mechanisms are given as follows;

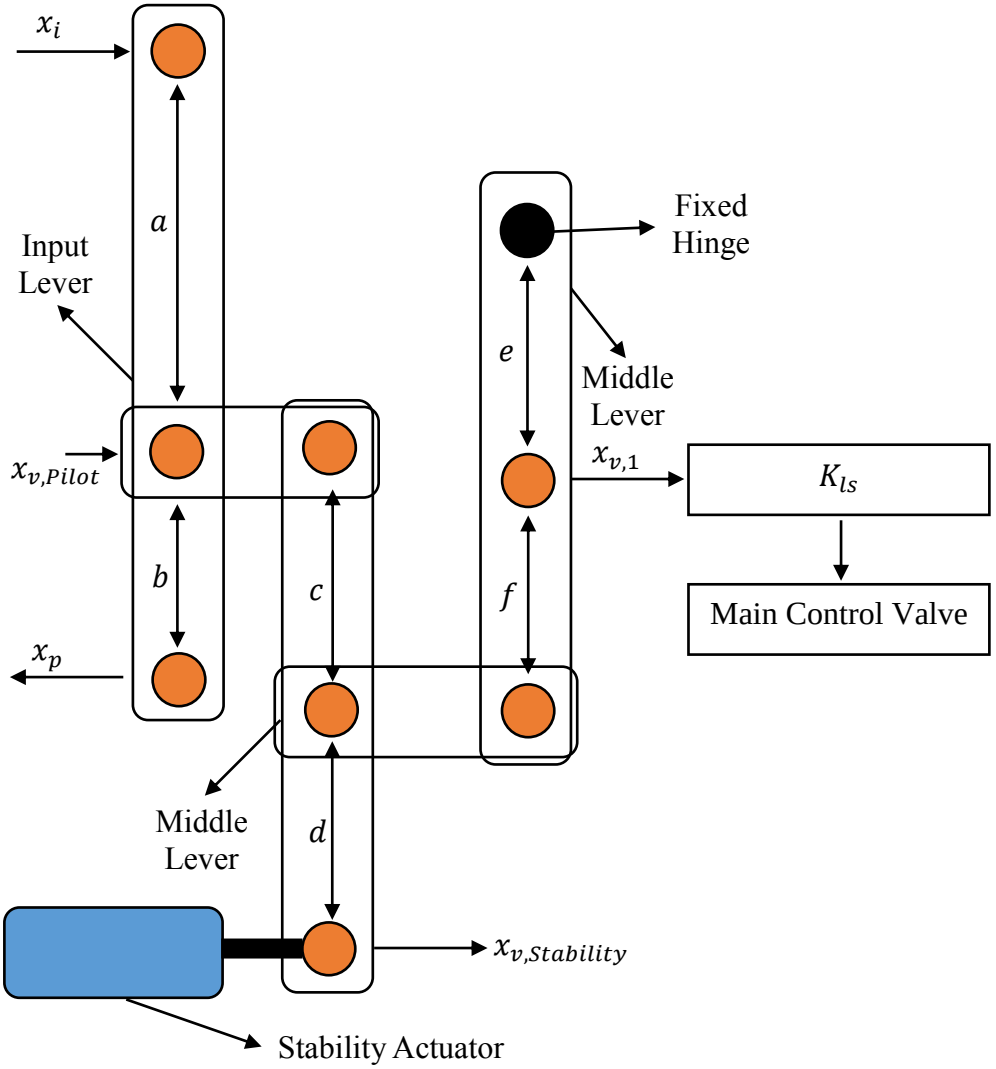

Figure 4.6 Original Control Loops and Mechanisms inside FCA (Non-modified)

There is input-output ratio between input of the stability actuator and cylinder steady state position, likewise pilot input, and actuator output. Considering ratio between open loop input and cylinder output, and assuming that pilot input is retained as zero, it can be written as;

$$\frac{x_{v,stability}}{x_p} = \frac{a}{(a+b)}\frac{d}{c} \tag{4.4}$$

Sign of the cylinder output is considered towards leftwards, which is opposite to the input of valve and stability actuator. Thus, minus sign is to be disappeared as it has

already been considered while determining positive direction of motion. Extracting cylinder output from (4.4) yields (4.5).

$$x_p = \frac{(a+b)cx_{v,stability}}{ad} \tag{4.5}$$

Total valve control input can be represented by $x_{v,1}$. Valve control input can be defined in terms of pilot and stability actuator input that is given in Figure 4.5.

$$\begin{aligned} x_{v,1} &= \frac{ce}{(c+d)(e+f)}x_{v,stability} + \frac{de}{(c+d)(e+f)}x_{v,Pilot} \\ &= \frac{e(cx_{v,stability} + dx_{v,pilot})}{(c+d)(e+f)} \end{aligned} \tag{4.6}$$

In (4.6), $x_{v,Pilot}$ can be reprsented in terms of cylinder output and pilot input. Thus, (4.6) transforms into (4.7) that can be found as follows;

$$x_{v,1} = \frac{e(cx_{v,stability} + d(\frac{b}{(a+b)}x_i + \frac{a}{(a+b)}x_p)}{(c+d)(e+f)} \tag{…}$$

$$x_{v,1} = \frac{e\left(cx_{v,stability} + dbx_i + dax_p\right)}{(a+b)(c+d)(e+f)} \tag{4.7}$$

It is easier to comprehend original system by a block diagram. It order to express block diagram in a compact and simplified way, vector definitions that are provided from (4.8) to (4.11) are introduced.

$$[\boldsymbol{X}_i^t]^T = [x_i^F \quad x_i^L \quad x_i^R] \tag{4.8}$$

$$[\boldsymbol{D}^t]^T = [D_1 \quad D_2 \quad D_3] \tag{4.9}$$

$$[\boldsymbol{\varphi}_{\boldsymbol{H}}^{\boldsymbol{t}}]^T = \begin{bmatrix} P_H & R_H & Z_H \\ \dot{P}_H & \dot{R}_H & \dot{Z}_H \end{bmatrix} \tag{4.10}$$

$$[\boldsymbol{I}_{\boldsymbol{XY}}^{\boldsymbol{t}}]^T = [x_1 \quad y_1 \quad y_2] \tag{4.11}$$

Block Diagram of original FCA with stability actuator only is provided in Figure 4.7.

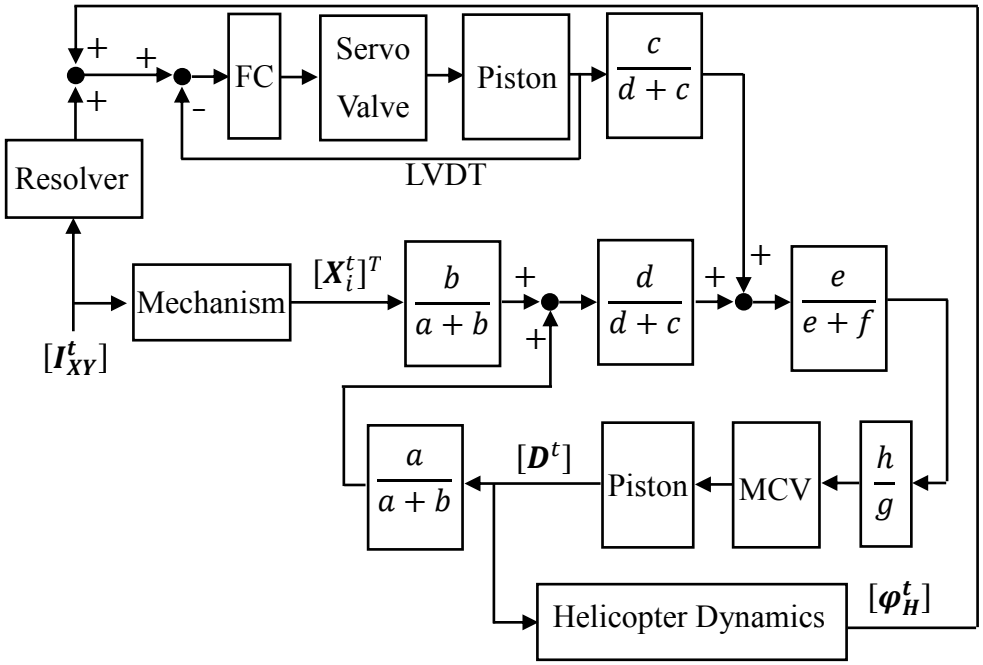

Figure 4.7 Block Diagram of Original System

4.3 Mathematical Model with SCA and Stability Actuator

Stability Control Actuator (SCA) is the actuator that is installed by a parallel linkage inside FCA to arrange PID gains of control computer that is used to provide stability of swashplate in case of any emergency condition that occurs on mechanical linkages between pilot control levers and input lever of FCA. In a FCA upgraded with SCA controller, cylinder output is still determined by only MCV inputs. Thus; pilot input lever, SCA and Stability Actuator are mechanically bounded to the MCV via linkages and ratio between these linkages is adjustable during designing of FCA. These actuators control cylinder output separately; however, they can operate simultaneously without any deficiency. Linkage between these actuators is provided in Figure 4.8.

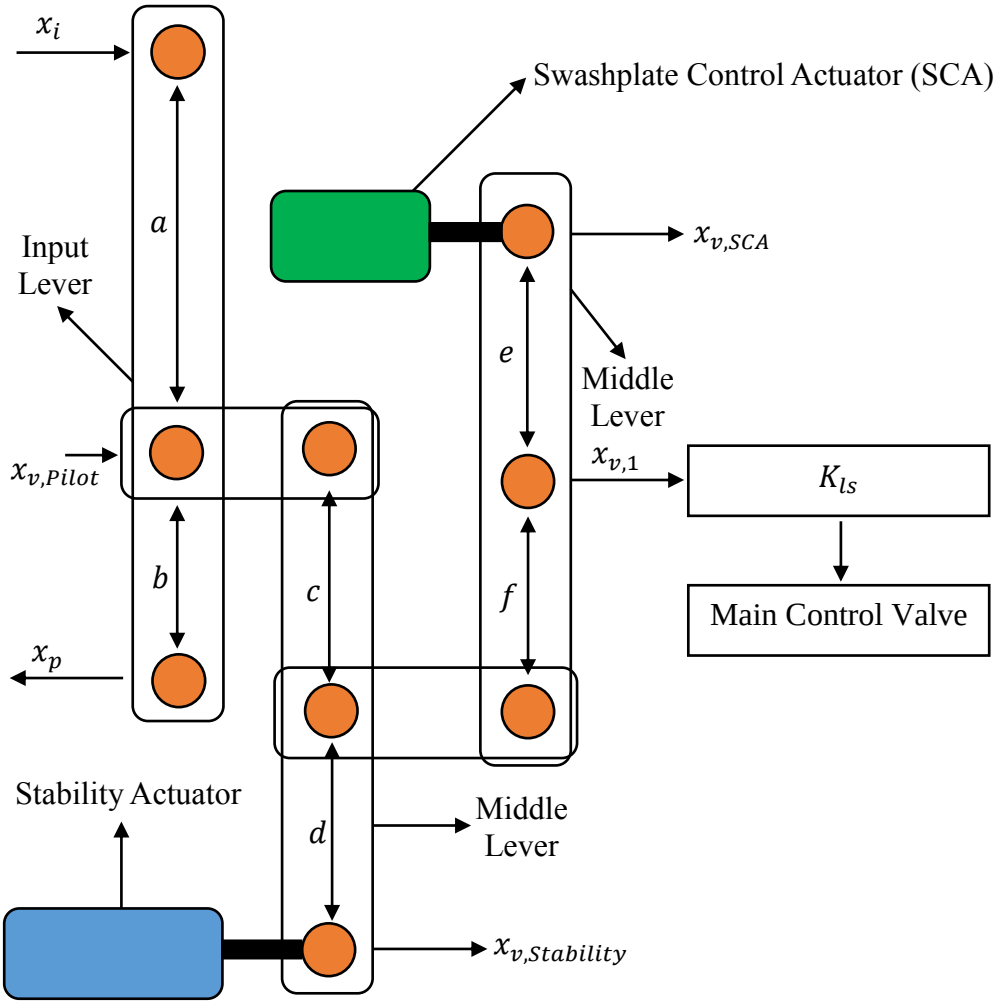

Figure 4.8 Linkage and Sub-Actuator Installation inside FCA

Ratio between input of SCA and $x_{v,1}$ is provided in (4.12).

$$x_{v,1} = \frac{f}{(e+f)} x_{v,SCA} \tag{4.12}$$

Relationship between input of SCA and steady-state output of cylinder is provided in (4.13).

$$\frac{x_{v,SCA}}{x_p} = \frac{a}{(a+b)} \frac{d}{(c+d)} \frac{f}{e} \tag{4.13}$$

Installation of sub-actuators are described as follows. Stability Actuator is linked to middle lever at the bottom end. Using links, input of Stability Actuator is transmitted

to MCV with a reduction ratio that is half of the given input. At the top end of middle lever, pilot input is linked. Between pilot input transmitter lever and middle lever, SCA that is used to provide stability of SSP is installed. Inputs of SCA is summed with mechanical pilot input and half of the total input is transmitted to main control valve. Before main control valve, a layshaft mechanism is used to reduce feedback ratio that is transmitted to MCV because direct transmission cause instabilities. Adding the middle lever has already decreased the ratio of transmission, layshaft design is reconsidered in a way that reduction ratio of layshaft is increased compared to mechanical FCA without controllers designed in previous chapters. Both of Stability actuator and SCA are equipped with a servo valve that is used to convert electrical input into flow rate for cylinder of sub-actuators. A more inclusive figure of linkage mechanisms inside FCA and feedbacks source are provided in Appendix 0.

Totally, there are three closed loop system involved in the control of complete helicopter motions. Initially, pilot control gives input to FCA and changes the orientation of SSP by taking feedback from each actuator. By changing orientation, compound of flight forces that are applied to helicopter body by rotor blades are also changed. Thus, helicopter moves at the desired direction. Secondly, control percentages of pilot inputs are read by Flight Computer (FC) as far as any input is given to main rotor actuators. From data of percentages, a particular orientation of helicopter is calculated by FC and helicopter is tried to be stabilized at that particular orientation in terms of angular positions and angular velocities. Feedback is taken from motions of helicopter body, and they are processed in FC. As a result of procession, Null positions of any FCA is changed using stability actuator to fight with disturbance that act on the motions of the helicopter such as gust, wind, and aerodynamic loads. Third loop arises immediately after implementation of SCA which takes from feedback of position input of any FCA likewise in the first loop and gives parallel inputs with pilot inputs to bring SSP in its desired position for enhancement of the overall stability of SSP, eventually the helicopter. In following chapters, only first and third control loops are deigned and analyzed because it is

required to implement a helicopter model to add second control loop. Instead, second control loop is overlooked by replaced with an open loop input given from FC to FCA computer input port. By making such an arrangement, it is demonstrated that designed controllers to increase stability of SSP operates perfectly well with Stability actuator inputs independent from the reference position of FCA at that instant, changed by stability actuator. Control Loops are demonstrated in Figure 4.9, and marked to express each loop clearly at Appendix C.

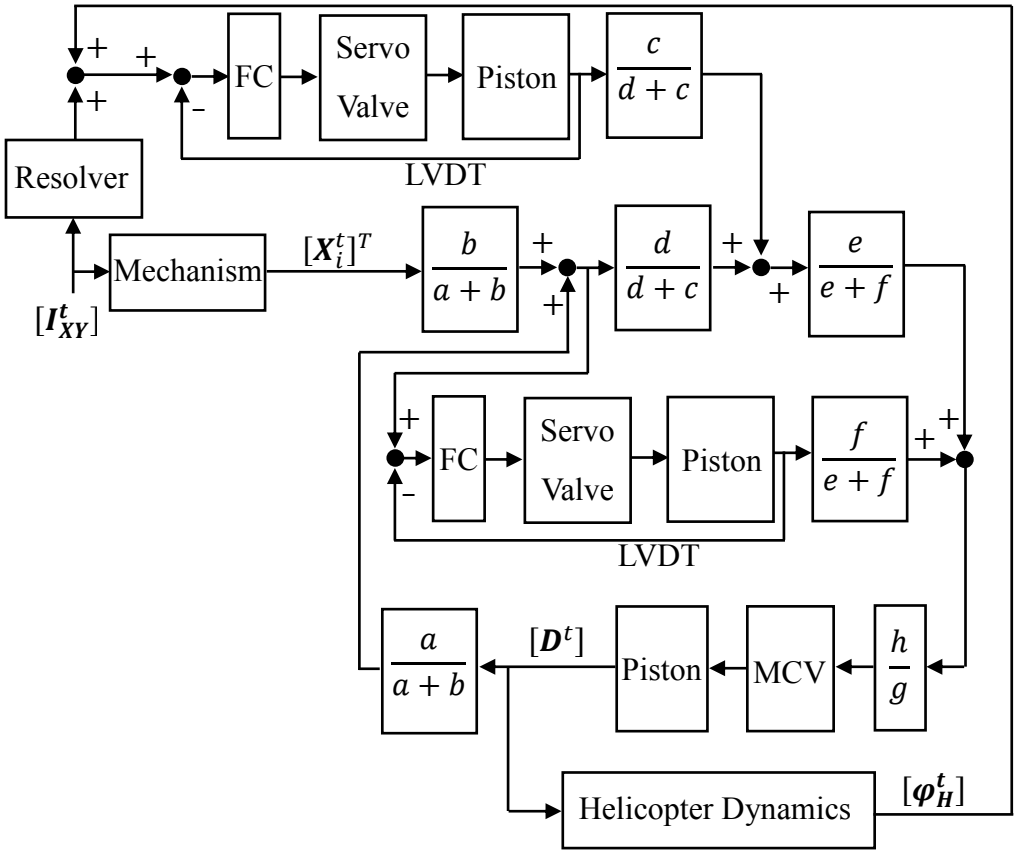

Figure 4.9 Modified Block Diagram with Swashplate Control Actuator (SCA)

4.4 SSP Control Applications

In this chapter, a Stability Control Actuator (SCA) is involved into position control application of SSP for the Purpose extending the frequency response margin and decreasing rise time (t_{rise}) without exceeding the limit peak value. SCA works upon

feedback control theory which is proposed for applying additional input to MCV during transient conditions to obtain better performance by decreasing the rise time of the cylinder output. Two types of different control strategies are developed using involvement of SCA, which are classical PID control method and model-based velocity control method. Defined control strategies are introduced and described in terms of their development idea and method as follows.

4.4.1 Classical PID Control Method

In classical PID control method, position of the cylinder output is given as feedback to control system using an LVDT. PID controller is used to correct the position of the cylinder based on reference input that is applied by pilot. In mechanical control system that is mentioned in (2.142), feedback is taken by mechanical feedback lever and cylinder output is corrected by only a proportional constant that can be arranged as layshaft transmission ratio. By adding a PID controller, a parallel closed loop can be performed. It has a significant benefit that can be proposed as a solution of two flight critical problem. Solution can be described as follows; in a conventional mechanical feedback, flight control capability is lost if there is a lost in the connection of valve input shaft and input lever that is indicated as point A in appendix 0. However, would not be lost if there is a second closed loop alternative which reads input of pilot electronically and gives closed loop control inputs to MCV considering pilot input lever position and LVDT signal from cylinder output. One drawback can be said that if the coefficient of PID controlled is arranged as limited authority, pilot would not be able to control helicopter as agile as it is desired. However, due to limited authority, helicopter would still be controllable although there is a lack of feel the control forces. Valve input the is obtained in PID control application is given in (4.14.

$$x_{v,SCA} = K_{P,SCA}e + K_{I,SCA}\int_0^t edt + K_{D,SCA}\frac{de}{dt} \tag{4.14}$$

Considering also mechanical pilot input to valve, total valve input can be found as follows;

$$x_{v,t} = x_{v,Pilot} + x_{v,SCA} + x_{v,0} \tag{4.15}$$

In (4.15), $x_{v,0}$ represents the null shift of MCV. Although cylinder is at the reference position and there is no pilot input is given to control system, valve can be at open condition. Thus, cylinder position is to be shifted from reference and become stable although it is not in reference position. Most of the cases, null can be neglected. By dropping the last terms, (4.15) can be written in open form as follows;

$$x_{v,SCA} = K_{P,Ls}((K_{P,SCA} + 1)e + K_{I,SCA}\int_0^t edt + K_{D,SCA}\frac{de}{dt}) \tag{4.16}$$

SCA can operate as integrated with Stability actuator. Total MCV input in terms of Stability Actuator, SCA and pilot input is given as follows;

$$\begin{aligned} x_{v,1} = {} & \frac{ce}{(c+d)(e+f)}x_{v,stability} + \frac{de}{(c+d)(e+f)}x_{v,Pilot} \\ & + \frac{f}{(e+f)}x_{v,SCA} \end{aligned} \tag{4.17}$$

In (4.17), $x_{v,Pilot}$ can be reprsented in terms of cylinder output and pilot input. Thus, (4.17) transforms into (4.18) that can be found as follows;

$$\begin{aligned} x_{v,1} = {} & \frac{ce}{(c+d)(e+f)}x_{v,stability} \\ & + \frac{de}{(c+d)(e+f)}\left(\frac{b}{(a+b)}x_i + \frac{a}{(a+b)}x_p\right) \\ & + \frac{f}{(e+f)}x_{v,SCA} \end{aligned} \tag{…}$$

$$\begin{aligned} x_{v,1} = {} & \frac{ce}{(c+d)(e+f)}x_{v,stability} \\ & + \frac{de}{(c+d)(e+f)(a+b)}(bx_i + ax_p) + \frac{f}{(e+f)}x_{v,SCA} \end{aligned} \tag{4.18}$$

Simulink® model starting from pilot input, SCA and Stability actuator to valve control input is given in Figure 4.10

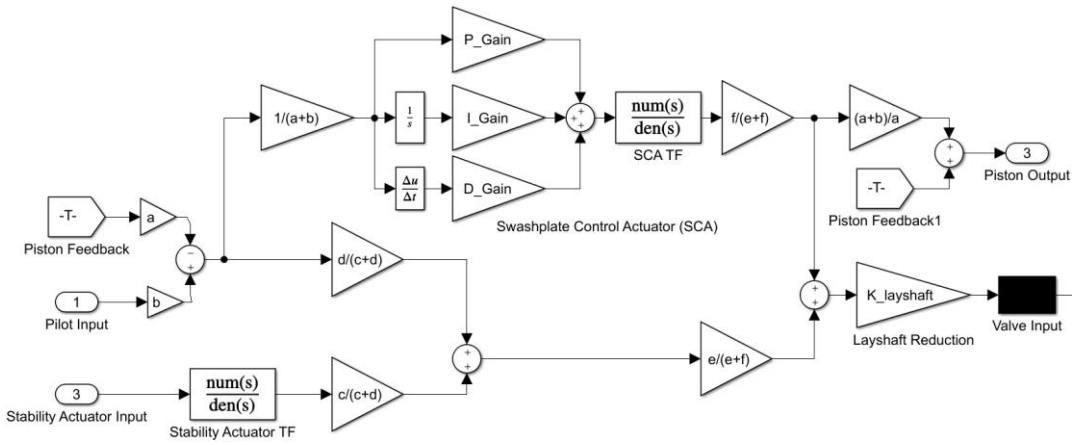

Figure 4.10 Control Inputs, Feedback and Ratios before Valve Input

4.4.2 2-Mass Position Control

Controller that are designated for performance improvement P and PI decreases rise time (t_{rise}) without increasing amplitude of response significant. Although amplitude of M_R does not increase, it has a natural frequency (ω_n) mode approximately at 2.3 Hz and at that frequency level, a significant amplification is observed. It is required to decrease amplitude of the response in case of obtaining more robust control of rotor system and escaping from resonant frequencies as far as 2.3 Hz is within the control band of helicopter rotor system for both automatic controllers and pilot. Besides, it is beneficial to extend bandwidth of output response to provide robustness and sensitive control. Until that point, only mass of piston (M_P) is controlled and other mass or masses are being under free movement. By having such a case for 2-mass system, bode plot between input lever position and output of free mass is given in Figure 4.11.

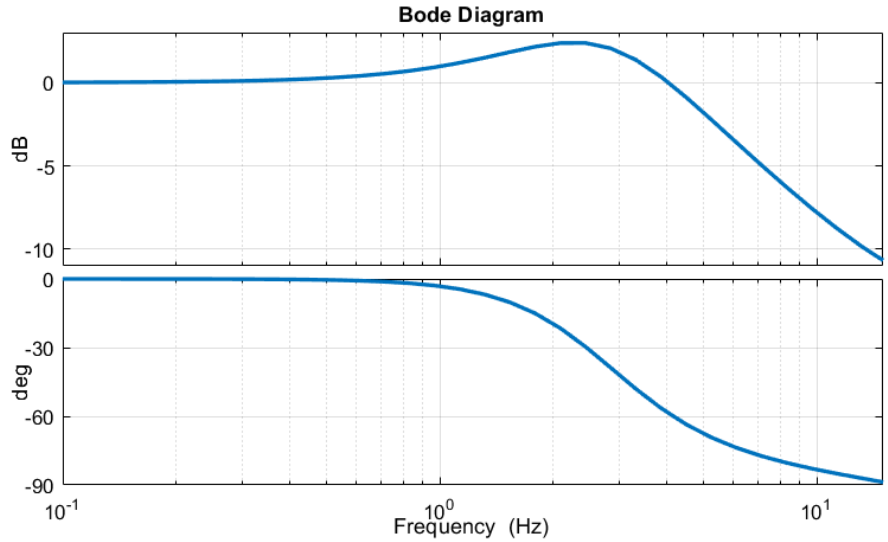

Figure 4.11 Bode Diagram of Single Mass Controlled System

A more robust control system can be proposed with a slight modification of feedback system. New control method is called "Two Mass Displacement Control System" [35], which proposes to take feedback not only from cylinder output but also from free mass output. By doing so, free mass in controlled under a wider frequency band without that much amplification. At the same time, cylinder output is also controlled in desired levels. Representative diagram of 2-mass position control system is given in Figure 4.12.

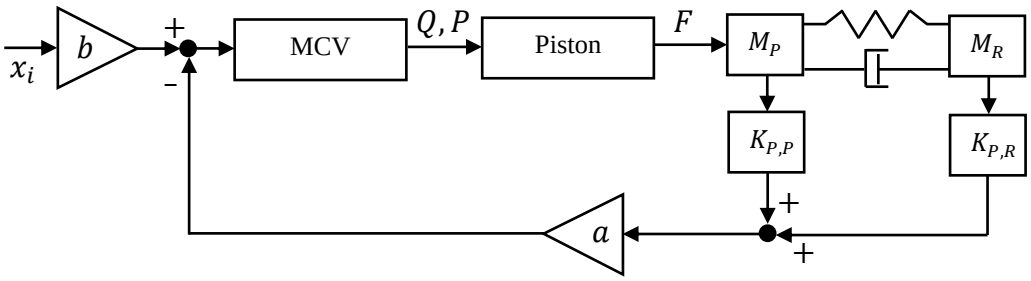

Figure 4.12 Two Mass Position Control

It is required to install a lever mechanism at the cylinder output of FCA to acquire combination of two feedbacks. Lever connection points are selected to determine influences of each independent feedback systems. It is known that modeled mass of

M_R represents rotating components of rotor system. Thus, feedback of this mass can be taken by using an LVDT and output of the LVDT is directly transmitted to an actuator, which is called Feedback Actuator. It is that is used to give feedback to Feedback Summer. Visual representation, inputs and output of Feedback Summer is provided in Figure 4.13 and approximate point on which the LVDT sensor is installed is demonstrated in Figure 4.14.

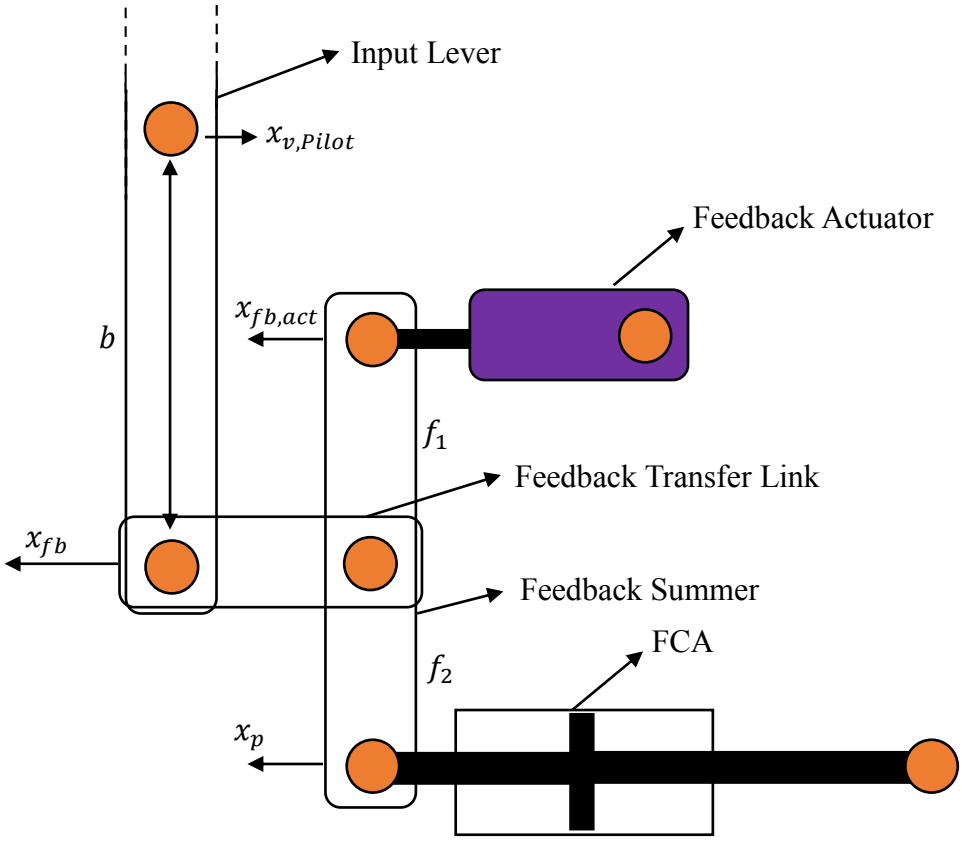

Figure 4.13 Visual Representation of Feedback Summer

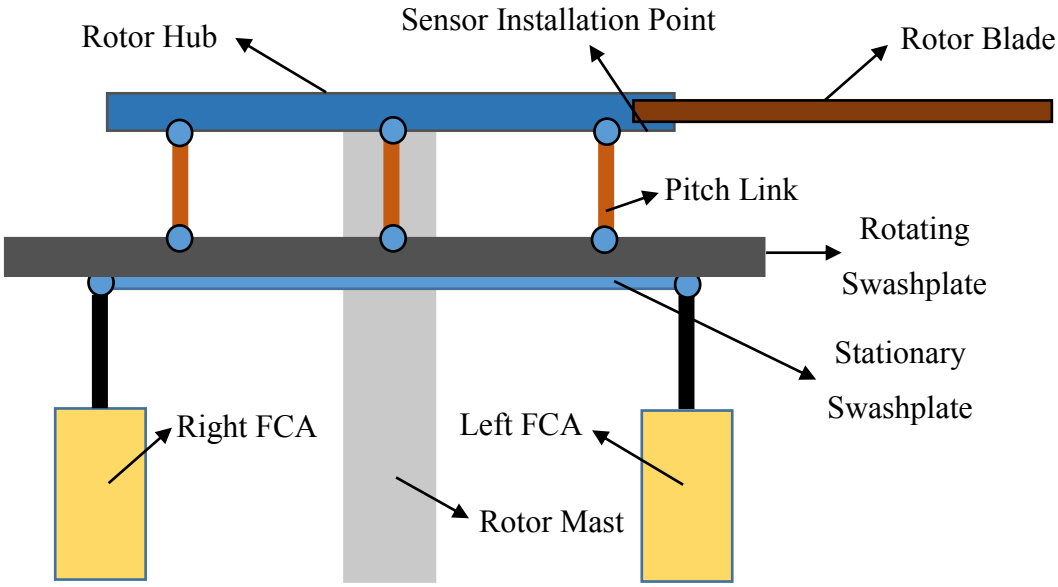

Figure 4.14 Position Transducer Installation Point

Mathematical representation of feedback given to cylinder end of input lever by addition of summer link is given in (4.19).

$$x_{fb} = \frac{f_1 x_p + f_2 x_{fb,act}}{f_1 + f_2} \tag{4.19}$$

Mathematical representation of $x_{v,Pilot}$ is given in (4.20).

$$x_{v,pilot} = \left(\frac{b}{(a+b)} x_i + \frac{af_1}{(a+b)(f_1+f_2)} x_p + \frac{af_2}{(a+b)(f_1+f_2)} x_{fb,act}\right) \tag{4.20}$$

Simulink model that includes modified feedback transmission system is provided in Figure 4.15.

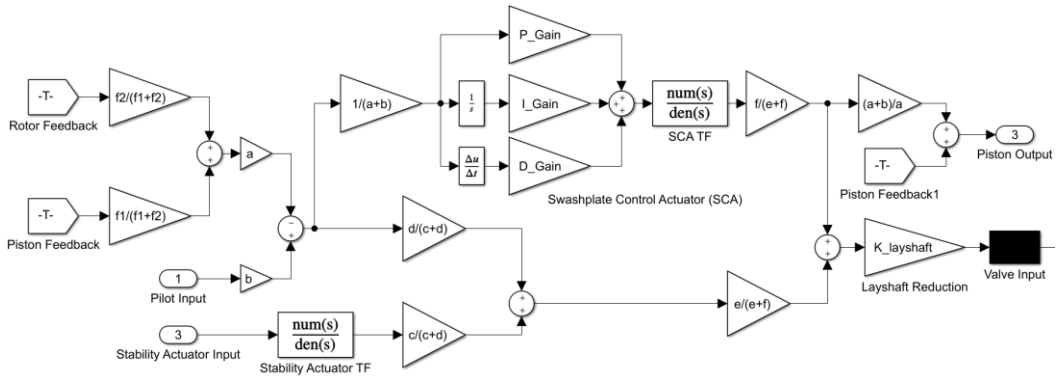

Figure 4.15 Simulink Model Including Modified Feedback

By using a summing link before given feedback to cylinder end of input lever, feedback ratios of two different masses can be arranged. Using mechanical ratios, the mass which is intended to be controlled more precisely can be given as a prior mass by arrangement of summer link ratios. Therefore, mass that is intended to be controlled is put into a control loop ore sensitively compared to other mass. However, even if the priority is given to mass of equivalent rotor components instead of mass of piston, control of piston mass is still provided with sufficient sensitivity because actuator itself is an overdamped actuator. Thus, it is favorable to give priority to mass of equivalent rotor components in terms of lever ratios. By doing so, feedback of rotor components mass is given to control system dominantly; therefore, two masses are controlled in synchronized and sufficiently precise way. Three different control strategies are selected and tried based on varying feedback ratios. Results of each feedback summation are obtained independently and compared. Three different feedback mechanisms that proposes different control strategies itself are provided in Table 4.1.

Table 4.1 Applied Control Strategies

Control Strategy	Mechanism Ratio ($^{f_2}/_{f_1}$)
No Control	0
Strategy 1: Cylinder Dominant	0.33
Strategy 2: Equally Dominant	1

4.4.3 Results of 2-Mass Position Control

Using these feedback summer links, a different amplitude gains and frequency bands are obtained which are demonstrated and compared in Figure 4.16 and Figure 4.17, for amplitude and phase lag respectively.

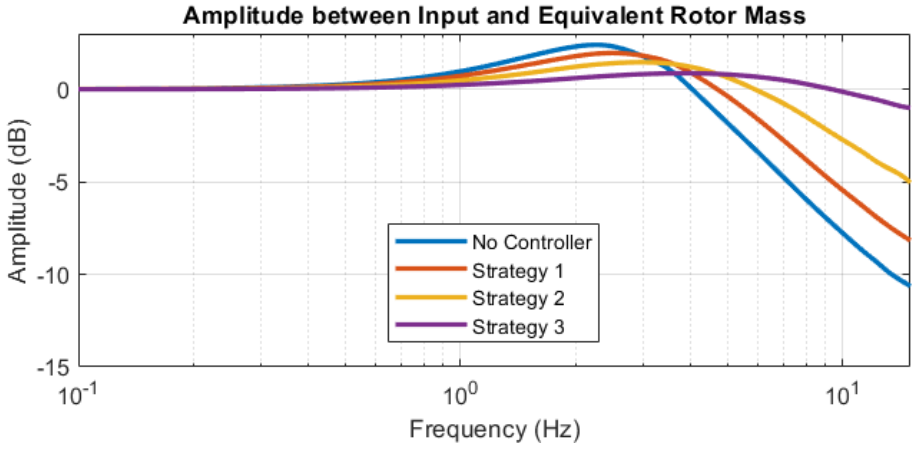

Figure 4.16 Amplitude Comparison of Different Control Strategies

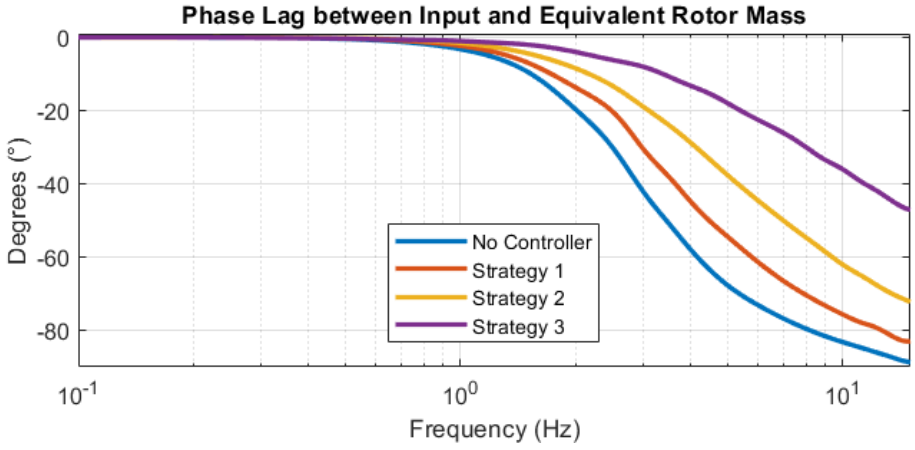

Figure 4.17 Phase Lag Comparison of Different Control Strategies

As it can be extracted from Figure 4.16 and Figure 4.17, control strategies that are proposed in chapter 4.4.2 work extremely beneficial especially with increasing dominancy of feedback from rotor equivalent mass. For example, frequency range

of above -3dB is expanded above 15 Hz. Resonant response of equivalent rotor mass is also decreased by increasing resonant frequency from 2.5 Hz up to 6 Hz by applying different strategies. Strategy 3 can be used to control rotor mass as it proposes the highest frequency margin and the lowest phase shift by increasing frequencies. Block diagram of completely modified system that includes both SCA, Stability Actuator and Feedback Actuator is provided in Figure 4.18.

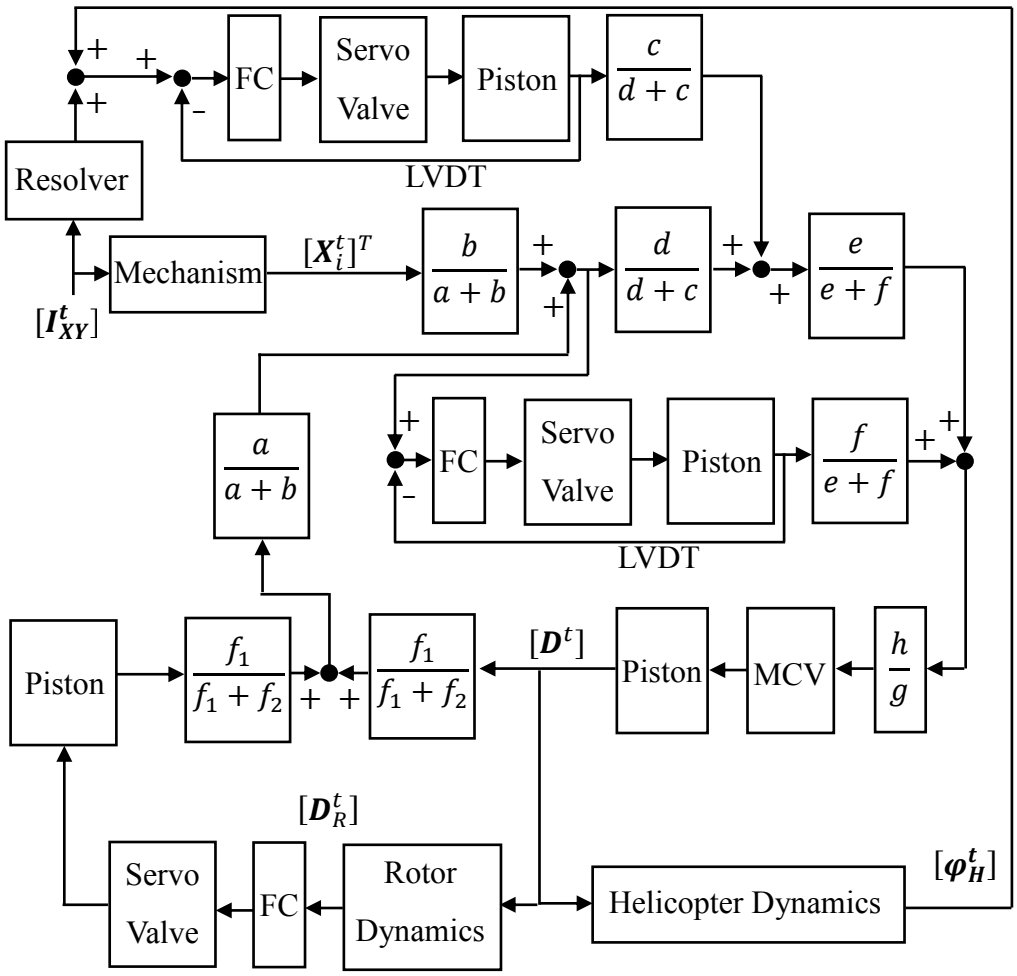

Figure 4.18 Modified Block Diagram with Swashplate Control Actuator (SCA), Stability Actuator and Feedback Actuator

Where displacement of equivalent rotor mass is represented as follows;

$$[D_R^t]^T = [D_{R,1} \quad D_{R,2} \quad D_{R,3}] \tag{4.21}$$

CHAPTER 5

CONCLUSION & RECOMMENDATION

5.1 Conclusion

Hydraulic control systems are widely used in position control of applications of helicopter main rotor as it is required to overcome and compete with high flight forces especially for heavy helicopters. For sensitive control, proportional control valves are used that operates with principle of feedback control. Position of main rotor is to be determined to arrange pitch angles of each rotor blade that creates main forces to direct and control helicopter. Each pitch angle is determined independent from each other on behalf of Stationary Swashplate (SSP). Position of SSP is determined via three Flight Control Actuators (FCA) that are installed as 120° separated from each other with a lug on SSP. Inputs for determination of position of SSP can be given manually by pilot and automatically by automatic control system.

Mathematical model of complete hydraulic control system is obtained by applying the following steps. Initially, helicopter input sources and their missions in a flight operation are introduced. Kinematic relationship between three FCAs that controls main rotor orientation and input sources are derived. As a result of these derivations, reference positions of FCAs can be obtained during controlling. Next, hydraulic subcomponents and driving/feedback mechanisms of FCA is modeled. Hydraulically driven components are mainly MCV and cylinder. Pressures of high-pressure source and low pressure tank are taken as constant as pressure drop of high pressure source is negligible during transient conditions. As far as null shift and leakage constant are able to be manipulated, they are taken as zero for simplicity in the analysis. Operation of a FCA is provided by feedback control theory. Positional feedback of cylinder output is taken as feedback to MCV for application of the theory. Additionally, dynamic system on motion is modeled as 2-Mass system represented by equivalent

masses of swashplate assembly and blade assemblies. Equivalent masses are taken as design parameters together with stiffness and damping coefficients that belongs to these masses.

Verification of the mathematical model is made by a test bench that is the reflection of hydraulic control system on helicopter. Designated tests are applied in the test bench. For external loading of FCAs, External Load Actuators (ELA) are used separately for each actuator instead of a rotor and swashplate mechanism. For source inputs of FCAs, Pilot Input Actuators (PIA) are used. Once the tests are executed, position output data of PIAs and FCAs are collected as well as force data of ELAs and pressure data of hydraulic pump that is used as the pressure source of test system. Theoretical results of linear and nonlinear system are compared with experimental results, and they are found as consistent to each other. Thus, validation of mathematical model is made by making such a comparison.

Apart from current control system, it is proposed a novel control system for performance improvement compared to current one. Two types of additional control algorithm are added for this purpose. First, classical PID controller is introduced by adding a Swashplate Control Actuator (SCA) which takes pilot inputs as reference as cylinder output as feedback but operates electronically. Although system interface is designed for PID controller, only P and PI controllers are used because derivative terms is evaluated as unnecessary. A preliminary performance improvement is provided by using the classical controller. Secondly, a new feedback system is designed by using a feedback actuator that gives position of equivalent rotor mass as feedback to MCV together with cylinder displacement. This control method is named as 2-Mass control system. It provides certain benefits which can be listed as increment of frequency band, decrement of amplitude in resonant frequency, moving of resonant frequency to a rarer frequency range. Mechanical explanation of proposed control methods is given.

Proposed controllers can be applied in a hydraulic rotor control system quite easily by implementing a two additional actuator. These actuators cooperate perfectly with

stability actuator which is used in current applications. Cooperation can be provided without any deficiency as far as new control actuator is installed by using a separate link and feedback actuator is linked to input lever with also a separate link. One of drawback can be said as installation of these actuator cause an increase of the weight of actuator.

5.2 Future Work & Recommendation

Hydraulic rotor control system consists of several critical details and complicated dynamics systems. Thus, some of these details are neglected or assumed and complicated dynamic system are reduced to a simpler system. Therefore, these details can be investigated as further research as they may contain an information that affects behavior of dynamics systems either positively or negatively. These details and simplifications by assumptions are explained and given as follows.

Initially, rotor dynamics system consist of many subcomponents and their behavior under varying environmental conditions are subjected to change. Some of information about dynamic behavior of them are lost by making assumptions as these subcomponents are taken as a simple mass-spring-damper system. In fact, overall dynamic characteristic of rotor system is determined by equivalent coefficients only. Thus; considering their life cycle, environmental changes, plastic deformations under such high loads, material characteristics, it is highly recommended to take equivalent parameters within a range instead of universal constants. This range can be determined by looking at the operational extremities of dynamic system considering missions of helicopter. By taking dynamic coefficient in a certain range, controlled dynamic plant experiences a change that excites any other frequencies that are to be controlled to provide overall control stability of the helicopter. Besides, rotor system is in overall reduced to a two-equivalent mass. However, if it is intended to make a more comprehensive analysis, some other masses can be added to dynamic system as they can also be connected in parallel as well as serial connections.

In hydraulically powered flight control actuator design, some assumptions are made as it is evaluated as non-critical for actuator in use. For example, leakage coefficient of actuator is taken as zero because it is known that leakage of this actuator is in quite low level; in fact, insignificant to affect system operation. However, if an actuator with high leakage rates are intended to be used, leakage coefficient is to be given correctly because higher leakage coefficient may create unexpected deficiencies in system operation. Besides, if the leakage is caused by a null shift and it is known, it is to be also given as a parameters. Leakage does not have to be a linearly changing value. In such a case, leakage is to be taken as a dependent function of pressure and spool position. In some actuators, friction between inside surface of actuator body and cylinder outer surface is dramatically high because of lack of sensitive manufacturing techniques or seal selection failures. In such cases, cylinder friction is to be implemented to mathematical model dependent to velocity of the cylinder.

In Chapter 3, verification and validation tests are executed in the exactly scaled test rig of main rotor control system. However, external loading that is applied by ELAs is not arranged considering inertial loads. Instead, combination of a static and dynamic load is applied to all actuators separately. It is recommended that external loads of all actuators are to be calculated and given to each actuator separately as a simulation of inertial effects as well as expected disturbances. Although it does not affect the mathematical model of hydraulic control system, loads that are caused by inertial effects are not to be verified and equivalent parameters of rotor system are kept as assumptions instead of verified parameters. It is also possible to add equivalent masses between ELAs and FCAs instead of connecting them each other. However, due to mobility of the test rig, inertial effects are recommended to be observable by adding a force control algorithm on the controllers of ELAs for simulation of external loads. By doing so, they can be quite easily manipulated and adapted for any design changes performed on the rotor system.

In Chapter 4, a novel control method is proposed by adding a certain sub-equipment on the flight control actuator. However, it cannot be tested as it requires a costly modification on the currently developed actuator. Thus, it is recommended to

implement Swashplate Control Actuator (SCA) and Feedback Actuator on the Flight Control Actuator is a manufacturing is to be performed. Some geometric modifications and design optimizations are to be made for reducing the volume of the component. Besides, as far as the proposed mechanisms are movable parts, it is highly recommended to have a kinematic model of intermediate and connection linkages in case of any jamming. It is possible to selected SCA and Feedback Actuator exactly same with Stability Actuator that have already been installed on the FCA. However, Stability actuator transfer function is an assumption of frequent applications, and it is not tested. However, it would be sufficient to use such an actuator to obtain desired performance of the control system.

Controller design in Chapter 4 is performed by reduction of the rotor dynamic system to a single mass to get rid of complexity. However, performance of control system may be enhanced to a further level by behaving rotor system as separate masses and making a position control from several locations on the rotor system. Besides, sensor location of displacement sensor is selected based on recommendations from rotor mechanical design criterion. However, any other location on the rotor assembly may reflect a more correct result in terms of equivalence of the rotor parameters. Additionally, velocity control can be applied to the equivalent masses as well as position control in order to obtain much higher performance in terms of defined criterion.

REFERENCES

1. Viswanath, S. and Nagarajan, R. 2002. Helicopter Hydraulic System (Design, Component Selection, Modular Construction, Integration and Testing), Rotary Wing Research & Design Centre, Hindustan Aeronautics Limited, Bangalore, India, ICAS 2022 CONGRESS, 693.1-8.

2. Kabai, S. January 2008. "Helicopter Tilt Control", WOLFRAM Demonstration Project, Open content licensed under CC BY-NC-SA, Accessed on: "https://demonstrations.wolfram.com/HelicopterTiltControl/", October 2021.

3. Yunjie, W. Jiang, C. Yuwen, Z. Haowen, W. 23 April 2020. Helicopter Safe Landing Trajectory after Main Rotor Actuator Failures, Applied Sciences 2020, 10, 2917, School of Aerospace Engineering, Tsinghua University, China.

4. Chatzakos, P. and Papadopulos, E. 2003. On Model-Based Control of Hydraulic Actuator. Proceedings of RAAD'03, 12th International Workshop on Robotics in Alpe-Adria-Danube Region Cassino.

5. Šıtum, Ž. 2011. Force and Position Control of a Hydraulic Press, Krmıljenje Hıdravlične Stıskalnıce. 314-320.

6. Efe, Yalcın.. 2014. Dynamic Model of a Hydraulic Servo System for a Manipulator Robot, M. Sc. Thesis, KTH Electrical Engineering, Stockholm, Sweden.

7. Liu, R. 1994. Nonlinear Control of Electro-Hydraulic Servosystems: Theory and Experiment, M. Sc. Thesis, University of Illinois at Urbana-Champaign, Mechanical Engineering Department, Urbana, Illinois.

8. Tenali, S. V. Simulation of Electro-Hydraulic Servo Actuator, M. Sc. Thesis, National Institute of Technology, Rourkela, Department of Mechanical Engineering, Rourkela, Orissa.

9. Loukianov, A, G. January 2004. Electro-hydraulic Actuator Trajectory Tracking, Conference Paper in Proceedings of the American Control Conference, Boston, Massachusetts, ThA19.5,2603-2608, DOI: 10.23919/ACC.2004.1383858 · Source: IEEE Xplore,

10. Kaddissi, C., Kenné, J. P., Saad, M., 2004. Position Control of an Electro-Hydraulic Servosystem – A non-linear backstepping approach. In Proceedings of the First International Conference on Informatics in Control (ICINCO), Automation and Robotics, pages 270-276, DOI: 10.5220/0001134402700276, SciTePress.

11. Vaidyanathan, S., Azar, A. T., 2021. Backstepping Control of Nonlinear Dynamical Systems, Advances in Nonlinear Dynamics and Chaos (ANDC), Pages 1-32, DOI: 10.1016/B978-0-12-817582-8.00008-8, Academic Press.

12. Maneetham, D., Afzulpurkar, N., 2010. Modeling, Simulation and Control of High Speed Nonlinear Hydraulic Servo System, World Journal of Modelling and Simulation, Vol. 6, No.1, pp.27-39, ISSN 1 746-7233, England, UK.

13. Sohl, G. A., Bobrow, E. J., March 1999. Experiments and Simulations on the Nonlinear Control of a Hydraulic Servosystem, IEEE Transactions on Control Systems Technology, Vol. 7, No. 2, 1063–6536/99$10.00.

14. Tamburrano, P., Distaso, E., Plummer, A. R., Amirante, R. April 2019. A Review of Electro-Hydraulic Servovalve Research and Development, Article in International Journal of Fluid Power, Vol. 20_1, 53-98, DOI: 10.13052/ijfp1439-9776.2013, River Publishers.

15. Naveen, Kumar, A., August 2018. Design and Implementation of Hydraulic Press System Using MATLAB, International Journal of Engineering Sciences & Research Technology, DOI: 10.5281/zenodo.1336656.

16. Kalyoncu, M., Haydim, M., January 2009. Mathematical Modeling and Fuzzy Logic Based Position Control of an Electrohydraulic Servosystem with Internal Leakage, Mechatronics 19, pages 847-858. DOI:10.1016/j.mechatronics.2009.04.010, ScienceDirect.

17. Li, L., February 2015. Simulation and Control of Servo Hydraulic Actuators for Test Applications. Doctor's Thesis, Graz University of Technology, Institute of Electronics, Graz.

18. Zhou, Y., Zhou, X., Modeling and Controller Design For An Experimental Test Bench For Aircraft Actuators, Advances in Mechanical Engineering, Vol. 10(12) 1-7, DOI: 10.1177/1687814018815362, SAGE.

19. Kővári, A., 2010. Real-Time Modeling of an Electro-Hydraulic Servo System, Computational Intelligence in Engineering, Studies in Computational Intelligence Vol. 313, 2010, pp 301-311, Print ISBN: 978-3-642-15219-1, DOI: 10.1007/978-3- 642-15220-7_24.

20. Bequette, W., 2022. Process Control: Modeling, Design and Simulation, International Series in the Physical and Chemical Engineering Sciences, Published Dec 26 by Pearson, ISBN-10: 0-13-353640-8 or ISBN-13: 978-0-13-353640-9.

21. Deakin, R., E. 2005. Chapter 7: Linearization Using Taylor's Theorem and the Derivation of Some Common Surveying Observation Equation, RMIT University, Geospatial Science, Lecture Notes on Least Squares.

22. Merritt H. E., 1967. Hydraulic Control Systems, John Wiley & Sons, Inc. New York, London, Sydney.

23. Rowell, D., Wormley, N. D., 1997. System Dynamics: An Introduction, Prentice Hall Inc. Upper Saddle River, New Jersey 07458.

24. Platin, E. B., Çalışkan, M., Özgüven, 1991. Dynamics of Engineering Systems, Middle East Technical University, Mechanical Engineering Department.

25. Dransfield, P., Bruce, D. M., March-April 1968. Leakage Flowrate past Pistons of Oil Hydraulic System Components, J. Aircraft, Vol. 5, No 156-160, DOI: 10.2514/3.43923.

26. Hružík, L. Vašina, M. Bureček, A., 2013. Evaluation of Bulk Modulus of Oil System with Hydraulic Line, EPJ Web of Conferences 45, 01041-p.1-6, EDP Sciences, DOI: 10.1051/epjconf/20134501041.

27. Varghese, S. Josephkunju, P. C. Karunanidhi, S., September 2014. Influence of Different Grades of Diamond Lapping Paste on Leakage, Pressure Gain, and Frequency Response of Hydraulic Valve, International Journal of Emerging Technology and Advanced Engineering, ISSN 2250-2459, ISO 9001:2008 Certified Journal, Volume 4, Issue 9, pages 263-274.

28. Lin, F., The Design and Simulation of Electro-Hydraulic Velocity Control System, 2011. IFIP International Federation for Information Processing, IFIP AICT 347, pp. 568-574.

29. SAE-AS-4059, Aerospace-Cleanliness Classification for Hydraulic Fluids, Revision A, 30.03.1990. A-6C1 Contamination and Filtration Committee, Published by SAE International, 5 Pages, DOI: https://doi.org/10.4271/AS4059A.

30. Ozturan, A. Duzagac, H. A. et. al., October 30, 2019. Flow Analysis in a Test Rig for System Characterization of a Helicopter Hydraulic Power System, 8th Asian/Australian Rotorcraft Forum, Ankara, Turkey.

31. MIL-H-83282D, Hydraulic Fluid, Fire Resistant, Synthetic Hydrocarbon Base, Aircraft, Metric, Nato Code Number H-537, 30.09.1997. Military Specification.

32. MIL-H-5606G, Hydraulic Fluid, Petroleum Base; Aircraft, Missile and Ordnance, 09.09.1994. Military Specification.

33. MIL-H-87257, Hydraulic Fluid, Fire Resistant; Low Temperature, Synthetic Hydrocarbon Base, Aircraft and Missile, Nato Code Number H-538, 02.03.1992. Military Specification.

34. Ellis. G., 2012. Control System Design Guide (Fourth Edition), Chapter 6 – Four Types of Controllers, Elsevier, Pages: 97-119, DOI: https://doi.org/10.1016/B978-0-12-385920-4.00006-0.

35. Sun. Z., Zahn, P., Verl, A., Lechler, A., 20 December 2016. A New Control Principle to Increase the Bandwidth of Feed Drives with Large Inertia Ratio, Int J Adv Manuf Technol (2017) 91:1747-1752, Springer-Verlag London 2016, DOI: 10.1007/s00170-016-9895-3.

APPENDICES

A. Experimental Setup Sensor Locations and Measurement Rates

Experimental Setup of helicopter Hydraulic control system involves several measurement sensors and data from these sensors are collected. Locations of these sensors on the installation are given as follows:

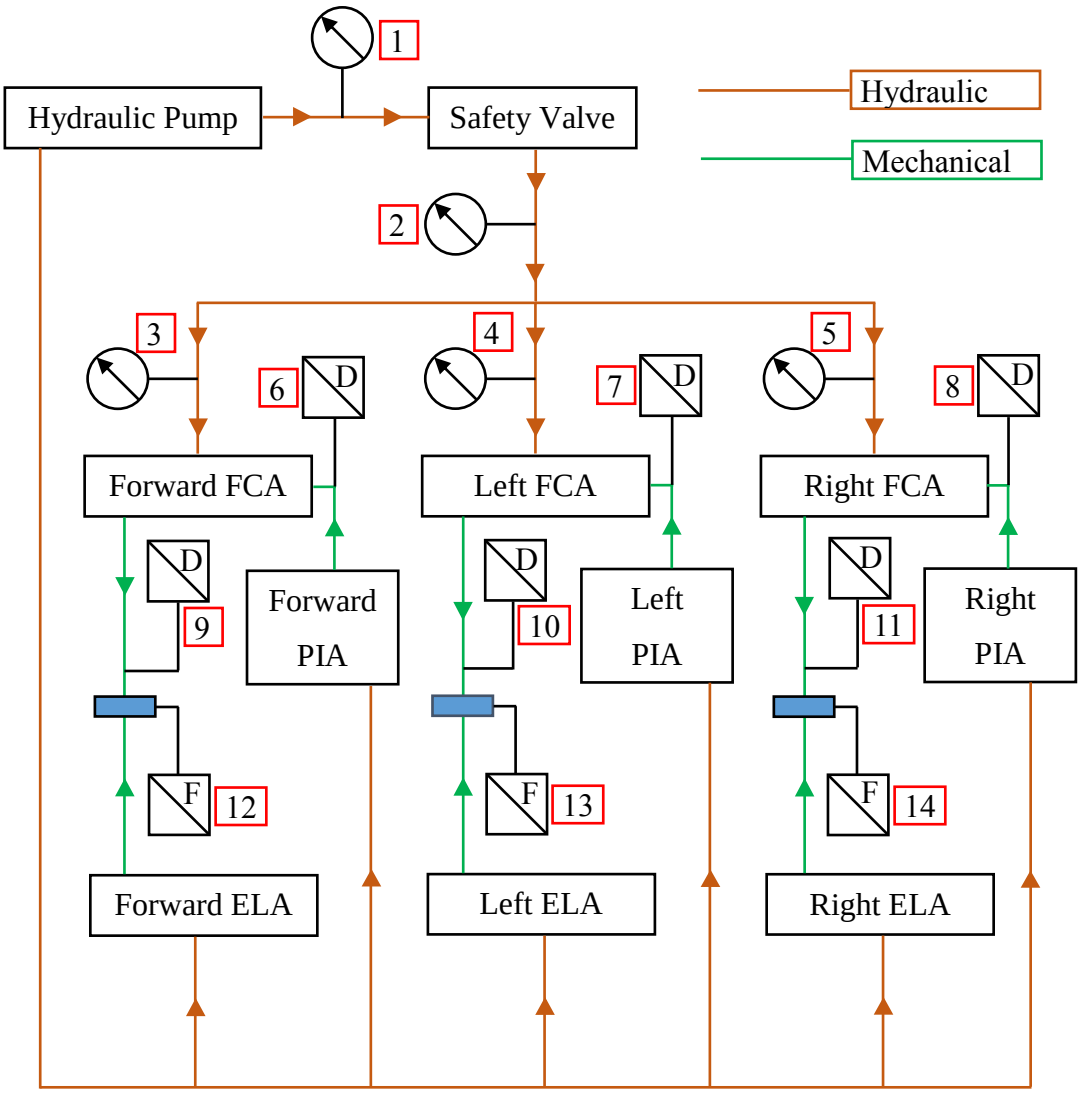

Demonstrated sensors are used ones to evaluate the necessary behavior of the system. There are fourteen sensors used and data is recorded in various frequencies. Sensor properties and their data collection rates are given as follows;

Sensor No	Sensor Type	Recording Rate	Sensor Name
1	Pressure Transducer	>1000 Hz	PUMP_PRES
2	Pressure Transducer	>1000 Hz	VALVE_PRES
3	Pressure Transducer	>1000 Hz	FFCA_PRES
4	Pressure Transducer	>1000 Hz	LFCA_PRES
5	Pressure Transducer	>1000 Hz	RFCA_PRES
6	Displacement Transducer	>100 Hz	FPIA_DISP
7	Displacement Transducer	>100 Hz	LPIA_DISP
8	Displacement Transducer	>100 Hz	RPIA_DISP
9	Displacement Transducer	>100 Hz	FFCA_DISP
10	Displacement Transducer	>100 Hz	LFCA_DISP
11	Displacement Transducer	>100 Hz	RFCA_DISP
12	Force Transducer	>100 Hz	FELA_LOAD
13	Force Transducer	>100 Hz	LELA_LOAD
14	Force Transducer	>100 Hz	RELA_LOAD

B. Linear Derivation of 2-Mass System

Physical representation of the reduced 2-Mass system is given below. Note that during derivation, several details are not entirely described as this derivation has already been performed for 1 and 3-Mass system is 2.2.2 and 2.3.1, respectively.

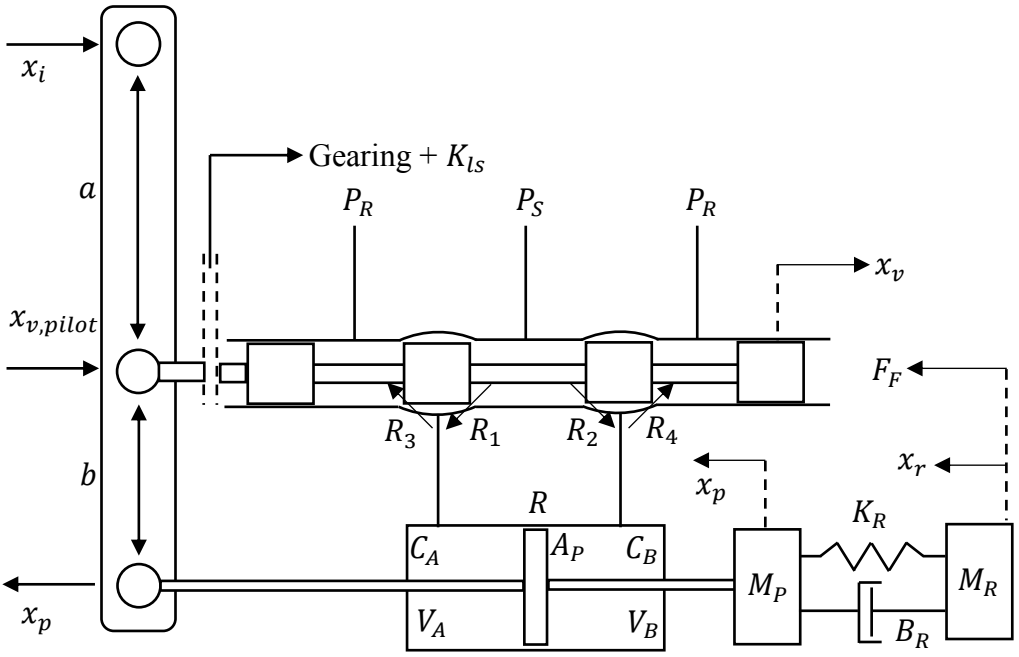

Linear Graph representation of the model is given as follows;

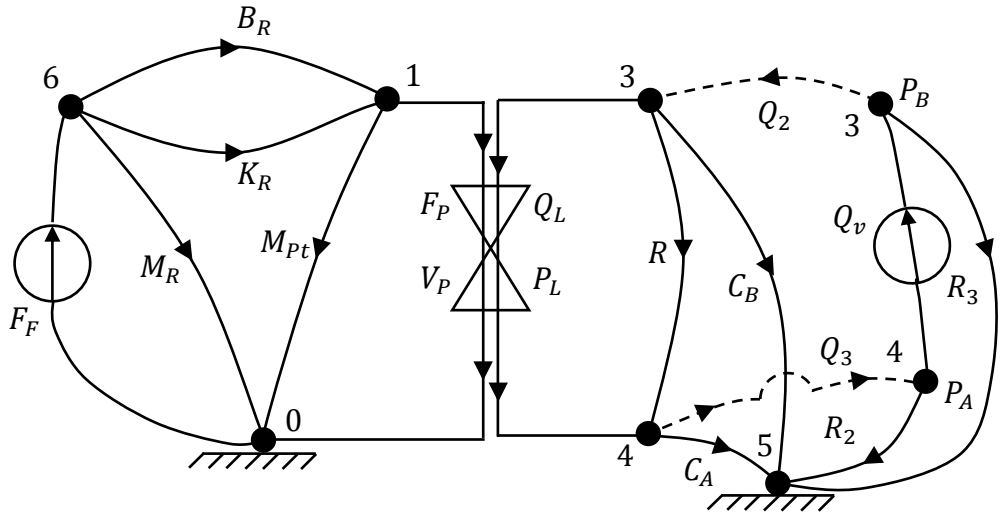

Properties of linear graph is given in the following table.

Linear Graph Property	# of the Property in Linear Graph
Branches (B)	13
Nodes (N)	7
Across Sources (S_A)	0
Through Sources (S_T)	2
Nodes in Normal Tree ($N - N_D$)	5
Variables ($2B$)	26

Normal Tree representation of the 2-mass system is given as follows.

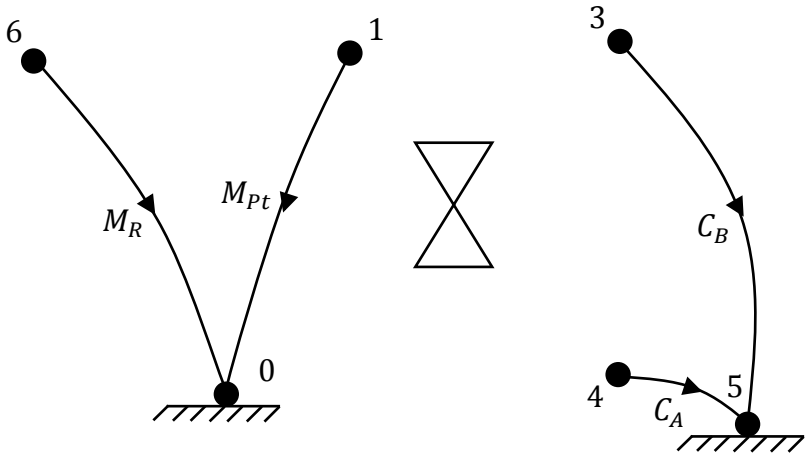

Primary and secondary variables of the system are provided below.

Primary Var.	V_R, V_P, P_A, P_B,Q_v, F_{BR}, F_{KR}, F_F, F_P, Q_L, Q_R, Q_{R2}, Q_{R3},
Secondary Var.	F_R, F_P, Q_A, Q_B, P_v, V_{BR}, V_{KR}, V_F, V_P, P_L, P_R,P_{R2}, P_{R3}

For 2-Mass representation, there are 11 different elemental equations can be found in total which are given as follows;

$$\dot{V}_R = \frac{1}{M_R} F_R$$

$$\dot{V}_{Pt} = \frac{1}{M_{Pt}} F_P$$

$$\dot{P}_A = \frac{1}{C_A} Q_A$$

$$\dot{P}_B = \frac{1}{C_B} Q_B$$

$$\dot{F}_{KR} = K_R V_{KR}$$

$$F_{BR} = B_R V_{BR}$$

$$F_P = A_P P_L$$

$$Q_L = -A_P V_P$$

$$Q_R = \frac{1}{R} P_R$$

$$Q_{R2} = \frac{1}{R_2} P_{R2}$$

$$Q_{R3} = \frac{1}{R_3} P_{R3}$$

Number of continuity equations that can be written for 2-Mass system is 4 and they are given as follows;

$$F_F = F_{BR} + F_{KR} + F_R$$

$$F_{BR} + F_{KR} = F_{Pt} + F_P$$

$$Q_A = Q_L + Q_R - Q_{R3} - Q_v$$

$$Q_B = -Q_L - Q_R + Q_{R2} + Q_v$$

Number of compatibility equations that can be written for 2-Mass system is 8 and 7 they are given as follows;

$$P_L = P_A - P_B$$

$$P_{R3} = P_A$$

$$P_R = P_A - P_B$$

$$P_{R2} = -P_B$$

$$V_{BR} = V_{KR}$$

$$V_R = V_{KR} + V_{Pt}$$

$$V_{Pt} = V_P$$

Starting with $\dot{V}_R$, 1st state equation can be found as;

$$\dot{V}_R = \frac{1}{M_R}(F_F - B_R(V_R - V_{Pt}) - F_{KR}) = \left(\frac{F_F}{M_R} - \frac{B_R V_R}{M_R} + \frac{B_R V_P}{M_R} - \frac{F_{KR}}{M_R}\right)$$

Continuing with $\dot{V}_P$, 2nd state equation can be found as;

$$\dot{V}_{Pt} = \frac{1}{M_{Pt}}(F_{KR} + B_R(V_R - V_{Pt}) - A_P P_C) = \left(\frac{F_{KR}}{M_{Pt}} + \frac{B_R V_R}{M_{Pt}} - \frac{B_R V_P}{M_{Pt}} - \frac{A_P P_C}{M_{Pt}}\right)$$

Continuing with $\dot{F}_{KR}$, 3rd state equation can be found as;

$$\dot{F}_{KR} = K_R V_{BR} = K_R(V_R - V_{Pt}) = K_R V_R - K_R V_{Pt}$$

Continuing with $\dot{P}_C$, 4th state equation can be found as;

$$\dot{P}_C = \dot{P}_A - \dot{P}_B = \frac{1}{C}\left(-2A_P V_{M1} + \frac{2}{R}P_C - 2K_{vf}x_v + K_{pf}P_C\right)$$

Although linear system can be represented by 4 state variables, it is required to add a dummy state in order to control the displacement of the cylinder and obtain a closed loop linear system. By adding a dummy state, 5th state equation can be written as;

$$\dot{X}_P = V_{Pt}$$

Besides, 4th state equation becomes as follows by representing x_v in terms of x_i and x_p.

$$\dot{P}_C = \frac{1}{C}\left(2A_P V_{M1} + \frac{2}{R}P_C - \frac{2K_{vf}K_{ls}b}{(a+b)}x_i + \frac{2K_{vf}K_{ls}a}{(a+b)}X_P - K_{pf}P_C\right)$$

State matrix, states, input matrix and inputs for 2-Mass system are found as follows;

$$\boldsymbol{A} = \begin{bmatrix} 0 & K_R & -K_R & 0 & 0 \\ -\frac{1}{M_R} & -\frac{B_R}{M_R} & \frac{B_R}{M_R} & 0 & 0 \\ \frac{1}{M_{Pt}} & \frac{B_R}{M_{Pt}} & -\frac{B_R}{M_{Pt}} & -\frac{A_P}{M_{Pt}} & 0 \\ 0 & 0 & \frac{2A_P}{C} & \frac{(-RK_{pf}+2)}{RC} & \frac{2K_{ls}K_{vf}a}{C(a+b)} \\ 0 & 0 & 1 & 0 & 0 \end{bmatrix}$$

$$x^T = [F_{KR} \quad V_R \quad V_{Pt} \quad P_C \quad X_P]$$

$$\boldsymbol{B}^T = \begin{bmatrix} 0 & \frac{1}{M_R} & 0 & 0 & 0 \\ 0 & 0 & 0 & 0 & -\frac{2K_{vf}K_{ls}b}{C(a+b)} \end{bmatrix}$$

$$u^T = [F_F \quad x_i]$$

Bode plot representation that demonstrates the relationship between pilot input and cylinder output is obtained and given in chapter 4.1.Linkages and Feedbacks of Flight Control Actuator

Main linkages and feedback sources inside Flight Control Actuator are demonstrated below.

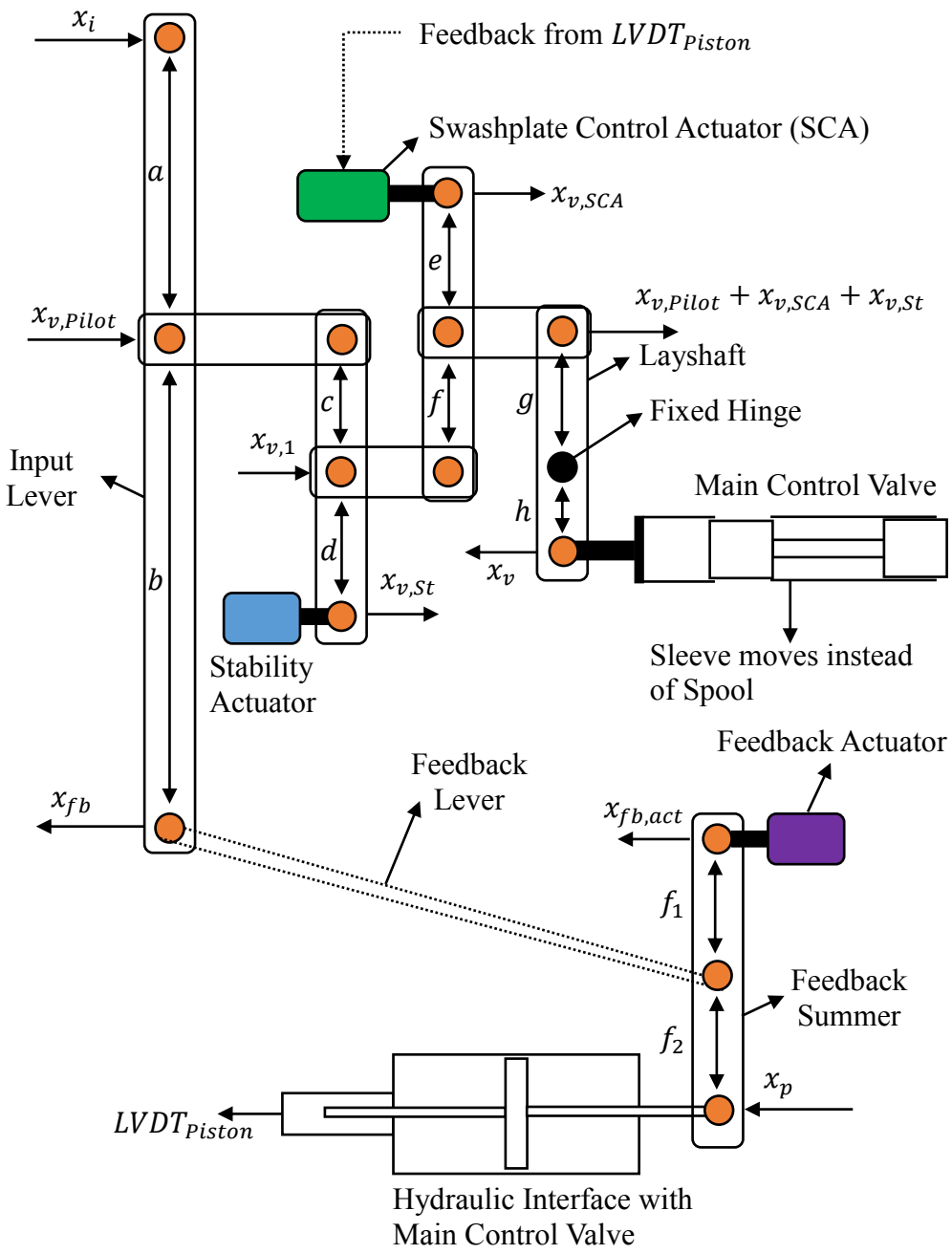

C. Control Loops in a Helicopter Control Application

Control Loop of Helicopter are demonstrated and marked as follows;

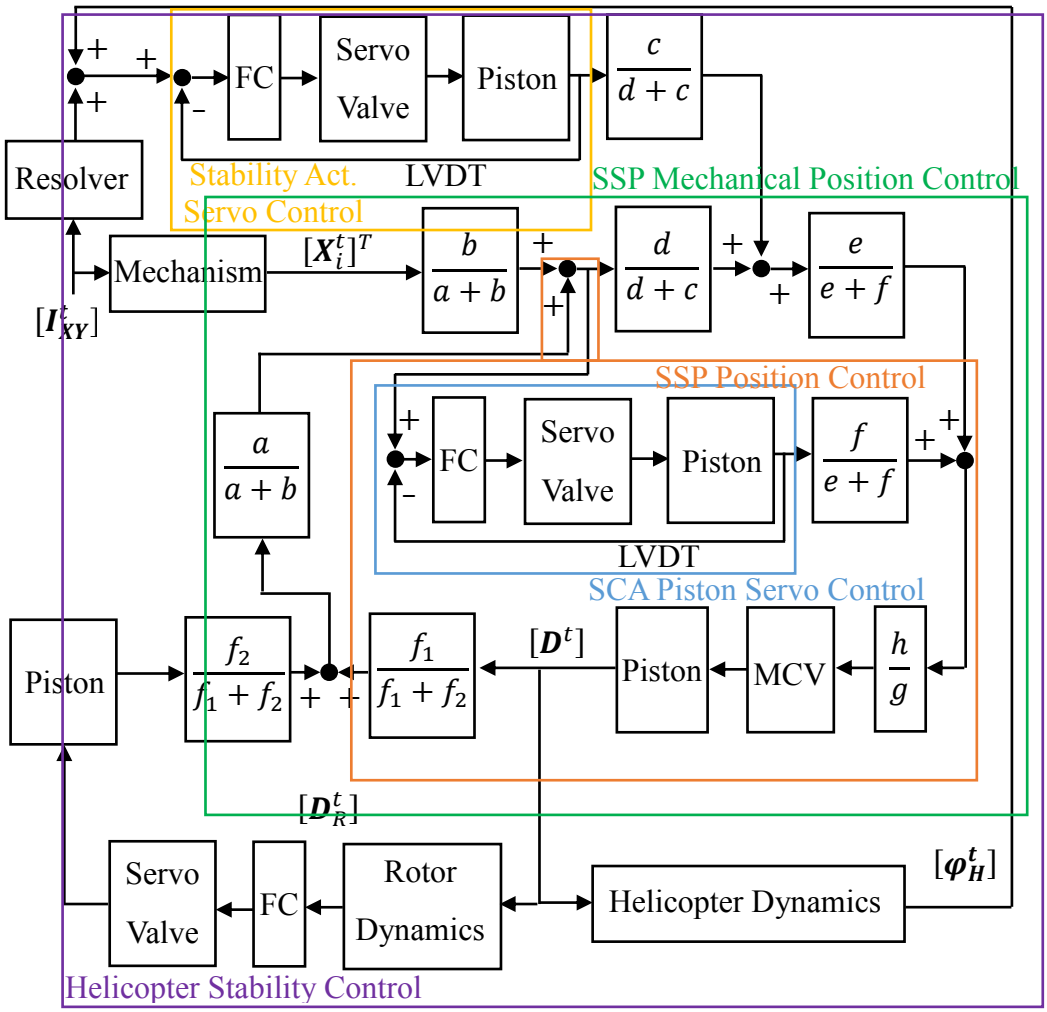
FC
Servo Valve
Piston
$\frac{c}{d+c}$
Resolver
Stability Act. Servo Control
LVDT
SSP Mechanical Position Control
Mechanism
$[X_i^t]^T$
$\frac{b}{a+b}$
$\frac{d}{d+c}$
$\frac{e}{e+f}$
$[I_{XY}^t]$
SSP Position Control
$\frac{a}{a+b}$
FC
Servo Valve
Piston
$\frac{f}{e+f}$
LVDT
SCA Piston Servo Control
Piston
$\frac{f_2}{f_1+f_2}$
$\frac{f_1}{f_1+f_2}$
$[D^t]$
Piston
MCV
$\frac{h}{g}$
$[D_R^t]$
Servo Valve
FC
Rotor Dynamics
Helicopter Dynamics
$[\varphi_H^t]$
Helicopter Stability Control